

Cranial osteology of the pampathere *Holmesina floridanus* (Xenarthra: Cingulata; Blanco NALMA), including a description of an isolated petrosal bone (#19901)

1

First submission

Please read the **Important notes** below, the **Review guidance** on page 2 and our **Standout reviewing tips** on page 3. When ready [submit online](#). The manuscript starts on page 4.

Important notes

Editor and deadline

Erik Seiffert / 7 Sep 2017

Files

12 Figure file(s)

5 Table file(s)

Please visit the overview page to [download and review](#) the files not included in this review PDF.

Declarations

No notable declarations are present



Please read in full before you begin

How to review






When ready [submit your review online](#). The review form is divided into 5 sections. Please consider these when composing your review:

- 1. BASIC REPORTING**
- 2. EXPERIMENTAL DESIGN**
- 3. VALIDITY OF THE FINDINGS**
4. General comments
5. Confidential notes to the editor

 You can also annotate this PDF and upload it as part of your review

To finish, enter your editorial recommendation (accept, revise or reject) and submit.

BASIC REPORTING

-  Clear, unambiguous, professional English language used throughout.
-  Intro & background to show context. Literature well referenced & relevant.
-  Structure conforms to [PeerJ standards](#), discipline norm, or improved for clarity.
-  Figures are relevant, high quality, well labelled & described.
-  Raw data supplied (see [PeerJ policy](#)).

EXPERIMENTAL DESIGN

-  Original primary research within [Scope of the journal](#).
-  Research question well defined, relevant & meaningful. It is stated how the research fills an identified knowledge gap.
-  Rigorous investigation performed to a high technical & ethical standard.
-  Methods described with sufficient detail & information to replicate.

VALIDITY OF THE FINDINGS

-  Impact and novelty not assessed. Negative/inconclusive results accepted. *Meaningful* replication encouraged where rationale & benefit to literature is clearly stated.
-  Data is robust, statistically sound, & controlled.
-  Conclusions are well stated, linked to original research question & limited to supporting results.
-  Speculation is welcome, but should be identified as such.

The above is the editorial criteria summary. To view in full visit <https://peerj.com/about/editorial-criteria/>

7 Standout reviewing tips

3



The best reviewers use these techniques

Tip

Example

Support criticisms with evidence from the text or from other sources

Smith et al (J of Methodology, 2005, V3, pp 123) have shown that the analysis you use in Lines 241-250 is not the most appropriate for this situation. Please explain why you used this method.

Give specific suggestions on how to improve the manuscript

Your introduction needs more detail. I suggest that you improve the description at lines 57- 86 to provide more justification for your study (specifically, you should expand upon the knowledge gap being filled).

Comment on language and grammar issues

The English language should be improved to ensure that your international audience can clearly understand your text. I suggest that you have a native English speaking colleague review your manuscript. Some examples where the language could be improved include lines 23, 77, 121, 128 - the current phrasing makes comprehension difficult.

Organize by importance of the issues, and number your points

1. Your most important issue
2. The next most important item
3. ...
4. The least important points

Give specific suggestions on how to improve the manuscript

Line 56: Note that experimental data on sprawling animals needs to be updated. Line 66: Please consider exchanging "modern" with "cursorial".

Please provide constructive criticism, and avoid personal opinions

I thank you for providing the raw data, however your supplemental files need more descriptive metadata identifiers to be useful to future readers. Although your results are compelling, the data analysis should be improved in the following ways: AA, BB, CC

Comment on strengths (as well as weaknesses) of the manuscript

I commend the authors for their extensive data set, compiled over many years of detailed fieldwork. In addition, the manuscript is clearly written in professional, unambiguous language. If there is a weakness, it is in the statistical analysis (as I have noted above) which should be improved upon before Acceptance.

Cranial osteology of the pampathere *Holmesina floridanus* (Xenarthra: Cingulata; Blacan NALMA), including a description of an isolated petrosal bone

Timothy J Gaudin ^{Corresp., 1}, Lauren M Lyon ²

¹ Department of Biology, Geology & Environmental Science, University of Tennessee - Chattanooga, Chattanooga, Tennessee 37403, United States

² Department of Geosciences and Don Sundquist Center of Excellence in Paleontology, East Tennessee State University, Johnson City, Tennessee 37614, United States

Corresponding Author: Timothy J Gaudin

Email address: Timothy-Gaudin@utc.edu

The present study entails descriptions of several well-preserved skulls from the pampathere species *Holmesina floridanus*, recovered from Pliocene localities in central Florida and housed in the collections of the Florida Museum of Natural History. Bone by bone descriptions have allowed detailed reconstructions of cranial morphology. Cranial foramina are described and illustrated in detail, and their contents inferred. The first ever description of an isolated pampathere petrosal is also included. Cranial osteology of *H. floridanus* is compared to that of Pleistocene species of *Holmesina* from both North and South America (*H. septentrionalis*, *H. occidentalis*), as well as to the other well-known pampathere genera, to closely related taxa among glyptodonts (*Propalaeohoplophorus*), and to extinct and extant armadillos (*Proeutatus*, *Euphractus*). This study identifies a suite of apomorphic cranial features that serve to diagnose a progressive series of more inclusive monophyletic groups, including the species *Holmesina floridanus*, the genus *Holmesina*, pampatheres, pampatheres plus glyptodonts, and a clade formed by pampatheres, glyptodonts, and *Proeutatus*. The study highlights the need for further anatomical investigations of pampathere cranial anatomy, especially those using modern scanning technology, and for analyses of pampathere phylogenetic relationships.

Cranial osteology of the pampathere *Holmesina floridanus* (Xenarthra: Cingulata; Blac-
NALMA), including a description of an isolated petrosal bone

Timothy J. Gaudin¹ and Lauren M. Lyon²

¹Department of Biology, Geology, and Environmental Science, University of Tennessee at
 Chattanooga, 615 McCallie Avenue, Dept. 2653, Chattanooga, TN 37403-2598, USA

²Department of Geosciences and Don Sundquist Center of Excellence in Paleontology, East
 Tennessee State University, 325 Treasure Lane, 70357, Johnson City, TN 37614-6502, USA

Corresponding author: Timothy J. Gaudin, Timothy-Gaudin@utc.edu

Key Words: Xenarthra, Cingulata, pampathere, *Holmesina*, cranial osteology, auditory region

15

16 Abstract - The present study entails descriptions of several well-preserved skulls from the
 17 pampathere species *Holmesina floridanus*, recovered from Pliocene localities in central Florida
 18 and housed in the collections of the Florida Museum of Natural History. Bone by bone
 19 descriptions have allowed detailed reconstructions of cranial morphology. Cranial foramina are
 20 described and illustrated in detail, and their contents inferred. The first ever description of an
 21 isolated pampathere petrosal is also included. Cranial osteology of *H. floridanus* is compared to
 22 that of Pleistocene species of *Holmesina* from both North and South America (*H. septentrionalis*,
 23 *H. occidentalis*), as well as to the other well-known pampathere genera, to closely related taxa
 24 among glyptodonts (*Propalaeohoplophorus*), and to extinct and extant armadillos (*Proeutatus*,
 25 *Euphractus*). This study identifies a suite of apomorphic cranial features that serve to diagnose a
 26 progressive series of more inclusive monophyletic groups, including the species *Holmesina*
 27 *floridanus*, the genus *Holmesina*, pampatheres, pampatheres plus glyptodonts, and a clade
 28 formed by pampatheres, glyptodonts, and *Proeutatus*. The study highlights the need for further
 29 anatomical investigations of pampathere cranial anatomy, especially those using modern
 30 scanning technology, and for analyses of pampathere phylogenetic relationships.

31

INTRODUCTION

Living armadillos, the only mammals to bear a carapace of dermal bony armor, are the most diverse of the extant groups of Xenarthra, numbering at least 21 of the 31 currently recognized xenarthran species (Aguiar and Fonseca 2008- although armadillo taxonomy is currently in flux; e.g., see Abba et al. 2015; Feijó and Cordeiro-Estrela 2016). However, the diversity of extinct armored xenarthrans, i.e., the Cingulata, far surpasses its extant representatives, not only in taxonomic diversity, but in terms of body size, locomotory diversity, and dietary diversity, even including a “horned” taxon *Peltephilus* (Fericola et al. 2008; Gaudin and Croft 2015; Croft 2016). Regarding diet, it is particularly noteworthy that there are omnivorous extant armadillos, but no herbivores (McDonough and Loughry 2008; Gaudin and Croft 2015), whereas the fossil cingulates include two herbivorous clades, pampatheres and glyptodonts. Both are comprised of large bodied taxa with complex dentitions (lobate teeth composed of multiple dental tissues of differing hardness; Kalthoff 2011). The former numbers only a few genera, whereas the latter encompasses at least 65 genera (McKenna and Bell 1997). Both are understudied, particularly given their conspicuous nature, often bizarre anatomies, and their abundance and ecological importance in late Cenozoic faunas of South and North America.

Pampatheres are a particularly poorly studied group. The oldest undoubted pampathere does not appear until the middle Miocene (Gaudin and Croft 2015; with the possible exception of a very poorly preserved taxon from the late Eocene of Patagonia, *Machlydothorium*, De Iuliis and Edmund 2002). The group’s basic taxonomy has long been unsettled. McKenna and Bell (1997) recognize only 4 valid pampathere genera, though several new taxa have since been added (Edmund and Theodor 1997; Góis et al. 2015). One of their genera, *Pampatherium*, includes as a

junior synonym at least one genus that is widely recognized as a separate, valid taxon, *Holmesina*; however, which of the species described in the literature belong in *Holmesina* and which in *Pampatherium* has been uncertain (Edmund 1987; De Iuliis et al. 2000). In addition, McKenna and Bell (1997) recognize the taxon name *Plaina* as a junior synonym of the genus *Kraglievichia*, whereas subsequently, De Iuliis and Edmund (2002) synonymize *Plaina* with McKenna and Bell's genus *Vassallia*. Part of the taxonomic difficulties lie with the paucity of fossil material. The majority of preserved pampathere remains consist of isolated osteoderms, which are often unreliable for taxonomic purposes (De Iuliis and Edmund 2002).

The nature of the pampathere record has also hindered an understanding of their basic skeletal anatomy. Most of the described postcranial skeletal remains are based on very incomplete material, have received only cursory descriptions, and are poorly illustrated, if at all, by unlabeled photographs showing only one or two views (Castellanos 1937; James 1957; Robertson 1976; Cartelle and Bohórquez 1985; Edmund 1985; Edmund and Theodor 1997; Góis et al. 2015). Despite the fact that several complete skeletal reconstructions have been published (James 1957; Edmund 1985), the postcranial osteology of pampatheres remains scarcely known.

For the skull, mandible, and dentition, the situation is somewhat better. A fair number of complete, or nearly complete skulls and mandibles are known from a variety of taxa, including *Kraglievichia* (Castellanos 1937), *Vassallia* (De Iuliis and Edmund 2002), *Pampatherium* (Bordas 1939; De Iuliis et al. 2000), and various species of *Holmesina* (Simpson 1930; James 1957; Cartelle and Bohórquez 1985; Edmund 1985; Vizcaíno et al. 1998). Although several other genera remain incompletely known (e.g., *Scirrotherium*, Edmund and Theodor 1997), *Tonnicius*, Góis et al. 2015). More detailed examinations of cranial anatomy have been published, including several studies of the ear region (in *Pampatherium*, Bordas 1939; Guth

1961; and in *Vassallia*, Patterson et al. 1989) and a recently published study on brain anatomy based on a digital endocast (Tambusso and Fariña 2015). However, many of these cranial descriptions are fairly cursory, and virtually all are illustrated with unlabeled photographs that leave out many details. Even the ear region studies fail to address or adequately illustrate the detailed anatomy of the petrosal bone, as is common among more modern treatments of mammalian auditory region osteology. To date, there remains no study of the cranial osteology of pampatheres that clearly illustrates suture patterns and provides a bone by bone description of the anatomy, including the cranial foramina and their likely contents.

Fossil pampatheres have been known from the state of Florida, in the extreme southeast of North America, for more than a century (Simpson 1930). Two species in the genus *Holmesina* are currently recognized: a late Pliocene-early Pleistocene (Blancan NALMA) form, *H. floridanus*; and, a middle to late Pleistocene taxon (Irvingtonian and Rancholabrean NALMA), *H. septentrionalis* (Hulbert and Webb 2001). Both are known from extensive material, but the older material is particularly complete, abundant, and well-preserved (see, e.g., the skull illustrated in Hulbert and Webb 2001, fig. 10.7, currently on exhibit at the Florida Museum of Natural History), though it remains mostly undescribed. Multiple individuals, including both adults and subadults, are derived largely from two sites: Haile 7G in Alachua County, Florida; and Inglis 1C in Citrus County, Florida. The goal of the present study is to describe the cranial osteology of *Holmesina floridanus*, based on this material. Because of the preservation quality, these fossils will allow us to conduct a thorough, bone by bone analysis of the skull, and to provide a fairly comprehensive view of the cranial foramina and their reconstructed contents. There is even an isolated petrosal among this material, which will allow us to describe the bony anatomy of the auditory region in unprecedented detail. These descriptions are accompanied by

a carefully executed series of drawings, including both drawings of the best preserved fossils themselves, as well as reconstructions of the anatomy as we believe it would have appeared in life. The present study will provide the most detailed glimpse yet into the cranial anatomy of pampatheres, and should serve as an important basis for future studies of the paleontology, systematics, and evolution of this enigmatic group of cingulate xenarthrans.

MATERIALS AND METHODS

Our goal was to base our description on the best preserved specimens of *Holmesina floridanus* available. Unfortunately for our purposes, the best preserved skull, UF 121742 (one of the best preserved fossil skulls we have ever seen!), is currently on exhibit at the Florida Museum of Natural History. Although the museum staff was kind enough to allow our examination of this specimen for an afternoon, it was not possible for us to borrow the skull for more careful study. Therefore, the descriptions below are based largely on three other specimens, UF 191448, UF 224450, and UF 248500, which were also in excellent condition and were available for loan. UF 191448 is an almost perfectly complete adult skull, with only minor damage in the orbital wall and nasopharyngeal roof; but, as an adult, most of the sutures are closed, and the specimen retains only four of eighteen teeth (left M3-5, and right M8). UF 224450 is an isolated but nearly perfectly preserved left mandible, however it retains only three of nine teeth (m2 and m6-7). UF 248500 is a subadult specimen with some significant damage to the middle portions of the skull, including parts of the skull roof, orbital wall, nasopharynx and left basicranium; but, it retains many if not most of its sutures, all its dentition is intact, and those portions of the skull that are present are very well preserved. In addition, it has a complete, isolated left petrosal that we were able to examine in three dimensions.

In order to examine interspecific variation, including ontogenetic variation, the three specimens that form the primary basis for this description were compared to the other skulls and mandibles of *H. floridanus* in the collections of the Florida Museum of Natural History. Most of these, with the exception of the aforementioned display specimen, are not fully prepared, several are incompletely preserved, and at least one represents a subadult likely even younger than UF 248500. These specimens include the following: UF 121742 [exhibit skull], UF 223813 [skull only], 248000 [partial mandible], 275496 [juvenile skull], 275497 [skull & mandible], 275498 [skull & mandible]; 278000 [partial skull & mandible]; 285000 [skull & mandible], 293000 [skull & mandible]. None of the *H. floridanus* material examined preserved any trace of the ectotympanic bone or the auditory ossicles, or showed any trace of an entotympanic (an element commonly present in other xenarthrans and likely a synapomorphy of Xenarthra; Patterson et al. 1992; Gaudin 2004; Gaudin and McDonald 2008), though, as noted above, some specimens are not yet fully prepared.

In order to assess generic level variation within *Holmesina*, the *H. floridanus* material described above was compared to two specimens of the North American Pleistocene species *H. septentrionalis* (UF 889 [partial skull only] and UF 234224 [cast skull only]) and one specimen of the South American Pleistocene species *H. occidentalis* (ROM 3881 [skull], ROM 4955 [mandible]), as well as any literature available on these taxa. Likewise, in order to gain a comparative perspective on pampathere cranial anatomy, our material was compared to one specimen of *Vassallia maxima* (FMNH P14424), as well as the available literature on this and other pampathere skulls. Finally, in order to place this anatomy in a broader context among cingulates, *H. floridanus* was compared to specimens of the basal glyptodont *Propalaeoplophorus* (YPM-PU 15007, 15291; FMNH 13205; glyptodonts are the putative

sister taxon to pampatheres; Gaudin and Wible 2006; Billet et al. 2011), the extinct eutatine armadillo *Proeutatus* (FMNH P13197, P13199; *Proeutatus* is the putative sister taxon to pampatheres and glyptodonts; Gaudin and Wible 2006; Billet et al. 2011), and the extant euphractine armadillo *Euphractus* (CM 6339; UTCM 1481, 1486, 1491, 1500; one of the living armadillos that is most closely related to pampatheres; Gaudin and Wible 2006; Billet et al. 2011).

Descriptions of the dorsal surface of the petrosal are only available for a small number of cingulate taxa. Therefore, we will be comparing the anatomy of the dorsal surface of our isolated petrosal in *Holmesina floridanus* to the detailed description of *Dasypus novemcinctus* by Wible (2010), to a bisected skull of *Euphractus sexcinctus* (UTCM 1486), and to the ~~Field Museum~~ specimen of *Vassallia maxima*, FMNH P14424, in which the braincase has been bisected (though its endocranial anatomy was never described; the cut is visible in De Iuliis and Edmund, 2002, figure 2). Because these are the only two cingulates for which we have information on the lateral surfaces of isolated petrosals, we shall restrict our comparisons of this surface to these two taxa, *H. floridanus* and *Dasypus novemcinctus* (Wible, 2010).

Anatomical terminology, wherever possible, follows that of Wible and Gaudin (2004) and Wible (2010). Stereophotographs of UF 248500 were prepared with the assistance of Dr. Stelios Chatzimanolis (Univ. of Tennessee at Chattanooga) in accordance with the procedure outlined in Gaudin (2011).

Institutional Abbreviations: CM, Carnegie Museum of Natural History, Pittsburgh, PA, USA; FMNH, Field Museum, Chicago, IL, USA; UF, Florida Museum of Natural History, University of Florida, Gainesville, FL, USA; UTCM, University of Tennessee at Chattanooga Museum of Natural History, University of Tennessee at Chattanooga, Chattanooga, TN, USA;



YPM-PU

Princeton University Collection, Peabody Museum of Natural History, Yale

University, New Haven, CT, USA.

Other abbreviations: c.n., cranial nerve; GSL, greatest skull length; M1-9, upper

molariform teeth; m1-9, lower molariform teeth; MML, maximum mandibular length; NALMA,

North American Land Mammal Age; SALMA, South American Land Mammal Age.

RESULTS (DESCRIPTIVE ANATOMY)



Nasal

The nasals in *Holmesina floridanus* (UF 191448, 248500) consist of two long, transversely convex bones that cover most of the visible surface of the snout in dorsal view (Figures 1, 2). The outline of the bones is somewhat variable, with the bones accounting for anywhere between 32-43% of the skull's total length, and the width to length ratio varying from 0.32-0.49 (Table 1, 2). The extant six-banded armadillo (*Euphractus sexcinctus*, UTCM 1491) falls into the same range for both values, whereas the nasals of the extinct eutatine armadillo *Proeutatus oenophorus* (FMNH P13197) are of similar length but narrower. The congeneric pampathere *H. septentrionalis* (UF 234224) has longer but narrower nasals, the pampathere *Vassalia maxima* (FMNH P14424) has longer nasals of comparable width, and the early glyptodont *Propalaeohoplophorus australis* (YPM-PU 15007) has nasals that are both shorter and wider (Table 1). A nasal bone greater than or equal to thirty-five percent of the skull length is a synapomorphy of *Proeutatus*, glyptodonts, and pampatheres (Gaudin and Wible 2006). In lateral view, the nasals of *H. floridanus* slope gently anteroventrally as in other pampatheres (Castellanos 1937; Bordas 1939; James 1957; Cartelle and Bohórquez 1985; Edmund 1985; Edmund and Theodor 1997; Vizcaíno et al. 1998; De Iuliis et al. 2000; De Iuliis and Edmund

2002), as well as in *Propalaeohoplophorus* (Scott 1903-4), and the extant *E. sexcinctus* (CM 6399, UTM 1486, 1491). This condition is exaggerated in *Proeutatus oenophorus* (FMNH P13197; Scott 1903-4), where the posterior half of the nasal bones curve upwards steeply towards the frontal bone.

In dorsal view, the anterior margin of the nasal bones in *H. floridanus* is convex, which is a synapomorphy of Cingulata (Gaudin and Wible 2006; Gaudin and McDonald 2008). UF 284500 has distinct lateral sutures running the length of the nasals, whereas the sutures with the maxilla and premaxilla are largely fused in UF 191448. Nasal width is uniform from the anterior tip to the maxillo-premaxillary suture, where it then gently narrows posteriorly as it approaches the frontal bone. There appears to be two major fronto-nasal suture patterns that occur in *H. floridanus*. One of the patterns occurs in UF 191448, as a roughly straight though highly irregular suture (Figure 1). The other pattern, observed in multiple specimens (UF 223813, 275496, 275497, 275498; 285000) is a shallow V-shaped suture with the apex directed anteriorly. The nasals of UF 248500 are fractured posteriorly, and the bone is clearly incomplete in places, making it hard to discern the course of its fronto-nasal suture. In *H. septentrionalis* (UF 889), the overall shape of the nasal is similar to that of *H. floridanus*. However, the fronto-nasal suture varies in form and may differ substantially from that of *H. floridanus*. In UF 889 it forms a distorted W-shape, due to a large median peak with a posteriorly directed apex. Conversely, in UF 234224 it is roughly straight, but irregular, as in *H. floridanus* (UF 191448). The fronto-nasal suture in *H. occidentalis* (ROM 3881) forms a very shallow, anteriorly concave jagged “U.” In *Vassallia* the suture is a shallow V-shape, reminiscent of some *H. floridanus* specimens, except that the apex in *Vassallia* is directed posteriorly. It is clear from our survey that the shape of the fronto-nasal suture varies widely among pampatheres, though in our

reconstruction of *H. floridanus* we have chosen to illustrate a condition like that in UF 191448 (Figure 2).

The suture is unknown in *Propalaeohoplophorus* (Scott 1903-4; Vizcaino et al. 1998). Like some *Holmesina*, the fronto-nasal suture of *Proeutatus* (FMNH P13197) forms a V-shape, with the apex pointing anteriorly. In *Euphractus* it is roughly straight near the lateral edges of the nasal bones, but as it approaches the median suture it too forms an anteriorly-directed V-shape, albeit a smaller one than that of *Proeutatus* (Wible and Gaudin 2004).

Premaxilla

In lateral view, the premaxilla has a broad rectangular facial process, with its dorsoventral height slightly exceeding its anteroposterior length (Figures 3, 4). The maxillo-premaxillary suture of the facial process in *H. floridanus* (UF 248500) forms a single posteriorly convex curve. The premaxillary sutures are harder to distinguish in UF 191448, but they appear similar. The dorsal suture between the premaxilla and nasal is relatively short in *Holmesina* (7-10% of GSL in *H. floridanus*; Table 1, 2 - though not listed in the table, the value for *H. occidentalis* [ROM 3881] is about 7% of GSL) relative to the extant *Euphractus* (15% of GSL, UTCM 1491), though not as short as in glyptodonts (4% of GSL, *Propalaeohoplophorus* YPM-PU 15291; Table 1). *Proeutatus* (11% of GSL, FMNH P13197) is similar in this regard to *Holmesina*.

The free anterior edge of the facial process is vertical but irregularly shaped. The dorsal portion of this edge has a deep and narrow notch in UF 248500 (Figure 3B, C) and UF 121742, which slopes anteroventrally into a large triangular prong. In both UF 191448 (Figure 3A) and UF 285000 the anterior edge is marked by a shallower, more rounded notch, ending in a small

bump on its ventral margin. *H. septentrionalis* and *Vassallia maxima* (Edmund 1985; De Iuliis and Edmund 2002) also have notches that are deep and narrow, as in UF 191448, whereas *H. occidentalis* (ROM 3881) has a shallower C-shaped notch more like UF 248500. *Propalaeohoplophorus* has a very shallow C-shaped notch on the anterior edge of its very tall and narrow premaxillary facial process (Scott 1903-4). In *Euphractus*, the anterior margin of the premaxilla is variable in shape – it may be a relatively straight edge sloping posteroventrally (Wible and Gaudin 2004), it may be marked by a wide, shallow, C-shaped notch (e.g., UTCM 1500), or the entire edge may form a single shallow concavity (e.g., UTCM 1486, 1491). The anterior edge of the premaxilla in *Proeutatus* (FMNH P13197) slopes posteroventrally in lateral view, as in *Euphractus*, and it lacks the notch that is present in pampatheres, glyptodonts, and some *Euphractus* (Wible and Gaudin 2004).

The external nares of *H. floridanus* are widest transversely near the nasopremaxillary suture. From there the premaxilla slopes steeply inward ventromedially. In anterior view UF 248500 appears to have irregularly rounded, upside-down triangular shaped nasal opening. The nares in UF 191448 have a more rounded, inverted pentagonal cross-section, much like that of *H. septentrionalis* (UF 234224). The nasal opening is more ovate and dorsoventrally compressed in both *Proeutatus* (FMNH P13197) and *Euphractus* (CM 6399; UTCM 1486, 1491).

In ventral view, the premaxilla of *H. floridanus* forms a rounded M-shaped palatal suture with the maxilla (Figures 5, 6), similar to that of *H. septentrionalis* (UF 889). The maxillo-premaxillary suture exhibits a high degree of variability in other species.

In *H. floridanus*, the anteroventral tip of the premaxilla extends forward in the midline as a rounded prong in UF 191448, though this prong is strongly reduced in UF 248500. *H. septentrionalis* (Edmund 1985) has a similar, though transversely broader, U-shaped

anteroventral prong, and a prong very like that of UF 191448 is also present in *Vassallia* (De Iuliis and Edmund 2002). *Propalaeohoplophorus* differs in that the anteroventral edge of the premaxilla forms extensions that project forward to form a distorted M-shape, with long anterolateral edges and a short V-shaped median notch. The premaxillae of *Proeutatus* and *Euphractus* lack anteroventral extensions (Scott, 1903-4; Wible and Gaudin 2004).

The palatal process of the premaxilla in *H. floridanus* is incised by a deep groove that emerges from the front of the incisive foramina (Figures 5, 6). The incisive foramen transmits the nasopalatine duct, which connects the oral and nasal cavities with the vomeronasal organ. It also transmits the nasopalatine nerve, artery and vein (Wible and Gaudin 2004). The incisive foramina themselves are deeply recessed posterodorsally, with separate left and right openings that empty into a single midline fossa. This appears to be a general feature of pampatheres, but it is an unusual morphology among cingulates. Other cingulates, such as *Proeutatus* (FMNH P13197) and *Euphractus* (CM 6399; UTCM 1481, 1486), have a common fossa that houses the two separate incisive foramina, and all cingulates (except perhaps glyptodonts; see Gillette and Ray 1981, fig. 11c) have close set incisive foramina. However, in no other cingulates are they as deeply recessed, and no other cingulates possess the deep anterior groove found in pampatheres. As in all other cingulates, aside from *Peltephilus* (Gaudin and Wible 2006), the incisive foramina in *H. floridanus* are completely encompassed by the premaxilla.

The premaxilla retains a single tooth near its posterior border with the maxilla. The right maxillary-premaxillary suture runs into the mesial portion of the socket of the second tooth. The premaxilla encompasses the labial half of the second tooth socket, but forms only the front of the socket on the lingual side. The presence of premaxillary teeth is a synapomorphy of euphractine armadillos, glyptodonts, and pampatheres (Node C; Gaudin and Wible 2006), though it is lost

secondarily in glyptodonts. The premaxillary tooth of *H. floridanus* is angled anteriorly and slightly medially. It has beveled wear facets on the occlusal surface. The surface area of the mesial facet is greater than that of the distal facet in most specimens, though the distal is larger in UF 293000 and highly reduced in UF 121742 and 275496, and the two facets lie at a 110 degree angle to one another. The overall outline of the occlusal surface is ovate, with its mesiodistal length exceeding its transverse width (Table 1). The left premaxillary tooth in UF 248500 possesses a small lenticular island of osteodentine in the center, whereas the right tooth has a narrow linear island of osteodentine. Presence of an elevated core of osteodentine is a synapomorphy of *Proeutatus*, glyptodonts, and pampatheres (Node 7; Gaudin and Wible 2006), as is the presence of beveled wear facets only in the anterior portion of the tooth row. In both *H. occidentalis* (ROM 3881), and *Proeutatus* (FMNH P13197) the premaxillary tooth has an ovate occlusal surface, similar to *H. floridanus*. In *Vassallia* and *H. septentrionalis* the premaxillary teeth are missing, (Edmund 1985; De Iuliis and Edmund 2002), but it can be ascertained from the shape of the tooth alveoli in these animals that they too had ovate occlusal surfaces, making this a shared trait among cingulate taxa that possess premaxillary teeth. In *Euphractus* (CM 6399; UTCM 1486, 1491) the premaxillary tooth is mostly flat at its tip, with a small discolored island in the center, likely formed from orthodentine (Ferigolo 1985; Kalthoff 2011).

Maxilla

The facial process of the maxilla contacts the nasal dorsally, the premaxilla anteriorly, and the frontal and lacrimal posteriorly (Figures 3-6). The large zygomatic process of the maxilla contacts the jugal posteriorly. The facial process is marked by a ridge that runs anteroposteriorly just below the nasomaxillary suture. In *Holmesina*, this ridge begins as an indistinct, broad

elevation above M2/M3 (=second and third molariform teeth; note all teeth in pampatheres and glyptodonts are molariform) that becomes a more pronounced, low ridge above M4, and finally forms a sharply defined ridge over M6. The ridge then curves posteroventrally to become confluent with the maxilla/jugal suture and a large rounded ridge that marks the anterior termination of the jugal and outlines the distinct antorbital fossa (Wible and Gaudin 2004; = buccinator fossa from Gaudin 2004). The antorbital fossa is particularly large and deep posteriorly behind the infraorbital foramen, as well as on the anterior surface of the zygomatic process of the maxilla. This fossa accommodates the nasiolabialis muscles (Smith and Redford 1990; Vizacaino et al. 1998; Wible and Gaudin 2004). In dorsal view, the maxilla forms a small portion of the roof of the snout as it touches the nasal bone (Figures 1, 2). It also comprises the majority of the lateral walls of the snout, which taper anteriorly in both lateral and dorsal views (Figures 1-4). A nearly identical lateral maxillary ridge is present in the other *Holmesina* species (*H. occidentalis*, *H. septentrionalis*). The ridge in *Vassallia*, though present, is less distinct (De Iuliis and Edmund 2002) than it is in *Holmesina*. *Euphractus* (CM 6399; UTM 1486, 1491) also has a distinct maxillary ridge that begins over M3 and marks the dorsal edge of a strong antorbital fossa (Wible and Gaudin, 2004). The antorbital fossa is less well marked in *Proeutatus*, and is absent in *Propalaeohoplophorus* (Scott, 1903-4; Gaudin and Wible 2006).

The palatine process of the maxilla is broadly concave anteroposteriorly from M1 to M7. The palate, including both maxillary and palatine contributions, is convex from M7 to the posterior edge of the palate, but concave transversely along its whole length. Both the longitudinal and transverse concavities are especially deep anteriorly, near the junction of the maxilla and premaxilla. The hard palate is marked by numerous foramina (Figures 5, 6), as in other xenarthrans (Gaudin and Wible 2006). This is due to the fact that the major palatine

arteries, veins, and nerves that travel within the palatal process of the maxilla (Wible and Gaudin, 2004), rather than on its ventral surface, as in other mammals (e.g., *Canis*, Evans and Christiansen 1979; *Homo*, Clemente 1985). These nerve and vessels finally emerge ventrally from their canal in the maxilla near the front of the palate, through the anterior palatal foramina. Anterior palatal foramina are typically located near M4 (e.g., in UF 248500) in *H. floridanus*, but they exhibit some variation in their position in different specimens. For example, in UF 191448, both are near the distal half of M3, but on the left side of UF 121742, they are as far back as the mesial half of M5. The anterior palatal foramina occupy similar, somewhat varying positions in *H. occidentalis*, *H. septentrionalis*, and *Vassallia*, showing only slightly greater variation than that found in *H. floridanus* itself - one specimen of *H. septentrionalis* (UF 234224) had the foramina situated a little further forward, at the mesial edge of M3 or between M2 and M3. In all of these species, the foramina open anteriorly into distinct grooves that travel forward, ending just short of the maxillo-premaxillary suture. This anterior palatal foramina and grooves are also present in glyptodonts (Gaudin 2004) and *Proeutatus* (FMNH P13197). The characteristic is convergent on similar features shared by pilosans (Gaudin 2004; Wible and Gaudin 2004; De Iuliis et al. 2011).

The median suture of the maxilla is slightly raised from the distal edge of M5 posteriorly to the junction with the palatine in *H. floridanus* (Figures 5, 6). This trait is also present in *H. occidentalis* (ROM 3881), *Vassallia* (De Iuliis and Edmund 2002), *Propalaeohoplophorus* (Scott 1903-4), *Proeutatus* (FMNH P13197), and *Euphractus* (CM 6399). In *H. floridanus*, the apex of the U-shaped maxillary/palatine suture reaches as far anteriorly as the middle of M8. The suture travels posteriorly just medial to the tooth alveoli of M8 and M9, and then curves laterally behind this last tooth in front of the pterygoid process. A U-shaped maxillo-palatine suture with

rounded anterolateral corners is a derived feature of *Proeutatus* and living euphractines (Node 6, Gaudin and Wible 2006), but this condition also occurs in *H. floridanus* and *H. occidentalis* (ROM 3881). The maxilla/palatine suture is unknown in *H. septentrionalis* and *Propalaeohoplophorus*, whereas in *Vassallia*, the suture is M-shaped (De Iuliis and Edmund 2002; Gaudin and Wible 2006).

The zygomatic process of the maxilla is sizeable, and forms most of the anterior wall of the orbit in pampatheres (Gaudin and Wible 2006). In ventral view, the zygomatic process is triangular with a broad base and narrow apex extending laterally at a right angle to the main body of the maxilla (Figures 5, 6). The ovate infraorbital foramen in *H. floridanus* is situated above M6, and opens anteriorly into a short groove. The maxillary foramen lies above the posterior half of M7 (UF 121742, 248500; 285000) or the anterior half of M8 (UF 191448). It is triangular in shape, and serves as the posterior entrance to a long infraorbital canal that perforates the base of the zygomatic process. This canal is riddled with many smaller foramina along its medial wall, as occurs in *Euphractus* (Gaudin and Wible 2004). In *H. occidentalis*, *H. septentrionalis* and *Vassallia*, the infraorbital canal also extends from M8-M6 (ROM 3881; UF 234224; Edmund 1985; De Iuliis and Edmund 2002); thus, this appears to be a characteristic of pampatheres in general. In contrast, *Propalaeohoplophorus* has a more dorsally situated infraorbital canal than that of pampatheres. The canal is relatively short, its entire length located above M6-M5 (Scott 1903-4). *Proeutatus* also has a short, dorsally positioned infraorbital canal that begins above M7 and exits above M5/M6, and lies above the antorbital fossa. In *Euphractus* (CM 6399), the canal is intermediate in length between that of *Proeutatus* and *Holmesina*, beginning over the posterior half of M7 and exiting over the anterior half of M6.

Sutures are fused or poorly marked in the orbit of UF 191448, and large portions of the orbital process of the maxilla are missing or heavily fractured in UF 248500, though the sutures are more clearly visible in the latter specimen. That said, the orbital process of the maxilla appears to comprise the anteroventral part of the medial wall of the orbit (Figure 7) as in most cingulates, with the exception of dasypodine armadillos (Gaudin and Wible 2006). The orbital exposure of the maxilla borders the lacrimal, anterodorsally, the frontal posterodorsally, and the alisphenoid, pterygoid (or palatine; see description of palatine below), and orbitosphenoid posteriorly. Atypical of other mammals and even other cingulates, pampatheres and glyptodonts possess a sphenopalatine foramen that is housed in a common fossa with the sphenorbital fissure. The opening of the sphenopalatine foramen is directed cranially (UF 121742). Within the orbit the maxilla forms the anterior edge of the sphenopalatine foramen, whereas the alisphenoid (or palatine; see description of palatine below) forms the posterior edge. In *Euphractus*, the sphenopalatine foramen lies between the maxilla and palatine (Wible and Gaudin 2004).

The presence of nine upper teeth is the primitive condition in *Proeutatus*, euphractine armadillos, and pampatheres (Node 3; Gaudin and Wible 2006), with all but the first (M2-M9) housed in the maxilla. *Propalaeohoplophorus* has only eight teeth, since it is missing the premaxillary tooth, as noted above. Therefore, we believe the first tooth in *Propalaeohoplophorus* is homologous with M2 in pampatheres, and we will label it as such for comparative purposes. UF 248500 preserves a complete dentition (Figure 5B), whereas in UF 191448 there are only four teeth remaining (the left M3-M5, and the right M8; Figure 5A). Among other *H. floridanus*, UF 121742 also has a complete dentition, whereas at least partial dentitions are visible in the incompletely prepared specimens UF 223813, 275496, 285000, and 293000. The upper molariforms in *H. floridanus* are relatively short and broad compared to

399 those in other pampatheres or glyptodonts (Table 1, 2). The occlusal surfaces of M2 and M3 are
 400 ovate in outline. The occlusal surface of M4 is ovate in UF 191448 and almost rectangular in UF
 401 293000, but reniform in UF 248500 and most other specimens, with an occlusal surface that is
 402 concave lingually and convex labially. In UF 191448, M5 is reniform and concave labially, and
 403 M5 is bilobate in UF 285000 and 275498, whereas in UF 248500 and the other *H. floridanus*
 404 specimens, M5-M7 are trilobate on the lingual side, and bilobate on the labial side of the tooth,
 405 though the middle lingual lobe is often poorly marked. This causes these teeth to retain a bilobate
 406 gestalt, as is typical for pampatheres (Hoffstetter 1958; Edmund 1985; Edmund and Theodor
 407 1997; De Iuliis and Edmund 2002). M8 and M9 are bilobate on both sides of the jaw. The
 408 presence of reniform occlusal surfaces on the anterior teeth and bilobate occlusal surfaces on the
 409 posterior teeth appears to be a characteristic of pampatheres. *H. septentrionalis* has occlusal
 410 surfaces that are kidney-shaped from M2-M4, but bilobate from M5-M9, as in *H. floridanus*
 411 (Edmund 1985). *H. occidentalis* (ROM 3881) differs from *H. floridanus* and *H. septentrionalis*
 412 in that M3-M4 are more ovate in outline, and the posterior lobes are displaced slightly laterally
 413 in M6-M9, whereas in other pampatheres the lobes are linearly arranged. *Vassallia* is missing
 414 most of its teeth, but the occlusal surface of the left M6 appears to be similar in shape to that of
 415 *H. floridanus*, albeit with deeper lateral lobes (De Iuliis and Edmund 2002). *Scirrotherium*,
 416 *Kraglievichia*, and *Pampatherium* appear to differ mainly in the size and shape of M4, with the
 417 tooth smaller and more ovate in *Scirrotherium* (Edmund and Theodor 1997) and relatively larger
 418 than *Holmesina* and bilobate in shape in the latter two genera (Simpson 1930; De Iuliis et al.
 419 2000). In *Propalaeohoplophorus*, the anterior teeth are reniform, or weakly lobate in the case of
 420 M4, reminiscent of the condition in pampatheres. However the posterior teeth are distinct in
 421 outline, with M5-M6 irregularly shaped, weakly bilobate labially and trilobate lingually, whereas

M7-M9 are strongly trilobate on both sides. This trilobate pattern is a defining feature of glyptodonts (Hoffstetter 1958; Gillette and Ray 1981). *Proeutatus* possesses anterior teeth with ovate cross-sections as in *Euphractus*, whereas the back teeth are shaped like tear drops with the apex pointing anteriorly and lingually (Scott 1903-4). *Euphractus* has ovate or circular occlusal surfaces on all its teeth, as in other armadillos (Wible and Gaudin 2004; Gaudin and Wible 2006).

In UF 248500, M2 possesses an oval island of osteodentine in the center of the tooth, which becomes narrow and linear in M3-M4 and M9. M5 through M8 have a line of osteodentine that is either Y-shaped or triangular at either end (Figure 5B). This osteodentine pattern was consistently present among the other *H. floridanus* specimens that were examined and appears in other pampatheres as well. In *Propalaeohoplophorus*, each lobe of the molariforms has a branched central ridge of osteodentine, as in other glyptodonts (Scott 1903-4; Gillette and Ray 1981; Ferigolo 1985; Kalthoff 2011). In *Proeutatus* the posterior teeth also possess an osteodentine core like glyptodonts and pampatheres, but this core forms a loop rather than a linear or branched structure (FMNH P13197; Scott 1903-4). In *Euphractus* (CM 6399; UTCM 1486, 1491), as in other armadillos, there is no osteodentine in the teeth. There is only an ovate region of modified dentine in the center of each tooth (Ferigolo, 1985; Gaudin and Wible 2006; Kalthoff, 2011).

M2 and M3 both have beveled crowns, with a mesial facet that is much larger than the distal facet. The angle between the mesial and distal facets on M2 is more acute than that of M1, whereas in M3 the two facets form nearly a right angle. M4 and all of the remaining teeth have but one flat occlusal surface. The long axis of the tooth crowns in UF 248500 are all angled anteroventrally in lateral view (Figures 5, 6). Additionally, M2 and M3 are lingually oriented in

anterior view, M5-M7 are vertical, and M8-M9 are tilted labially. The corresponding occlusal surfaces form a gently rolling planar surface that faces slightly ventrolaterally in the posterior teeth, and faces progressively more ventromedially near the front of the toothrow. This is similar to the condition occurring in glyptodonts, where the upper teeth slant lingually anteriorly and labially posteriorly (Gaudin 2004). The posterior molariforms take on a stairstep appearance in lateral view, with the occlusal surfaces slanting posteroventrally (Figures 5, 6). In both *Holmesina* and *Vassallia*, the anterior left and right toothrows bend inward to form a nearly closed dentition (Figures 3, 4). This is also the case in *Kraglievichia* and (to a lesser extent) *Pampatherium* (Simpson 1930; Bordas 1939; De Iuliis et al. 2000), and likely represents a derived trait of pampatheres. This feature is unusual among cingulates, but it is also present in *Macroeuphractus* (Vizcaíno and De Iuliis 2003). This differs from the condition that occurs in the extinct “horned” armadillo *Peltephilus*, where the dentition is fully closed anteriorly (Gaudin and Wible 2006).

Palatine

The palatine bone consists in part of a large horizontal process that forms the back of the hard palate, with the left and right bones separated medially by a raised suture (Figures 3, 4). This elongated median ridge is a synapomorphy among euphractine armadillos, *Eutatus*, *Proeutatus*, glyptodonts, and pampatheres (Node A, Gaudin and Wible 2006). However, the median palatine ridge in both *Euphractus* and *Proeutatus* is more sharply defined than that of *H. floridanus*. As noted above, the anterior apex of the maxillo-palatine suture in *H. floridanus* (UF 248500) lies opposite the midpoint of M8. The ventral surface of the horizontal process has a few small perforations that appear to accommodate branches of the major palatine arteries, veins,

and nerves. The posterior-most region of the palatal surface may have one or two minor palatine foramina of varying size (size and number vary both bilaterally and among specimens), and the posterior margin in some specimens is marked (on one side or both right and left) by a deep notch that presumably served the same purpose, accommodating the minor palatine nerves and vessels that service the soft palate (Wible and Gaudin 2004). The minor palatine foramen in UF 248500 opens into a caudal palatine foramen that is situated in the floor of the sphenopalatine canal, just medial and anterior to the aperture of the sphenopalatine foramen.

The posterior edge of the palatine, which forms the anteroventral margin of the choanae, takes on a narrow U-shape. This configuration is a synapomorphy of glyptodonts and pampatheres (Gaudin and Wible 2006). Moreover, the palatine extends only a short distance beyond the tooththrow posteriorly, which is a synapomorphy among *Tolypeutes*, euphractine armadillos, *Eutatus*, *Proeutatus*, glyptodonts, and pampatheres (Node 5, Gaudin and Wible 2006).

In several *H. floridanus* specimens examined, there was a transverse crack present behind M9 but anterior to the minor palatine foramina. Although it is more or less symmetrical on the right and left sides in UF 248500 (Figure 5B), and a similar crack is present in roughly the same place in a couple of other specimens (UF 223813, 275496 [juvenile]), we have ultimately decided that it is just a crack in the palatine, and not a suture. The posterolateral corner of the palatine's horizontal process curves ventrally to form a large triangular flange. This flange covers the robust pterygoid process on its anterior, ventral, medial surface. In *H. floridanus* (UF 248500) this flange forms distinct sutures laterally and posteriorly with the pterygoid bone.

In lateral view, there is typically no exposure of the palatine in the orbit (UF 191448, UF 121742; Figure 7). In the juvenile specimen, UF 248500, there is a narrow portion of the

palatine's perpendicular process visible as a vertical splint lying between the maxilla anteriorly, and the alisphenoid and pterygoid posteriorly. As noted above, this may be a temporary condition, and the alisphenoid may have grown over it to cover the maxilla later in life. The dorsal edge of the palatine bone is broken in UF 248500, and the orbital sutures are fused in UF 191448. Thus the connections with the orbitosphenoid are unclear, though there is clearly no contact with the squamosal. The lack of an orbital palatine exposure is likely an autapomorphy of *Holmesina*, since an exposure is present in *Vassallia* (De Iuliis and Edmund 2002), glyptodonts (Guth 1961) and *Proeutatus* and *Euphractus* (Wible and Gaudin 2004). The vertical process of the palatine forms the anterolateral wall of the nasopharynx, contacting the presphenoid, basisphenoid, and probably the vomer dorsally, although sutural fusion in UF 191448 and UF 121742 and damage to UF 248500 make it difficult to determine the posterior extent of this part of the palatine.

Pterygoid

The pterygoid in cingulates is generally a small bone that forms the posteroventral margin of the orbit's medial wall, extending posteroventrally into a short pterygoid process or hamulus. It typically forms a somewhat larger portion of the posterolateral wall of the nasopharynx (Wible and Gaudin 2004). Although the sutures in this region of the skull are difficult to interpret in the various specimens of *H. floridanus*, it would appear the pterygoid bone occupies a similar position in this taxon. Its small, rectangular lateral surface contacts the alisphenoid dorsally and the maxilla (and perhaps the palatine) anteriorly (Figures 3, 4, 7). There is no contact between the pterygoid and squamosal bones, which is designated a derived feature of Cingulata by Gaudin and Wible (2006), though it is likely a primitive feature of eutherian

mammals (Novacek 1986; Wible et al. 2004; Wible et al. 2009). Therefore, among xenarthrans, the presence of a pterygoid/squamosal contact should be considered a derived feature of pilosans instead.

The pterygoid of *H. floridanus* forms a blunt, triangular, and quite rugose pterygoid process. This kind of blunt, rough, thickened pterygoid process is a synapomorphy of glyptodonts and pampatheres (Gaudin and Wible 2006). In *H. floridanus*, *H. occidentalis* (ROM 3881; Vizcaíno et al. 1998) and *Vassallia* (FMNH P 14424; the relevant area in *H. septentrionalis* is not preserved in the specimens we examined), the lateral surface of the pterygoid is covered with a variable number of rugose ridges, typically around six, which are slanted in a generally anterodorsal to posteroventral orientation. These ridges are also present in *Propalaeohoplophorus* (Scott 1903-4) although the pterygoid is much more dorsoventrally elongate in this genus. These ridges serve as an attachment point for the robust medial pterygoid muscle in these herbivorous cingulates. There are similar ridges on the lateral surface of the pterygoid of some sloths, although they are less densely packed and organized somewhat differently (Gaudin 2004, 2011). The pterygoid process is positioned lateral to the toothrow in ventral view (Figures 5, 6), which is also a synapomorphy of pampatheres and glyptodonts (Gaudin and Wible, 2006).

In ventral view, the pterygoid of UF 248500 forms an L-shaped exposure that contributes to the posterolateral corner of the hard palate, with a narrow portion comprising the pterygoid process/lateral exposure of the pterygoid extending anteroposteriorly, and a narrow transverse portion that extends medially (Figure 5B). A similar morphology is probably present in UF 121742, though the sutures are not always clear, whereas in some specimens (e.g., UF 191448, UF 223813, UF 275496) there is no evidence of a suture between the pterygoid process and

palatine, though we suspect that this is the result of fusion. A palatal exposure of the pterygoid is an unusual feature among cingulates (and among placental mammals in general; O'Leary et al., 2013), but is a synapomorphy of the dasypodine armadillos *Dasypus* and *Stegotherium* (Gaudin and Wible, 2006). At least the pterygoid process contribution to the palate may be more widespread among pampatheres and glyptodonts. Though it is not mentioned in De Iuliis and Edmund (2002), such a contribution is visible in *Vassallia* (FMNH P14424), and Guth illustrates a similar morphology in *Glyptodon* (Guth 1961, fig. 123).

The dorsal portion of the pterygoid in UF 248500, which normally forms much of the posterolateral wall of the nasopharynx in cingulates (Wible and Gaudin 2004), is strongly reduced, extending dorsally as a triangular wedge only a short distance. In UF 121742, the dorsal and medial exposure of the pterygoid appears larger, but still does not reach the roof of the nasopharynx. Because of suture closure, it is unclear whether the area dorsal to the pterygoid in the latter specimen is formed by palatine extending posterodorsally, or basisphenoid extending ventrally.

We have observed several unusual morphologies associated with the pterygoid region in individual specimens of *H. floridanus*. UF 121742 possesses two pterygoid processes - a large, more laterally situated process that is clearly homologous to the pterygoid process of the other *H. floridanus* specimens and other cingulates, and a smaller, more medially situated process extending posteriorly from the back margin of the hard palate. The presence of two pterygoid processes or crests, an entopterygoid process/crest and an ectopterygoid process/crest, is a feature that is widely observed among primitive eutherians [e.g., *Zalambdalestes* (Wible et al., 2004); *Leptacris* (Novacek, 1986)] and many extant placental mammals [e.g., *Atelerix* (UTCM 727, 1553; Frost et al., 1991); *Tupaia* (UTCM 1980; Wible 2011); *Elephantulus* (UTCM 1482,

1512)]. The ectopterygoid process/crest is typically formed mostly by the alisphenoid, so for those taxa with a single pterygoid process or hamulus formed by the pterygoid, it is generally homologized with the entopterygoid process/crest, as has been done for the armadillo *Euphractus* by Wible and Gaudin (2004). If the lateral pterygoid process of UF 121742 is indeed the entopterygoid process, as seems almost certain, then the more medial process represents a neomorph. We suspect this process represents an attachment point for enlarged pharyngeal or masticatory muscles. If the muscular anatomy of *Canis* (Evans and Christiansen, 1979) can be used as a model, the pterygopharygeus seems a likely candidate.

In UF 191448, there is an unusual, vertical mass of cancellous pneumatized bone that lies at the junction between the medial wall of the orbit and the lateral wall of the choanae. This mass may be part of the pterygoid, due to its position in the skull, and the fact that it has a small palatal exposure along the posterior margin of the palate that appears to match the medial, transverse portion of the pterygoid palatal exposure in UF 248500 and other *H. floridanus* specimens. On the other hand, this mass appears to be completely surrounded by sutures (including the palatal exposure), which would suggest that it too is a neomorphic feature. Pneumatization of the pterygoid is rare among cingulates. However, it is commonplace among pilosans, where inflated, often bullate pterygoids are known among myrmecophagid anteaters, *Megalocnus*, *Mylodon*, some nothrotheriid sloths, the three-toed sloth *Bradypus torquatus*, and the two-toed sloth genus *Choloepus* (Stock 1925; Guth 1961; Patterson et al. 1992; Gaudin 2004; De Iuliis et al. 2011). This separate pneumatized mass of bone is only present in UF 191448, but other *H. floridanus* specimens did display pneumatized bone around the posteromedial edge of the choanae. This mass of bone in UF 191448 forms a discrete suture with the palatine and

basisphenoid anteriorly and dorsally, the palatine anteriorly and ventrally, and the pterygoid and alisphenoid bones laterally.

Lacrima

The lacrima is shaped roughly like a parallelogram, with its long axis tilted anterodorsally (Figures 3, 4). It contacts the maxilla anteriorly and posteroventrally, the frontal posterodorsally, and the jugal ventrally. The lacrima consists of a facial and orbital process; the boundary between these two processes is not particularly distinct. In Wible and Gaudin (2004), the low ridge that runs from the postorbital process of the frontal ventrally onto the jugal, the antorbital ridge, was used as a rough boundary between the facial and orbital processes. The antorbital ridge exhibits some variation in its development among *H. floridanus* specimens. The position of the lacrima foramen also varies among pampatheres. In the majority of pampathere specimens examined in this study, the lacrima foramen is located on the antorbital ridge, that is, on the boundary between the facial and orbital processes, as it is in *Proeutatus* (FMNH P13199) and *Euphractus* (Wible and Gaudin 2004). In *H. septentrionalis* (UF 889, 243224) and *Vassallia* (P 14424), however, the lacrima foramen is located anterior to the antorbital ridge; therefore, it is clearly situated on the facial process. This is apparently also the condition in primitive glyptodonts (Scott 1903-4). In *Euphractus*, *Proeutatus*, and most of the pampatheres and glyptodonts examined, the lacrima foramen is relatively small. However, in *H. septentrionalis* (UF 889) the lacrima foramen is situated within a much larger, circular depression. A similar, but more dorsoventrally ovate depression appears to be present in *H. septentrionalis* (UF 243224), as well as in *Propalaeohoplophorus* (YPM-PU 15007), although in this specimen the depression opens posteriorly. Just dorsal to the lacrima foramen is a rugose area, the lacrima tubercle. In UF 191448, the tubercle is small, and continuous with a crest that extends ventrally

onto the zygoma anterior to the lacrimal foramen (Wible and Gaudin 2004). The lacrimal tubercle is much larger in UF 248500, and contacts not only this anterior crest, but the antorbital ridge as well. A lacrimal tubercle is present in all cingulates, with the exception of *Dasypus* and *Stegotherium* (Gaudin and Wible 2006), and is distinct from the rest of the lacrimal surface, which is generally smooth.

The facial process of the lacrimal bone in *H. floridanus* (UF 191448, et al.), and other pampatheres (*H. occidentalis*; *Vassallia*), is typically triangular in shape (Figures 3, 4). The shape is more variable in *H. septentrionalis*. In UF 889, it is triangular as in other pampatheres, but the anterodorsal apex of the triangle is elongated with a rounded tip, whereas in UF 234224 the facial process is more ovate than triangular, elongated dorsoventrally. *Euphractus* has a quadrangular facial process (Wible and Gaudin 2004; Gaudin and Wible 2006). According to Gaudin and Wible (2006), a quadrangular facial process is a synapomorphy of the clade including *Eutatus*, euphractine armadillos, *Proeutatus*, glyptodonts, and pampatheres (Node B), although the latter revert to the triangular shape characteristic of dasypodine and tolypeutine armadillos.

The orbital process of the lacrimal bone in *H. floridanus* is also triangular, but it is somewhat smaller than the facial process. The lacrimal contributes to a small portion of the anterior orbital wall, where it contacts the jugal anterolaterally, and the frontal posteriorly. There is also a small lacrimal contact with the maxilla posteroventrally, on the orbital side of the jugal in *H. floridanus* (UF 191448, 248500), as in *Euphractus* (UTCM 1486, 1491; Wible and Gaudin 2004). This trait, the presence of lacrimal contact with the orbital process of the maxilla, is a synapomorphy of *Tolypeutes*, *Eutatus*, euphractine armadillos, *Proeutatus*, pampatheres, and glyptodonts (Node 4, Gaudin and Wible 2006). The lacrimal fenestra, which perforates the lower

edge of the orbital process of the lacrimal, serves as the site of origin for the inferior oblique muscle, and is present at the intersection of the lacrimal, frontal, and maxilla in *H. floridanus* (Gaudin and Wible 2006; Wible and Gaudin 2004). This condition is primitive, and occurs in all cingulates with the exception of *Dasypus*, *Stegotherium*, *Zaedyus*, and *Chlamyphorus* (Gaudin and Wible 2006).

Jugal

The jugal forms the anterior portion of the zygomatic arch. In *H. floridanus* (UF 248500, UF 191448) the dorsal edge of the jugal is U-shaped, whereas the ventral edge is irregular (Figures 3, 4). The jugal can be divided into two processes, facial and zygomatic. Roughly half of the anterior root of the zygoma is comprised of the transversely broad facial process of the jugal bone, which contacts the lacrimal dorsally, the maxilla anteriorly, ventrally, and medially. The zygomatic process is oriented almost perpendicular to the facial process, and is strongly compressed mediolaterally and deep dorsoventrally. It has a dorsoventrally convex surface laterally, and is concave medially. In lateral view it broadens posteriorly toward its posterior contact with the squamosal, near the middle of the zygomatic arch. The jugal-squamosal suture in UF 248500 is asymmetrically concave posteriorly, with the anterodorsally oriented ventral portion more elongate than posterodorsally sloped dorsal portion (Figure 3B, C). In UF 191448, the junction between these dorsal and ventral portions is more angular (Figure 3A). In UF 248500, the posterodorsal edge of the zygomatic process is extended into a sharp, triangular postorbital process. In UF 191448, the postorbital process is more rounded, and formed jointly by the jugal and squamosal. The jugal/squamosal contact in *H. occidentalis* (ROM 3881) and *Vassallia* (De Iuliis and Edmund 2002) shows a similar pattern, though in the latter the

postorbital process is carried largely by the squamosal rather than the jugal. In contrast to the pampathere condition, in both *Propalaeohoplophorus* and *Proeutatus* (Scott 1903-4) there is a substantial posterior extension of the jugal underneath the zygomatic process of the squamosal, so that much of the jugal/squamosal suture is horizontal, as in euphractine armadillos (Wetzel 1985; Wible and Gaudin 2004). The postorbital process on the zygomatic arch is also less well developed in *Euphractus* (but not *Chaetophractus* or *Zaedyus*; Wetzel 1985; Wible and Gaudin 2004), *Proeutatus* (FMNH 13197; Scott 1903-4), and some specimens of *Propalaeohoplophorus* (e.g., FMNH P13205; *P. australis*, Scott 1903-4 plate 23; but not YPM-PU 15007 or *P. minor*, Scott 1903-4 plate 27).

The facial process extends ventrally and slightly laterally into a prominent ventral (or descending) process of the zygomatic arch. This ventral process is in fact an anteromedial to posterolaterally extended, cresecent-shaped complex, comprised of a variable number of strong rugose bumps or transverse ridges. In UF 248500, there are only two bumps/ridges (Figure 3B), with the more anterior being formed in part by the jugal and in part by the maxilla. In other specimens, there may be as many as four (e.g., UF 275498, 285000 on L only). In some specimens, this ventral zygomatic process (or complex of processes) appears worn, although it is unclear if this is reflective of the age of the specimen (they do seem less “worn” in juvenile specimens) or due to some sort of post-mortem abrasion.

Holmesina occidentalis and *Vassallia* have ventral zygomatic processes quite similar to those in *H. floridanus*, with three bumps or ridges that are heavily worn in the *Vassallia* specimen [FMNH P14424; De Iuliis and Edmund (2002), who also report a similar morphology in *Pampatherium*; Vizcaino et al. (1998: p. 297-298) note that the ventral process is “narrower and less rugose” in *H. occidentalis* than in *Vassallia*]. The ventral zygomatic process of

pamphateres is comparable in position to the small boss present in *Euphractus* (Wible and Gaudin 2004; Gaudin and Wible 2006) and *Proeutatus* (FMNH P13197; Gaudin and Wible 2006), but is much larger in size. *Propalaeohoplophorus* and other glyptodonts possess a gigantic descending process (Hoffstetter 1958; Gaudin and Wible 2006) that forms a greatly elongated, anteroposteriorly compressed plate of bone, but unlike *Holmesina*, this process is primarily formed by the maxilla (YPM-PU 15007; Gillette and Ray 1981), the jugal forming only a small portion of the dorsolateral margin. This descending process is greatly enlarged in order to accommodate the bulky masseter muscle in glyptodonts (Gillette and Ray 1981), and this is likely the case in pamphateres, though the masseter would have been enlarged to a lesser degree.

Frontal

The frontal ~~bone~~ in *H. floridanus* forms slightly less than a third of the total skull length, including the anterior half of the braincase. It is shaped roughly like a pentagon in dorsal view, broadening dramatically in its anterior reaches (Figures 1, 2). This is due to the presence of enlarged sinuses beneath the frontal bone, a feature present in many other cingulates (Gaudin and Wible 2006). The frontal bone contacts the nasal, maxilla, and lacrimal bones anteriorly and the parietal posteriorly on the skull roof. It dips ventrally and laterally into the orbit to form a sizeable portion of the medial orbital wall (Figures 3, 4, 7). The orbital portion of the frontal likely contacts the maxilla, orbitosphenoid and alisphenoid ventrally, and the squamosal posteroventrally, creating a triangular exposure in lateral view that is similar to that of *Euphractus* (UTCM 1491; Wible and Gaudin 2006). The fronto-parietal suture is a very irregular and jagged line that travels slightly anterodorsally across the top of the braincase from a position

even with the anterior edge of the glenoid fossa, as in *Proeuphractus*, *Proeutatus*, other pampatheres, and glyptodonts (Node E; Gaudin and Wible 2006). This differs from *Euphractus* in which the most lateral part of fronto-parietal suture lies posterior to the anterior edge of the glenoid fossa (Wible and Gaudin 2004; Gaudin and Wible 2006).

The frontal bone in *H. floridanus* has very distinct temporal lines curving posteromedially from the large, blunt postorbital processes (Figures 1, 2). The posterior half of the fused interfrontal suture is elevated by a prominent midline crest in UF 248500, that extends unbroken between the temporal lines back along the midline of the parietal, all the way to the nuchal crest. A ridge of similar extent is present in UF 191448, but it is much more weakly developed. Wible and Gaudin (2004) describe a weakly developed crest in a similar position in *Euphractus*, where it serves as a site of origin for the orbito-auricularis muscle. The crest is also present in *H. occidentalis* and *Proeutatus* (FMNH P1319; Scott 1903-4). It is present on the frontal only in *H. septentrionalis* (UF 889) and *Vassallia* (FMNH P14424), being replaced posteriorly by a true sagittal crest. It is missing entirely in *Propalaeohoplophorus*, where again there is a strong sagittal crest (FMNH P13205; YPM-PU 15007; Scott 1903-4). It is likely that the presence of a strong ridge in this position is related to the presence of large pinnae for the ears.

As is typical of euphractine armadillos, *Proeutatus*, pampatheres and glyptodonts, there are numerous small foramina in UF 191448 that coalesce around the midline of the frontal dorsally, just anterior to the frontal-parietal suture, in a depression between the temporal lines and behind the frontal sinuses (Node C, Gaudin and Wible 2006). These foramina are less evident in UF 248500. In lateral view, within the temporal fossa, there are also foramina along the posterolateral region of the frontal bone in eutatine armadillos, euphractine armadillos,

Proeutatus, *Vassallia* and glyptodonts (Node A; Gaudin and Wible 2006). These appear to be absent in *H. floridanus*, though they are present in *H. occidentalis* (ROM 3881).

In addition to these foramina, the frontal is marked by two other types of foramina within the orbit (Figure 7). UF 191448 has a pair of asymmetrical foramina for the frontal diploic vein (sensu Wible and Gaudin 2004; =supraorbital foramina of Gaudin 2004 and others). On the left, there is a single opening situated ventral and posterior to the broad, low, rugose area that marks the postorbital process. On the right, there are two foramina, one mirroring the opening on the left, the other, smaller opening situated further anterior and dorsal, virtually on the process itself. The left side of UF 248500 is damaged in the region of the postorbital process, but the right side has a single foramen like that described for UF 191448. In UF 121742, the foramen is more anteriorly situated, lying in front of a strong infratemporal crest that extends posteroventrally from the postorbital process, a crest that is only weakly developed in UF 191448. The morphology of UF 121742 is also found in *H. septentrionalis* (UF 889, UF 234224) and *Vassallia* (UF P14424). The foramen for the frontal diploic vein also occurs in a similar position in glyptodonts (Gaudin 2004), whereas in *Proeutatus* it is situated more posteriorly (FMNH P13197).

The ventral portion of the orbital wing in UF 121742 is marked by a ventrally directed foramen that lies between the infratemporal crest and a rounded ridge that marks the dorsal margin of the optic foramen. Given the position of this opening, anterodorsal to the optic foramen, and its orientation, we identify it as the ethmoid foramen (sensu Wible and Gaudin 2004). Other cingulates may have as many as three ethmoid foramina (Gaudin and Wible 2006). Although sutures are not unambiguous in this area, the opening appears to be contained entirely within the frontal, in contrast to some cingulates in which there is orbitosphenoid participation in

the rim (Gaudin and Wible 2006). In UF 248500, there appears to be a second ethmoid foramen, just dorsal to the first and separated from it by the infratemporal crest.

Parietal

The parietal bone is roughly rectangular and forms the posterior half of the braincase (Figures 1-4). It contacts the frontal anteriorly, the squamosal ventrolaterally, and the supraoccipital posteriorly. As in most cingulates, with the exception of *Peltephilus*, there is no contact between the parietal and the alisphenoid bones (Figure 7) due to an extensive contact between the frontal and squamosal bones (Node 2; Gaudin and Wible 2006; see also Novacek and Wyss 1986; Rose and Emry 1993; Gaudin et al. 1996). Although the parietal tends to be relatively flat transversely in eutatine and euphractine armadillos and in glyptodonts (Gaudin and Wible 2006), in *H. floridanus* and other pampatheres (Cartelle and Bohórquez 1985; De Iuliis et al. 2000; De Iuliis and Edmund 2002) it is strongly convex transversely, giving the braincase a much more tubular appearance. The parietals are marked by strong temporal lines, which approach one another, but do not unite to form a midline sagittal crest. As noted above in the description of the frontal, the parietals do carry a midline crest for the extrinsic ear muscles between the temporal lines. This morphology, which also characterizes *H. occidentalis* (ROM 3881), is very reminiscent of the pattern in *Proeutatus* (FMNH 13197; Scott 1903-4) and some specimens of *Euphractus* (Wible and Gaudin 2004). A true sagittal crest is present on the parietals in *H. septentrionalis* (UF 889), *Vassallia* (De Iuliis and Edmund 2002), and *Propalaeohoplophorus* (Scott 1903-4) and other glyptodonts (Gillette and Ray, 1981), as noted above. Both the temporal lines and the midline crest unite posteriorly with a robust nuchal crest. The nuchal crest is of uniform thickness along the posterior edge of the skull, as is characteristic

of *Tolypeutes*, eutatine armadillos, euphractine armadillos, *Proeutatus*, pampatheres, and glyptodonts (Node 5; Gaudin and Wible 2006). It is strongly convex posteriorly, overhanging the dorsal portion of the occiput.

Within the temporal fossa in *H. floridanus*, the parietal surface is heavily pitted with a large but variable number of foramina (12-16 in UF 191448 and 248500), especially in the ventrolateral half of the bone. The more dorsally located foramina open into distinct grooves, traveling at various angles, through which the rami temporales emerge. The presence of so many temporal foramina (greater than 5) is a synapomorphy of *Priodontes*, *Tolypeutes*, eutatine armadillos, euphractine armadillos, *Proeutatus*, pampatheres, and glyptodonts (Node 3; Gaudin and Wible 2006).

Squamosal

The squamosal consists of two broad regions, the squamous part and the zygomatic process (Figures 1-7). The squamous part comprises a roughly rectangular, vertical exposure in the lateral wall of the braincase, contacting the frontal anteriorly, the alisphenoid and petrosal ventrally, and the parietal dorsally. It also has a lappet that wraps around the nuchal crest to form a small, triangular exposure on the occiput, contacting the occipital exposure of the mastoid petrosal ventrally, and the supraoccipital dorsally. *Euphractus* has a very similar occipital exposure of the squamosal (Wible and Gaudin 2004), and according to Gaudin and Wible (2006), this feature is a synapomorphy of euphractine armadillos, pampatheres and glyptodonts (Node C of Gaudin and Wible 2006). The anterior portions of the squamosal/ parietal suture and the dorsal portions of the squamosal/frontal suture form a slightly raised ridge, as they do in some *Euphractus* (Wible and Gaudin 2004) and in *Vassallia* (De Iuliis and Edmund 2002) and

Propalaeohoplophorus (YPM-PU 15007). Like the parietal, the squamous region's posterior and dorsal surface is marked by a variable number (5-12 in UF 191448 and UF 248500) of foramina for the rami temporales. This is a common feature in cingulates. The squamous part of the squamosal is crossed horizontally by a crest that connects dorsal edge of the zygomatic process to the nuchal crest, marking the lower limit of the temporal fossa (Figures 3, 4). This is also a feature in *H. occidentalis* (ROM 3881) and *H. septentrionalis* (UF 234224), as well as *Proeutatus* (FMNH P13197) and *Propalaeohoplophorus* (YPM-PU 15007; Scott 1903-4), whereas in *Vassallia* (De Iuliis and Edmund 2002) the ventral end of the nuchal crest passes lateral to the crest extending posteriorly from the dorsal edge of the zygoma, so that the two approach but do not contact. The latter is similar to the condition in *Euphractus* (Wible and Gaudin 2004).

The region of the squamosal immediately ventral to the lower ridge of the temporal fossa is strongly convex anteroposteriorly, forming a porus acousticus that would have accommodated the external auditory meatus. The posterior wall of the porus is formed by a flat, roughly ovate ventral projection that abuts the anterior base of the petrosal's paroccipital process (=mastoid process of Patterson et al. 1989; Gaudin 1995). This projection is the posttympanic process of the squamosal (Figure 7). In UF 191448, it has a somewhat thickened ventral edge that may have participated in the facet for the posterior crus of the ectotympanic. The lower anterior wall of the porus is formed by a freestanding ridge, the postglenoid process (Figure 8). As in *Euphractus* (Wible and Gaudin 2004) and a few other eutherians (e.g., *Zalambdalestes*, Wible et al. 2004), the postglenoid process lies posterior to the postglenoid foramen in *H. floridanus*. The postglenoid process and posttympanic process approach one another medially at roughly a 60°-75° angle in ventral view (it is more acute in UF 248500 than in UF 191448), with the porus

narrowing accordingly (Figures 6, 8). The morphology of this region of the skull in *Vassallia* (FMNH P14424) is very similar to that of *H. floridanus*. *Propalaeohoplophorus* (YPM-PU 15007) is also similar, though the porus is narrower, with a much more acute angle ($< 20^\circ$) between the postglenoid and posttympanic process, and the former is much larger than it is in *H. floridanus*. *Proeutatus* (FMNH P13197) has a very odd morphology in this region of the skull. The glenoid is situated so far posteriorly that it approaches the ventral end of the nuchal crest. As a consequence, the porus acousticus is reduced to a narrow vertical groove, and the process identified as the posttympanic process by Patterson et al. (1989) is actually two processes, the posttympanic process and the immediately adjacent postglenoid process (the two distinct tips of these processes are visible in the lateral view of the skull in Patterson et al. 1989, fig. 13A). In *H. floridanus* 191448, there is a bilateral foramen just lateral and dorsal to the anterior end of the postglenoid process. This is likely homologous to the suprimeatal foramen found in some *Euphractus* specimens (Wible and Gaudin 2004). Like *Euphractus*, the presence of this foramen may be variable in *Holmesina*, because it is absent in UF 248500 and UF 121742.

Anterior and medial to the postglenoid process is a small, circular depression that represents the squamosal contribution to the epitympanic recess, accommodating the mallear/incudal articulation. The squamosal forms roughly 2/3 of this depression, the remainder formed by the lateral reaches of the petrosal. In *Propalaeohoplophorus* (YPM-PU 15007), the epitympanic recess is ovate rather than circular, elongated along a posterolateral to anteromedial axis.

Anterior and medial to the epitympanic recess is a massive process that extends as a broad ridge laterally and ventrally, forming the anterolateral wall to the tympanic cavity. This is the entoglenoid process, which extends across the squamosal/alispheoid suture and onto the

alisphenoid behind the foramen ovale (Figure 8). The posterior surface of this process is marked by a circular depression that almost certainly represents the facet for the anterior crus of the ectotympanic. At its posterior, dorsal and medial extremity, the entoglenoid process abuts the small anteroventral process of the tegmen tympani on the petrosal (=processus crista facialis of Patterson et al. 1989; Gaudin 1995; Wible and Gaudin 2004), which may have a small contribution to the ectotympanic facet. A similar entoglenoid process is present in *Vassallia* (FMNH P14424), *Propalaeohoplophorus* (YPM-PU 15007), and *Proeutatus* (FMNH P13197). In the latter two, it appears to be somewhat inflated.

In ventral view, the root of the zygomatic process is triangular, extending (and narrowing) laterally, as it does in all pampatheres and glyptodonts (Node 8, Gaudin and Wible 2006). Its dorsal surface is deeply concave transversely to house the temporalis muscles. On its ventral surface, it carries the glenoid articulation for the mandible. Just beyond the lateral edge of the glenoid, the process curves anteriorly in a graceful arc. In lateral view, it deepens considerably in a dorsoventral plane as it approaches its anterior contact with the jugal, with which it forms the zygomatic arch. As noted above, it may or may not contribute to the postorbital process on the zygoma. *Propalaeohoplophorus* (Scott 1903-4), *Proeutatus* (Scott 1903-4), and *Euphractus* (Wible and Gaudin 2004) and other euphractine armadillos (Wetzel 1985) all lack the anterior broadening of the zygomatic process seen in pampatheres (Cartelle and Bohórquez 1985; De Iuliis et al. 2000; De Iuliis and Edmund 2002). Like the zygomatic portions of the jugal, the zygomatic region of the squamosal is convex laterally and concave medially.

The glenoid articular surface on the ventral side of the zygomatic root is convex in both transverse and anteroposterior planes, as it is in most eutatine and euphractine armadillos and in

glyptodonts and other pampatheres (Node B, Gaudin and Wible 2004; Vizcaíno et al. 1998). Its shape is somewhat more unusual however, forming a rounded triangle, narrowing laterally, with its transverse width much greater than its anteroposterior length (Tables 1, 2). Glyptodonts show similar transverse extension of the glenoid, though the shape of the facet is generally more rectangular and even narrower anteroposteriorly (Scott 1903-4; Gaudin 2004; Gaudin and Wible 2006), whereas in eutatine and euphractine armadillos the glenoid is more U-shaped, and as long or longer in the anteroposterior as opposed to the transverse dimension (Gaudin and Wible 2006). As in other cingulates, there is a postglenoid foramen in *H. floridanus*. Like other pampatheres and glyptodonts, this foramen is clearly visible in ventral view (Figures 6, 8), because the external auditory meatus is positioned well behind the glenoid, exposing the postglenoid fossa in which the foramen is situated (Gaudin and Wible 2006). In euphractine and eutatine armadillos this area tends to be obscured by the nearby ectotympanic.

Petrosal

The petrosal bone is preserved in situ in UF 191448 and on the right side of UF 248500 (Figures 6, 8), whereas a nearly complete, isolated left petrosal is available in the latter specimen (Figure 9). This will allow us to describe in detail not only the ventral exposure of the bone, but also its dorsal and lateral surfaces. The petrosal, which houses the inner ear, is bordered by the squamosal laterally, the exoccipital posteromedially, the supraoccipital dorsally, and the basioccipital and basisphenoid medially. It is comprised of two primary regions, the pars canicularis housing the semicircular canals and vestibular apparatus, and the pars cochlearis housing the cochlea (MacIntyre 1972). In ventral and lateral view, these are represented most notably by the mastoid region and promontorium, respectively.

The promontorium of *H. floridanus* is globose, and lacks any clear grooves for arteries or nerves, as is typical for cingulates (Guth 1961; Bugge 1979; Patterson et al. 1989; Wible and Gaudin 2004; Wible 2010). At its anterior pole, it is marked by a distinctive, elongate triangular process, the rostral tympanic process of the petrosal (Figures 6, 8, 9). Wible (2010) describes a small blunt rostral tympanic process that is present to a varying degree in some *Dasypus novemcinctus*, but no such process is present in *Euphractus* (Wible and Gaudin 2004). In *Vassallia*, *Propalaeohoplophorus* and other glyptodonts, and *Proeutatus* (Guth 1961; Patterson et al. 1989), the entire promontorium is elongated anteromedially, giving the promontorium a teardrop shape in ventral view. It seems likely that the anteromedial elongation of the promontorium in the pampathere/glyptodont/*Proeutatus* clade is homologous to the rostral tympanic process in *Holmesina*, with the process in *Holmesina* being substantially reduced in length and breadth. The anterolateral surface of the promontorium in UF 248500 is marked by a large, slightly raised circular boss of unclear function. This feature is also present in UF 223813, but is less clear in UF 191448, and is not at all evident in *Vassallia* (FMNH P14424).

Extensive shelving surrounds the promontorium of *H. floridanus* in ventral view. This includes not only the lateral facial sulcus and crista parotica typical of mammalian petrosals (MacIntyre 1972; Wible et al. 2009), but also an extensive epitympanic wing anteriorly and a medial flange medially (Figure 9A-D). The epitympanic wing is separated by a sizable gap from the underlying rostral tympanic process. In its anterolateral corner, it carries a fossa, particularly well developed in UF 191448 (also UF 223813, 275496), which likely served as the site of origin for the tensor tympani muscle. A small epitympanic wing is present in *Dasypus* (Wible 2010), but is much better developed in *Euphractus* (Wible and Gaudin 2004). An epitympanic wing is also present in *Vassallia* (FMNH P14424), though it is somewhat less extensive anteriorly. Like

904 *Holmesina*, there is a depression between it and the anteromedial extension of the promontorium.
 905 The epitympanic wing is evidently absent in *Proeutatus* (Patterson et al. 1989) and
 906 *Propalaeohoplophorus* (YPM-PU 15007; FMNH P13205). The tensor tympani muscle appears
 907 to originate on the epitympanic wing in *Vassallia* (FMNH P14424) as in *Holmesina*, whereas in
 908 *Dasypus* (Wible 2010) and *Euphractus* (Wible and Gaudin 2004) it attaches to the tegmen
 909 tympani, and it likely originated on the anterolateral surface of the promontorium in *Proeutatus*
 910 (Patterson et al. 1989) and *Propalaeohoplophorus* (YPM-PU 15007; FMNH P13205).

911 The medial flange of the petrosal in *H. floridanus* is quite extensive both transversely and
 912 anteroposteriorly (especially in juvenile specimen UF 275496) when compared to that of
 913 *Dasypus* (Wible 2010). In contrast to the latter, it extends as far forward as the epitympanic
 914 wing, creating a squared off anterior edge for the petrosal, and it is covered by a variety of pits
 915 and low ridges. The most prominent of these is a pit that is situated at roughly the midpoint of
 916 the medial flange, which serves as a point of attachment for the basioccipital (Figure 9A-D). In
 917 *Dasypus*, a patent basicochlear fissure is maintained into adulthood, so that there is no medial
 918 connection between the petrosal and the floor of the basicranium (Wible 2010). Immediately
 919 behind this basioccipital facet is a prominent foramen, the cochlear canaliculus (for the
 920 perilymphatic duct –see Clemente 1985; Evans and Christiansen 1979; Wible 2010). The medial
 921 flange in *H. floridanus* also differs from that of *Dasypus* in that it extends posteriorly beyond the
 922 cochlear canaliculus, reaching the region termed the “triangular shelf” in *Dasypus* (Wible 2010),
 923 that is, the roof of the post-promontorial sinus. In so doing it forms a shallow jugular notch, i.e.,
 924 the anteromedial edge to the jugular foramen. The medial flange of the petrosal is difficult to
 925 observe in *Vassallia*, *Propalaeohoplophorus*, *Proeutatus*, and even the extant *Euphractus*,
 926 because of the lack of preserved, isolated petrosals in these taxa. However, it is clear the latter

has an extensive contact between petrosal and basicranium, whereas only a small basioccipital/petrosal contact is present in *Vassallia* (FMNH P14424) and *Proeutatus* (FMNH P13197), as in *Holmesina*.

Holmesina floridanus has three prominent foramina in the ventral exposure of the pars cochlearis. The most anterior of these is the laterally directed primary facial foramen, which is hidden in ventral view by a low ridge at the base of the promontorium, and in lateral view by the anteroventral process of the tegmen tympani. In some *Dasypus* (as in most therians – Wible 1990, 2003), the space immediately lateral to the primary facial foramen, the cavum supracochleare, has a bony floor, creating a discrete hiatus Fallopii and secondary facial foramen anterior and posterior to the cavum, respectively (Wible 2010). This floor is not present in any *Holmesina floridanus* specimen, nor is it known to occur in *Euphractus* (Wible and Gaudin 2004), *Proeutatus* (FMNH P13197), *Vassallia* (FMNH P14424), or any glyptodont (e.g., *Propalaeohoplophorus*, YPM-PU 15007, FMNH P13205; see also Patterson et al. 1989).


The second foramen in the ventral pars cochlearis is a larger, laterally directed opening posterior to the primary facial foramen, the fenestra vestibuli, which accommodates the footplate of the stapes (Figure 9A-F). As in *Dasypus* and *Euphractus* (Wible and Gaudin 2004; Wible 2010), the opening of the fenestra vestibuli is somewhat recessed, and surrounded by a narrow rim of bone. The opening is rounder in *H. floridanus* than in the extant forms, with a stapedial ratio (sensu Segall, 1970; Length/width) of ~1.4, whereas it is 1.9 in *Dasypus* and 1.9-2.0 in *Euphractus*. *Proeutatus* (FMNH P13197) and *Propalaeohoplophorus* (FMNH P13205) also resemble the living taxa in this regard, with ratios of 2.4 and 1.8 respectively.

The third opening in the pars cochlearis' ventral surface is a posteriorly directed foramen separated from the rim of the fenestra vestibuli by a broad bar of bone, the crista interfenestralis,


This opening is generally called the fenestra cochleae (we follow Patterson et al. 1992; Gaudin 1995; Wible and Gaudin 2004 in using this widely recognized term), although, as Wible (2010) points out, the latter is actually a separate hole recessed within the cochlear fossula, and this more superficial, posteriorly facing foramen is actually the aperture of the cochlear fossula. The “fenestra cochleae” of *H. floridanus* is unusual in several respects. First, it is very wide and low, with a ratio of width to depth equal to approximately 3.4. In *Dasypus* (Wible 2010) and *Propalaeohoplophorus* (FMNH P13205), the ratio is closer to 2, whereas in *Euphractus* (UTCM 1491) and *Proeutatus* (FMNH P13197, P13199) the ratio is between 1.0—1.2. Although we could not obtain measurements for *Vassallia*, it appears similar in dimensions to *Holmesina*. The fenestra cochleae is also unusual in *Holmesina* in that it is shielded in ventral view by a prominent ridge, and, in UF 191448, it is divided by a ventral process into two separate openings. Neither feature is known to occur in other cingulates.

The crista interfenestralis, between the fenestrae vestibuli and cochleae, also exhibits unusual characteristics in *H. floridanus*. For one, it is quite broad, its maximum width clearly exceeding the maximum diameters of either of the openings flanking it. This is a feature that also occurs in *Vassallia* (FMNH P14424), but not in extant armadillos (Wible and Gaudin 2004; Wible 2010), *Proeutatus* (FMNH P13197, 13199), or *Propalaeohoplophorus* (YPM-PU 15007, FMNH P13205). In addition, the crista is connected laterally by a bony bridge to the base of the tympanohyal, the bridge forming a partial floor to the facial sulcus. This bridge is broken in most specimens of *H. floridanus*, as it is in the isolated left petrosal of UF 248500 (Figure 9A, B), but is intact on the right side of that specimen (Figure 8), as well as in UF 275496. This appears to be a unique apomorphy of *Holmesina*, although there are low ridges on the crista

972 interfenestralis of *Vassallia* (FMNH P14424), and low tubera in *Euphractus* (UTCM 1491) and
973 *Proeutatus* (FMNH P13197).

974 There is a narrow elongate groove that runs lateral to the promontorium along its entire
975 length (Figure 9 C, D). Anterior to the primary facial foramen, this groove accommodates the
976 greater petrosal ne  The portion posterior to the primary facial foramen is the facial sulcus for
977 the facial nerve (c.n. VII). The sulci are bordered laterally by a well-developed, sharp edge crista
978 parotica. The latter forms a rounded, U-shaped ventral extension immediately opposite the
979 primary facial foramen. This extension is somewhat rugose and broadened mediolaterally
980 relative to the rest of the crista, and likely represents the anteroventral process of the tegmen
981 tympani (Figure 9 C-F). The anteroventral process, which is termed the processus crista facialis
982 by Patterson et al. (1989) and others (e.g., Gaudin, 1995; Wible and Gaudin 2004), is much
983 better developed in extant armadillos, where it typically forms a mediolaterally expanded, cup-
984 shaped depression (Patterson et al. 1989; Wible and Gaudin 2004; Wible 2010). It may also
985 contact the squamosal, malleus, ectotympanic, entotympanic or alisphenoid bones in living
986 armadillos (Wible and Gaudin 2004; Wible 2010), whereas in *H. floridanus* it is much reduced,
987 and only contacts the squamosal. The anteroventral process is also small in *Vassallia* (FMNH
988 P14424), *Proeutatus* (FMNH P13197), and *Propalaeohoplophorus* (FMNH P13205), lacking
989 any concavity and contacting only the squamosal.

990 Just posterior to the fenestra vestibuli, the facial sulcus traverses the ventral surface of the
991 petrosal pars cochlearis, becoming confluent medially with a large, ovate depression, the
992 stapedius fossa for the stapedius muscle (Figure 9 C, D). The sulcus then turns laterally and
993 ventrally, terminating at a shallow stylomastoid notch in the isolated left petrosal of UF 248500.
994 However, on the right, the facial sulcus passes posterior to the tympanohyal, which abuts the

995 large caudal tympanic process of the petrosal posteriorly, enclosing a stylomastoid foramen for
 996 the emerging facial nerve (Figure 8). An enclosed stylomastoid foramen is also present in
 997 *Dasypus* (Wible 2010) and *Euphractus* (Wible and Gaudin 2004). Patterson et al. (1989, fig.
 998 15B) illustrate a very similar morphology for *Vassallia*, though our inspection of their specimen
 999 (FMNH P14424) reveals the tympanohyal has subsequently broken off. An enclosed
 1000 stylomastoid foramen is lacking, however, in both *Proeutatus* and *Propalaeohoplophorus*, where
 1001 the tympanohyal and the paroccipital and caudal tympanic processes of the petrosal frame only
 1002  3 or $\frac{3}{4}$ of an opening. The tympanohyal of UF 248500 is broken through its base on the left,
 1003 at the posterior terminus of the crista parotica, but on the right it is straight, elongated ventrally
 1004 and expanded distally, forming a concave, ovate stylohyal fossa similar to, but much smaller and
 1005 simpler than the structure of the same name so characteristic of sloths (Patterson et al., 1992;
 1006 Gaudin 1995, 2004). A similar anatomy was apparently present in *Vassallia* (Patterson et al.,
 1007 1989; though, as noted above, the tympanohyal in this specimen is now broken), but not in
 1008 *Dasypus* (Wible 2010), *Proeutatus* (FMNH P13197, P13199) or *Propalaeohoplophorus* (YPM-
 1009 PU 15007, FMNH P13205). In *Euphractus* (Wible and Gaudin 2004), the circular depression
 1010 that Wible and Gaudin (2004) label a stylohyal fossa has a small tympanohyal exposure in its
 1011 center, but is formed largely by the ectotympanic anteriorly, and the mastoid region of the
 1012 petrosal posteriorly and laterally. The tympanohyal is typically not straight in other cingulates,
 1013 as it is in *Holmesina*. It curves medially and posteriorly at its distal end in *Dasypus* (Wible
 1014 2010) and *Proeutatus* (Patterson et al. 1989, figure 13C), it is posteroventrally directed in
 1015 *Euphractus* (Wible and Gaudin 2004), and it bends laterally at its distal end in
 1016 *Propalaeohoplophorus* (YPM-PU 15007, FMNH P13205).

Although it is not evident in the isolated petrosal (due to postmortem breakage), both the right petrosal in UF 248500 and both left and right petrosals in UF 191448 are characterized by a massive caudal tympanic process of the petrosal on the ventral pars cochlearis (Figure 8). The process is concave posteriorly in both specimens, apparently articulating posteriorly with a small elevation on the anterior edge of the exoccipital, although the petrosal is anteriorly displaced from its suture with the exoccipital in both specimens. The caudal tympanic process forms the lateral half of the posterior wall to the stapedius fossa, and lies well lateral to the fenestra cochleae. It occupies a similar position in *Vassallia* (FMNH P14424) and *Dasypus* (Wible 2010), though it is less massive in both taxa. In *Proeutatus* (FMNH P13197) and *Propalaeohoplophorus* (YPM-PU 15007, FMNH P13205) it is both smaller and more medially placed. The caudal tympanic process of *H. floridanus* is separated laterally by a deep notch from the massively enlarged paroccipital process of the petrosal (=mastoid process of Patterson et al. 1989; Gaudin 1995; and others). This huge paroccipital process is slightly hooked medially and angled anteriorly at its distal extremity, and extends ventral to the level of the basicranial plate (Figures 3-8). Though almost cylindrical in appearance, its transverse diameter is in fact a good deal larger than its anteroposterior diameter, and it tapers distally to a rounded tip. The great enlargement of the paroccipital process is evidently a feature of pampatheres in general, because it is present in *H. septentrionalis* (UF 234224; Edmund 1985), *H. occidentalis* (ROM 3881), *Vassallia* (Patterson et al. 1989; De Iuliis and Edmund 2002), and *Pampatherium* (Bordas 1939; Guth 1961; Paula Couto 1984). The paroccipital process of glyptodonts is massive, but not as elongated as that of pampatheres (YPM PU 15007; Patterson et al. 1989), whereas the process is much smaller, though still sizable, in *Proeutatus* (labeled as “mastoid process” in Patterson et al. 1989) and *Euphractus* (Wible and Gaudin 2004). It is also flattened in the latter two taxa,

anteroposteriorly in *Euphractus* and obliquely in *Proeutatus* (in an anterolateral/posteromedial plane). The notch separating the caudal tympanic and paroccipital processes of the petrosal in *H. floridanus* is saddle shaped, separating the stylomastoid foramen anteriorly from the sulcus for the occipital artery posteriorly (Figure 8).

The caudal tympanic process is also separated by a medial notch from a small process attached to the back of a broad shelf of bone that lies behind the promontorium. The notch is likely for the auricular branch of the vagus nerve (c.n. X) based on comparisons with *Dasypus* (Wible 2010). The broad shelf, which is trapezoidal in shape, widening anteriorly (Figure 9A-D), is the roof of the postpromontorial sinus, the structure Wible (2010) terms the “triangular shelf” in *Dasypus*. This shelf is considerably broader in *H. floridanus*, as it is in *Vassallia* (FMNH P14424) and *Propalaeohoplophorus* (YPM-PU 15007, FMNH P13205). The shelf is semicircular but similar in size to that of *Dasypus* in *Proeutatus* (FMNH P13197), whereas in *Euphractus* (UTCM1491) it remains triangular but is larger and extends further anterolaterally than in *Dasypus*.

As a final aspect visible in ventral view, we note that the area of the petrosal lateral to the crista parotica in *H. floridanus* is a concavity that forms the medial half of the epitympanic recess, which accommodates the mallear and incudal heads in mammals. The lateral half of the recess is formed by squamosal, and is bisected transversely by the postglenoid process. The petrosal portion of the recess has a small divot in the lateral portion of its posterior wall that presumably represents the fossa incudis. The fossa lies immediately above a low ridge that extends anteromedially from the base of the tympanohyal. In *Dasypus*, the lateral wall of the anterolaterally facing fossa incudis is formed by the squamosal (Wible 2010), but this does not appear to be the case in *Holmesina*, nor in *Vassallia* (FMNH P14424), *Propalaeohoplophorus*

(FMNH P13205), or *Proeutatus* (FMNH P13197), where the fossa is more anteriorly oriented. *Euphractus* also lacks squamosal participation in the fossa incudis, but in this case it is due to the presence of an open epitympanic sinus above the ossicles (Wible and Gaudin 2004), as is typical for euphractine armadillos (Patterson et al. 1989; Gaudin 1995; Gaudin and Wible 2006, node 6).

Because of the presence of an isolated petrosal, we are able to describe and illustrate (Figure 9G, H) details of the dorsal surface of the petrosal that have never been described before in pampatheres. The most distinctive feature visible in a dorsal view of the *H. floridanus* petrosal is a large opening in the anteroventral region of the endocranial exposure (in the pars cochlearis), the internal acoustic meatus. This opening is much deeper than that of *Dasypus* (Wible 2010), and is ventrally displaced, so that it is separated from the endocranial roof of the basicranial plate by only a thin, sharp crest. This arrangement also differs from that in both *Vassallia* and *Euphractus*, in which the meatus is equally deep but more dorsally positioned.

At the bottom of the internal acoustic meatus is a series of openings that have been identified (Figure 9G, H) based on Wible's (2010) description of *Dasypus*. The openings are clustered into two groups, separated by a sharp transverse crest. In *Dasypus*, the transverse crest is broad and rounded, whereas in *Euphractus* it is broad but with a sharp medial edge. The anatomy in *Vassallia* is much like that of *Holmesina*. The two openings above (i.e., dorsal and lateral to) the transverse crest are the facial foramen for the facial nerve (c.n. VII), and posterior to that and roughly equivalent in size, the superior vestibular area. Below the transverse crest there are three openings: anteromedially, the large spiral cribriform tract, separated by a strong crest from two smaller, more posterior openings in a common fossa, a more posteromedial foramen singulare and a more anterolateral inferior vestibular area. The arrangement of these openings is very similar in *Vassallia*, whereas in *Dasypus* there is no real crest separating the

spiral cribriform tract from the more posterior foramina. Moreover, the posterior foramina are clearly visible in medial view in pampatheres, whereas in *Dasypus* they face more anteriorly (foramen singulare) or ventrally (inferior vestibular area; Wible 2010; UTCM 801[isolated petrosal]). *Euphractus* also lacks the septum between the spiral cribriform tract and the two posterior foramina, which are quite small, and located in close proximity along the posterior wall of the lower opening of the internal acoustic meatus (UTCM 1486). At the medioventral edge of the petrosal's endocranial surface, slightly posterior to the internal acoustic meatus, lies the opening of the cochlear canaliculus. It occupies the same position in *Vassallia* and *Dasypus* (Wible 2010), whereas in *Euphractus*, where the ventromedial edge of the petrosal contacts the basicranial plate along its whole length, the cochlear canaliculus occupies a more dorsal, endocranial position.

Anterior to the internal acoustic meatus is a distinct concavity, which may have accommodated the inferior petrosal sinus. A similar concavity is present in *Vassallia* and *Euphractus*, but is absent in *Dasypus* (Wible 2010). The region immediately dorsolateral to the meatus, the so-called prefacial commissure, is broad and swollen in both pampatheres. In *Dasypus* it is a narrow bar of bone (Wible 2010), whereas in *Euphractus* it is broad like the pampatheres, but flat rather than swollen. The prefacial commissure in *Holmesina* is surmounted by a rounded crista petrosa that at its posterodorsal end is divided into medial and lateral ridges by a vascular groove. This groove is situated too far medially to carry the postglenoid vein described by Wible (2010) in *Dasypus*, and so we suspect it carried the superior petrosal sinus. This groove is also present in *Vassallia*, though it is missing in both *Dasypus* and *Euphractus*, both of which have a much sharper crista petrosa. Indeed, in *Euphractus* (UTCM 1486), the crista petrosa is so elevated that it resembles a low ossified tentorium, like that of pangolins and

carnivorans (Gaudin et al. 2016), extending a short distance dorsally between the cerebrum and cerebellum—*Euphractus* also has a very large, concave cerebral surface of the petrosal, whereas in *Dasypus* (Wible 2010) and in pampatheres this surface is much smaller.

The endocranial exposure of the pars canalicularis is occupied by a broad, deeply concave subarcuate fossa in all the cingulates examined in this report. It is narrower anteroposteriorly in *Euphractus* than in *Dasypus* or pampatheres. In the latter forms it takes on a rounded triangular shape, with its apex pointing ventromedially. In pampatheres and *Euphractus*, it is divided by a low, rounded, roughly transverse ridge into upper and lower concavities. The upper concavity is further divided by a low ridge into anterior and posterior concavities in *Holmesina* and *Vassallia*. The first, more horizontal ridge is almost certainly created by the lower portion of the posterior semicircular canal, whereas the second, more vertical ridge is created by the crus commune of the anterior and posterior semicircular canals. The aqueductus vestibuli, which transmits the endolymphatic duct, takes the form of a vertical slit opening into the ventromedial corner of the subarcuate fossa (Figure 9G, H). It has the same shape and position in *Vassallia*. In *Euphractus*, this opening is quite close to the exoccipital bone posteriorly, in contrast to pampatheres, and in *Dasypus* (Wible 2010) it is located outside the subarcuate fossa, in a more ventral, medial and anterior position. A small opening into the recessus angularis, like that described for *Dasypus* by Wible (2010), is present on the dorsolateral rim of the subarcuate fossa in *H. floridanus*. On the right side of the UTCM 1486 specimen of *Euphractus* there is a similar opening; however, on the left side, there are three or four small vascular foramina in this area, some within and some outside the subarcuate fossa, the middle opening on the rim the largest. As noted by Wible (2010), the recessus angularis opening may or may not lie within the subarcuate fossa in *Dasypus*.

We have illustrated the isolated left petrosal of *H. floridanus* (UF 248500) in lateral view (Figure 9E, F), much as Wible (2010) has done for *Dasypus*. As in *Dasypus*, there are three broad regions of the petrosal of *Holmesina* recognizable in lateral view. There is a cerebral surface, exposed in the floor of the middle cranial fossa of the endocranium. Like *Dasypus* this surface is elongated along an anteroventrolateral to posterodorsomedial axis, and is relatively narrow transversely, though it is less triangular and more ovate in *Holmesina*. The tympanic exposure includes the promontorium, with its prominent elongated rostral tympanic process and large lateral, circular boss of unknown function. The fenestra vestibuli is also visible laterally, but not the primary facial foramen, which is hidden by a distinct ventral, semicircular ventral extension, the anteroventral process of the tegmen tympani. This process is present in *Dasypus* (Wible 2010), but does not extend ventrally to the same degree. Like *Dasypus*, this tympanic exposure also includes portions of the epitympanic recess situated lateral to the crista parotica. The petrosal contribution to the fossa incudis lies at the posterior and dorsal extremity of this surface, as in *Dasypus* (Wible 2010), but is less clearly marked. The tympanohyal is prominently exposed in *Dasypus* in lateral view, but is broken off in UF 248500. The remainder of the lateral exposure in UF 248500 is comprised of a posterodorsal contact surface for the squamosal, and the broken remains of the paroccipital process. Because the latter is so much larger in *Holmesina* than in *Dasypus*, it accounts for a much larger portion of this lateral surface, despite the fact that most of the process is broken off in the illustrated specimen.

The mastoid exposure of the petrosal is largely missing from the isolated petrosal, due to postmortem breakage, and so this region of the petrosal will be described based on the in situ right petrosal from UF 248500, and on UF 191448. In lateral view, the dominant feature of the mastoid exposure in *H. floridanus* is the gigantic paroccipital process (Figures 3, 4, 7), which, as

noted above, has a slight medial hook and is angled anteriorly at its distal extremity, extends ventral to the level of the basicranial plate, and is slightly compressed anteroposteriorly with a rounded tip. It has a clear, sigmoid suture dorsally with the squamosal (and its posttympanic process) in both specimens, extending in a posterodorsal to anteroventral direction. The lateral edge of the paroccipital process is continuous dorsally with the nuchal crest. As previously observed, the morphology of this region is similar in all pampatheres (Bordas 1939; Guth 1961; Paula Couto 1984; Edmund 1985; Patterson et al. 1989; De Iuliis and Edmund 2002), whereas the shape and size of the paroccipital process is variable in other cingulates (Patterson et al. 1989; Wible and Gaudin 2004; Wible 2010).

In posterior view, the mastoid region has a broad, rectangular (UF 191448) or rhomboid (UF 248500) exposure on the occiput (Figure 10). In UF 191448, the transversely elongated exposure is marked by two narrow vertical depressions. The deeper and more medial of these is the sulcus for the occipital artery, which arises as a deep notch between the paracondylar process of the exoccipital and the paroccipital process, and terminates dorsally at the posttemporal foramen (the posterior opening of the posttemporal canal for the arteria diploetica magna – see Wible and Gaudin 2004). This opening lies just below the suture between the mastoid and the occipital exposure of the squamosal. The second, more lateral and much shallower vertical depression represents the attachment surface for the digastric muscle, travelling along the inside edge of the nuchal crest. This depression does not reach the tip of the paroccipital process ventrally, but dorsally it extends beyond the mastoid, crossing the occipital surface of the squamosal onto the supraoccipital. It terminates just below a large muscular boss on the nuchal crest. The morphology of UF 248500 differs from that of UF 191448 in several respects. Most importantly, the shape of the occipital exposure is different – it is more rhomboid than

rectangular, with its dorsal border sloping ventrolaterally. Additionally, the digastric fossa is shallower, and has a sigmoid shape. In *H. septentrionalis* (UF 234224), the digastric fossa takes on a shape similar to that in UF 248500, and the occipital artery sulcus is bowed medially. The mastoid occipital exposure is even broader mediolaterally in *Vassallia* than in *Holmesina*, taking on a “Y-shape” as indicated by De Iuliis and Edmund (2002: p. 56), with medial and lateral extensions passing dorsal to the posttemporal foramen (= “mastoid foramen” of De Iuliis and Edmund 2002). In *Propalaeohoplophorus* (YPM-PU 15007), *Proeutatus* (FMNH P13197), and *Euphractus* (UTCM 1491), the digastric fossa is much shorter vertically than in pampatheres, restricted to the posterior surface of the paroccipital process, and not extending dorsally onto the squamosal and supraoccipital. *Holmesina floridanus*, *H. septentrionalis* (UF 234224), and *Vassallia* (FMNH P14424) all have a groove for the occipital artery extending dorsally from the posttemporal foramen across the squamosal and onto the supraoccipital. This condition was also described in *Euphractus* by Wible and Gaudin (2004), and is optimized as a cingulate synapomorphy by Gaudin and Wible (2006).

Ectotympanic, Entotympanic, Ear ossicles

To our knowledge, no remnant of the ectotympanic or ear ossicles has ever been recovered in any pampathere, and our specimens, well-preserved though they are, have proven no exception [Guth (1961) described partial stapes elements in several glyptodonts, but not any portion of the ectotympanic or other ossicles]. There appear to be facets for the attachment of the anterior and posterior crura of the ectotympanic preserved in UF 248500, on the ventromedial surface of the squamosal’s entoglenoid process, and on the anterior surface of the tympanohyal and the portion of the petrosal forming the anterior wall of the stylomastoid

foramen, respectively. This suggests that the ectotympanic formed a loosely attached, dorsally incomplete ring. There is also no indication of the presence of an entotympanic element – indeed, none has ever been described in any pampathere or glyptodont, despite its occurrence in *Euphractus* (Wible and Gaudin 2004) and many other cingulates (Patterson et al. 1989; Wible 2010).

Vomer

The vomer of *H. floridanus* is only partially visible in two places. It can be seen anteriorly through the external narial opening of UF 248500, as an elongate ridge extending dorsally from the roof of the maxillary palatine processes into the nasal cavity. Here it is Y-shaped in cross section, with the base in the midsagittal plane and the dorsal arms of the “Y” supporting the ossified portion of the median nasal septum. It appears to come to an abrupt anterior termination well behind the internal openings of the incisive foramina, therefore it likely did not contact the premaxilla, in contrast to *Vassallia*, *Propalaeohoplophorus* and most other cingulates (Gaudin and Wible 2006). The vomer is also visible looking posteriorly through the choanae of UF 191448, as a pair of nearly vertical alae extending along the lateral edge of the presphenoid, converging anteriorly until they meet in the midline, perhaps covering the anteriormost tip of the presphenoid ventrally. Much of the posterior and ventral reaches of these alae are broken, but they likely contacted the maxilla and perhaps the palatine ventrally along the lateral walls of the nasal passage.

Presphenoid/Orbitosphenoid

There is a clear suture between the presphenoid and basisphenoid in UF 248500, and the posterior portion of the presphenoid is visible in ventral view extending a short distance posterior to the choanae, although most of the anterior presphenoid is missing (Figures 5, 6). The entire presphenoid is preserved in UF 191448, though it is fused into the surrounding elements, so that its precise boundaries are no longer evident. Nevertheless, it can be inferred from the two specimens that the presphenoid takes the form of a narrow, elongate triangle that tapers anteriorly until disappearing beneath the vomer within the nasal cavity. As noted above, the anterior presphenoid connects laterally with the vomerine alae inside the nasal cavity, and likely contacts the palatine and pterygoid posterolaterally, although UF 248500 has ventrolateral flanges of the basisphenoid that extend lateral to the posteriormost parts of the presphenoid, and could preclude contact with the pterygoid. The presphenoid has a very similar form in other cingulates. In *Vassallia*, there is a ventrolateral projection of the basisphenoid that extends forward to preclude pterygoid/presphenoid contact, as in *H. floridanus*.

The lateral portions of the orbitosphenoid, i.e., the areas where it would normally be exposed at the surface along the medial orbital wall, are badly damaged in UF 248500. There is also some damage in this area in UF 191448, and the orbital sutures are all closed in this specimen, making it difficult to assess orbitosphenoid anatomy. However, two additional specimens of *H. floridanus*, UF121742 and UF 223813, provide better insight. The former is an exquisitely preserved display specimen and shows the surface exposure in the orbital wall, the latter a fragmentary specimen that preserves the endocranial portion of the orbitosphenoid (which can also be glimpsed through breaks in UF 248500). The specimens taken together show that the optic nerve is completely enclosed in a canal formed by the orbitosphenoid bone (Figure 7), as is typical for placental mammals (Novacek 1993). The lateral wall of this canal forms the

medial wall of a combined sphenorbital fissure (transmitting c.n. III, IV, V₁, and VI, as well various orbital blood vessels) and foramen rotundum (transmitting c.n. V₂). In nearly all cingulates, these two openings are fused.

The endocranial surface of the presphenoid/orbitosphenoid is marked by a strong, continuous orbitosphenoid crest surmounting the internal apertures of the left and right optic canals, but the jugulum sphenoidale (i.e., the surface of the presphenoid/orbitosphenoid rostral to the orbitosphenoid crest - using terminology of Evans and Christiansen 1979; Wible 2008) is only weakly convex in the midline. In many cingulates, including *Euphractus*, there is a strong midline crest in this area (Gaudin and Wible 2006 – note *Euphractus* is coded as lacking this feature, but should be coded as variably present, because a sharp crest is present in UTCM 1491, and a weaker, rounded crest is present in UTCM 1500). As in *Holmesina*, the midline crest itself is only weakly developed in *Vassallia*, but the entire jugulum singulare is swollen and convex, quite unlike the condition in *Holmesina*.

The surface exposure of the orbitosphenoid in the medial orbital wall is relatively small and ovate in UF 121742, and elongated along a posteroventral to anterodorsal axis (Figure 7). It contacts the frontal anteriorly and dorsally, the maxilla and alisphenoid ventrally, and is separated by a gap from the lateral wall of the common opening for the optic foramen and sphenorbital fissure. The orbitosphenoid forms the medial wall of this common opening. In contrast to *Euphractus* (Wible and Gaudin 2004) and *Proeutatus* (Gaudin and Wible 2006: fig. 6.6a), there does not appear to be contact between the palatine and orbitosphenoid, although it is possible that there is a connection at the base of the medial wall for the common fossa that holds the optic foramen/ sphenorbital fissure and sphenopalatine canal.

The orbitosphenoid does not participate in the rim of either the sphenopalatine foramen or the ethmoid foramen in UF 121742. Both conditions are known to occur at least variably in euphractine armadillos (Gaudin and Wible 2006), but Gaudin and Wible (2006) code both as absent in *Vassallia*, as they are in *Holmesina*. Like *Vassallia*, *Propalaeohoplophorus*, and *Proeutatus* (Gaudin and Wible 2006 – an unambiguous synapomorphy of Node 7), the optic foramen (i.e., the lateral opening of the optic canal) is hidden in lateral view by the lateral wall of the fossa housing the combined optic foramen/sphenorbital fissure, unlike *Euphractus* and most other extant armadillos (Gaudin and Wible 2006), in which the optic foramen is visible laterally. The small opening to the pterygoid canal lies on the suture between the orbitosphenoid and alisphenoid, just anterior to the optic foramen/sphenorbital fissure common opening, and at the base of a bony bridge that connects the alisphenoid and maxilla and forms a partial lateral wall to the common fossa for the sphenopalatine canal and the optic foramen/sphenorbital fissure (Figure 7). The position of the pterygoid canal foramen is similar in *Vassallia*, *Proeutatus*, and *Euphractus* (Wible and Gaudin 2004; Gaudin and Wible 2006), whereas in *Propalaeohoplophorus*, this foramen lies within the common fossa for the optic foramen and sphenorbital fissure (Gaudin and Wible 2006). The lateral surface of the orbitosphenoid is marked by a rounded, anterodorsally directed ridge in UF 121742. This ridge lies ventral to a groove emerging from the optic foramen; a similar ridge is formed by the frontal bone above this groove, separating it from the ethmoid foramen.

Alisphenoid

The alisphenoid is apparently quite large in *H. floridanus*, with a shallow bowl-like surface contour (Figure 7). It has sutural connections dorsally with the orbitosphenoid, frontal,

and squamosal, the first being the shortest, most anterior, and roughly horizontal. The middle section is positioned more dorsally, and travels posterodorsally, meeting at a point with the squamosal suture, which sweeps posteriorly and ventrally in a great semicircular curve, crossing the entoglenoid process at its posteriormost extremity, so that the alisphenoid forms roughly the anterior third of this process. The alisphenoid has a generally horizontal suture ventrally with the pterygoid, taking part in the dorsalmost lateral rugosities of this element. As noted above, it contacts either a thin sliver of palatine or the maxilla anteriorly, and forms the posterior half of the rim for the sphenopalatine foramen. There is no contact between alisphenoid and parietal, as noted above.

The large foramen ovale is housed completely within the alisphenoid, as in most cingulates (Gaudin et al. 1996), though the squamosal does closely approach its dorsal margin. There is a small transverse canal foramen (for a vein from the cavernous sinus – see Wible and Gaudin 2004) anteroventral to the foramen ovale in UF 121742, and on the left side of UF 191448. On the right side of UF 191448, and in UF 275496, there are two small foramina in this position, whereas the foramen appears to be absent in UF 248500. This feature is present in most cingulates (it is an ambiguous synapomorphy of Node 3 in Gaudin and Wible 2006). The alisphenoid also likely forms at least the lateralmost parts of the piriform fenestra's anterior edge, though it is difficult to be certain of the contribution because of fusion between the alisphenoid and basisphenoid posteromedially.

The alisphenoid has a prominent, rounded posterior edge that forms the terminus for the lateral wall of the nasopharynx. Just below its suture with the frontal, it is traversed by a sharp crest that originates on the anteromedial corner of the glenoid articular surface and extends anteriorly across the squamosal and alisphenoid. This is a posterior section of the infratemporal

crest. It terminates anteriorly at a large boss, where it joins the anterior portion of the infratemporal crest described above in connection with the frontal bone. This boss likely serves as the site of origin for most of the extrinsic eye muscles, and would therefore be homologous with the ossified ala hypochiasmatica described by Wible and Gaudin (2004) in *Euphractus*, though it is carried by the alisphenoid rather than the orbitosphenoid. The anatomy of these crests is very similar to *H. floridanus* in *H. septentrionalis* (UF 234224), *Vassallia* (FMNH P14424), and *Propalaeohoplophorus* (YPM-PU 15007). The alisphenoid terminates anteriorly in a thin, freestanding crest that marks the lateral margin of the fossa housing the optic foramen/sphenorbital fissure and the sphenopalatine canal. As noted above, it also forms a bony bridge lateral to this fossa that connects anteriorly with the maxilla. The entoglenoid portion of the alisphenoid in UF 248500 bears a shallow groove that runs anteroventromedially towards the foramen ovale, which likely accommodated the chorda tympani nerve.

Basisphenoid

The basisphenoid and basioccipital are fused in all the *H. floridanus* specimens available to us, so we cannot determine the boundary between the two with certainty. In other cingulates for which the suture is known (Gillette and Ray 1981; Patterson et al. 1989; Wible and Gaudin 2004; Wible 2010), the boundary lies anterior to the basioccipital tubera, roughly at the level of the carotid foramina. We will assume a similarly positioned boundary here (Figure 6).

The main body of the basisphenoid has a flat ventral surface contour and is trapezoidal in outline, tapering anteriorly. It contacts the presphenoid anteriorly and the basioccipital posteriorly. Along its lateral margins, it bears a prominent, ventrally curving flange. In UF 248500, this flange has a sutural outline anteriorly, although, due to damage in this area it is

unclear if the bone to which it is sutured is palatine, pterygoid, or perhaps even alisphenoid. More posteriorly, this flange, if present, is fused to the alisphenoid – there are vague indications of a basisphenoid/alisphenoid contact emerging from the piriform fenestra, crossing the anteriormost region of the entoglenoid process and extending anteriorly onto the nasopharyngeal wall in UF 121742. The ventral basisphenoid flange is visible in UF 275496 (a juvenile specimen), but is not visible in UF 191448 due to sutural fusion. The ventral flange is also present in *Vassallia* (FMNH P14424). In both *Holmesina* and *Vassallia* this flange has a triangular anterior extension that reaches forward beyond the level of the presphenoid/basisphenoid suture, presumably separating the vomerine alae from the palatine and/or pterygoid. Although it is not illustrated by Wible and Gaudin (2004), at least three specimens of *Euphractus* (UTCM 1486, 1491, and 1500) examined for this study have a small ventral flange of the basisphenoid. It is much smaller than in pampatheres, restricted anteriorly and triangular in shape. It extends laterally between the nasopharyngeal exposures of the pterygoid and palatine.

The posterolateral corner of the basisphenoid bears a concave, semicircular indentation for the carotid foramen (Figures 5, 6, 8). As noted in our description of the alisphenoid, these two sphenoid elements also form the anterior margin of the piriform fenestra (along with the entoglenoid process of the squamosal), though their relative contributions are unclear due to sutural fusion in this area. A short distance anterior to this indentation, a longitudinal groove forms in both UF 248500 and UF 191448. It travels anteriorly across the basisphenoid, beginning near the junction of its ventral flange and body, but shortly thereafter curving ventrally and then traveling straight for the remainder of its course across the ventral flange. This is the groove for the vidian nerve. Its anterior terminus is missing in UF 248500, but in UF 191448 it

terminates at the medial opening for the pterygoid canal, located at the junction of the ventral basisphenoid flange and the perpendicular plate of the palatine. This open groove for the vidian nerve is nearly identical in form in *Vassallia* (FMNH P14424), and an open groove of somewhat different form is preserved in *Proeutatus*, whereas in some cingulates, like *Euphractus*, the nerve is partially enclosed by a canal, and in others, e.g., *Propalaeohoplophorus*, it is fully enclosed by a canal (Gaudin and Wible 2006).

The dorsal surface of the basisphenoid is exposed in UF 223813. It is marked by a large, deep, circular hypophyseal fossa, flanked laterally by prominent grooves for the internal carotid arteries. In the roof of the internal carotid sulci are bilaterally symmetrical openings – small breaks in the basisphenoid show that these are connected to a canal within the tuberculum sellae (i.e., the eminence in front of the hypophyseal fossa), and are likely part of the cavernous sinus system, accommodating the veins that open at the transverse canal foramen anteroventral to the foramen ovale.

Basioccipital

The basioccipital forms the remainder of the basicranial surface, accounting for over half its length (if we are reconstructing the position of the basisphenoid/basioccipital suture correctly). It has straight lateral margins that converge only slightly anteriorly in *H. floridanus* (Figure 6). The basioccipital is considerably shorter and wider in *H. septentrionalis* (UF 234224) and *H. occidentalis* (ROM 3881), with lateral margins that are more steeply inclined, whereas the proportions of the basioccipital in *Vassallia* (De Iuliis and Edmund 2002), *Propalaeohoplophorus* (Scott 1903-4), and *Proeutatus* (Patterson et al. 1989) are more like those of *H. floridanus*. The basioccipital lateral margins are largely separate from the petrosal in *H.*

floridanus, although, as noted above, there is an articulation between the two bones, with a knob forming on the dorsal edge of the basioccipital's lateral margin, fitting into a depression in the medial flange of the petrosal and interrupting the otherwise open **basicochlear** commissure. At its posterior limit, the lateral margin of the basioccipital curves laterally, forming the anterior half of the notch for the jugular foramen. UF 248500 retains the suture between the exoccipital and basioccipital, showing it as a nearly horizontal contact that extends from the medial margin of the jugular foramen to the anterior portion of the ventral rim of the foramen magnum (Figure 6). In *Euphractus* (Wible and Gaudin 2004), this suture runs more diagonally, contacting the rim of the jugular foramen further anteriorly and the foramen magnum further posteriorly.

The ventral surface of the basioccipital is convex transversely and highly irregular, marked by several prominent elevations and depressions. The anteriormost of these include two prominent lateral tubercles flanking an even taller median crest (Figure 5). These represent the basioccipital tubera and pharyngeal tubercle, respectively [based on comparison with *Canis* (Evans and Christiansen, 1979) and *Homo* (Clemente 1985)], the former serving as the site of attachment for the m. longus capitis. Behind the basioccipital tubera are large, shallow depressions, elongated along a posterolateral to anteromedial axis that accommodated the insertion of the m. rectus capitis ventralis. In *H. septentrionalis* (UF 234224) and *H. occidentalis* (ROM 3881), the pharyngeal tubercle and rectus capitis fossae are less well-developed, whereas only the latter is reduced in *Vassallia* (Gaudin and Wible 2006). *Proeutatus* resembles the morphology in *H. floridanus*, but the basioccipital tubera are more elongated along an oblique axis, whereas the basioccipital surface relief is much reduced in both *Propalaeohoplophorus* and *Euphractus* (Wible and Gaudin 2004; Gaudin and Wible 2006).

Exoccipital/Supraoccipital

The occiput is a single fused plate in UF 191448, as is typical among adult mammals, but in the subadult UF 248500 the demarcations among its constituent elements are still visible, including the contact between just described basioccipital and the exoccipital elements on the skull base, as well as the junction between the exoccipitals and supraoccipital on the posterior surface of the skull.

The paired exoccipitals have two primary sections: a horizontal moiety on the skull base; and a vertical portion that forms part of the occipital surface. The former joins the basioccipital at its anteroventral extremity, at a suture that passes medially from the jugular foramen. It is not clear if the suture enters the rim of the foramen magnum, or meets its opposite anterior to the rim of the foramen magnum. Damage to the medial portions of both the left and right exoccipitals of UF 248500 leaves a sizable gap in this area (Figure 5B). The posterior, vertical segment of the exoccipital shares a lateral suture with the mastoid part of the petrosal. This suture extends from the base of the paracondylar process dorsally to the base of the supraoccipital. Any connection between the occipital exposure of the squamosal and the exoccipital is precluded by a dorsal contact between the mastoid petrosal and the supraoccipital (Figure 10). The crack that we interpret as the exoccipital/supraoccipital suture in UF 248500 is not perfectly symmetrical, and so may not represent the actual suture, but it occupies almost an identical position as that of the extant armadillo *Euphractus* (Wible and Gaudin 2004: fig. 5), extending ventromedially from the supraoccipital/mastoid suture to the dorsal rim of the foramen magnum. A specimen of *Propalaeohoplophorus*, YPM-PU 15007, has a nearly identical suture on the left side only. Lastly, there is an asymmetrical crack in roughly the same area of the occiput in *Vassallia*

(FMNH P14424), though it is oriented at a shallower angle and so does not appear to enter the dorsal rim of the foramen magnum, which would then be formed entirely by the exoccipital.

The lateral edge of the exoccipital's basicranial segment is marked by a distinct concavity that represents the jugular notch, i.e., the medial edge of the jugular foramen. As noted above, the anterior portion of the jugular notch is formed by the basioccipital. Extending more laterally than posteriorly from this notch is a sutural contact between exoccipital and mastoid. This suture is broadly open in both UF 191448 and UF 248500 (Figure 8), but this is presumably due to postmortem displacement of the petrosal. At the lateral extremity of this contact surface, the exoccipital bears a strong, free-standing ventral projection, the paracondylar process (=paroccipital process of Patterson et al. 1989; Gaudin 1995; =jugular process of Wible and Gaudin 2004). In posterior view, the paracondylar process has a convex lateral border and a concave medial border, giving it a hooked appearance, and it is separated by a distinct notch from the lateral edge of the occipital condyle (Figures 6, 8, 10). This morphology is apparently a general feature of pampatheres, because it is also present in *H. septentrionalis* (UF 234224), *H. occidentalis* (ROM 3881), *H. paulacoutoi* (Cartelle and Bohórquez 1985), *Vassallia* (FMNH P14424), and *Pampatherium* (Bordas 1939; Guth 1961). In *Propalaeohoplophorus* (YPM-PU 15007) the paracondylar process is well developed, but more blunt, and neither hooked medially nor separated by a notch from the occipital condyle. The process is dramatically reduced by comparison in both *Proeutatus* (FMNH P13197) and *Euphractus* (Wible and Gaudin 2004). Just medial to the jugular notch is a strong fossa that houses the hypoglossal foramen at its base. In UF 248500, there are two hypoglossal foramina, each connecting to a corresponding opening just inside the foramen magnum within the cranial cavity. In UF 191448, there appears to be a single opening. This mirrors the variation noted for *Euphractus* by Wible and Gaudin (2004), whereas

1451 Gaudin and Wible (2006, char. 153) record only a single hypoglossal foramen in *Vassallia*,
1452 *Propalaeohoplophorus*, and *Proeutatus*.

1453 The hypoglossal fossa of *H. floridanus* sits at the medial edge of a second, broader and
1454 shallower fossa that lies just anterior to the occipital condyle, the ventral condyloid fossa of
1455 Wible and Gaudin (2004). Medial to these two depressions, the ventral surface of the exoccipital
1456 is transversely convex, and terminates at a strong, rounded ridge, which is the lateral edge of the
1457 foramen magnum. The transverse convexity of the exoccipital's basicranial exposure is another
1458 general feature of pampatheres, present in *H. septentrionalis* (UF 234224), *H. occidentalis*
1459 (ROM 3881), and *Vassallia* (FMNH P14424); but not in *Propalaeohoplophorus* (YPM-PU
1460 15007), *Proeutatus* (FMNH P13197) or *Euphractus* (Wible and Gaudin 2004), where the
1461 basicranial portion of the exoccipital is flat.

1462 Prominent occipital condyles join the vertical and horizontal segments of the exoccipital
1463 (Figures 5, 6, 10). The condyles are cylindrical (=“roughly rectangular” in ventral view, char.
1464 155[1] in Gaudin and Wible 2006) in shape, an unambiguous synapomorphy of Cingulata
1465 according to Gaudin and Wible (2006). The lateral edge bears a distinct indentation that is
1466 present in all cingulates except *Peltephilus* (Gaudin and Wible 2006, node 2). The portion of the
1467 condyle anterior and ventral to this indentation extends much further laterally than the more
1468 dorsal and posterior portion. This is also a feature of in *H. septentrionalis* (UF 234224), *H.*
1469 *occidentalis* (ROM 3881), and *Propalaeohoplophorus* (YPM-PU 15007), whereas in *Proeutatus*
1470 (FMNH P13197) and *Euphractus* (UTCM 1486, 1491, 1500) the condyle is more symmetrical
1471 about this indentation, and in *Vassallia* (FMNH P14424) the indentation itself is dramatically
1472 reduced. In ventral view, the condyle appears to be somewhat wider transversely in pampatheres
1473 and glyptodonts than in armadillos (as represented by *Proeutatus* and *Euphractus*). The

measurements reflect this, with the ratio of width to length greater than or equal to 1.5 in *H. floridanus*, *H. septentrionalis*, *H. occidentalis*, *Vassallia*, and *Propalaeohoplophorus*, and substantially less in *Proeutatus* and *Euphractus* (Tables 1, 2).

The surface of the exoccipital immediately medial to the condyles is deeply impressed by a fossa that extends anteromedially almost to the front of the foramen magnum's ventral rim. Based on comparison with other placental mammals (see *Homo*, Clemente 1985; *Canis*, Evans and Christiansen 1979; in which the condyles are much smaller and shallower) we identify this depression as the site of insertion for the alar ligaments extending forward from the dens of the axis. It is not at all clear why these ligaments would be so large in *H. floridanus*, but they appear similarly enlarged in other pampatheres, based on the presence of this fossa in *H. septentrionalis* (UF 234224), *H. occidentalis* (ROM 3881), and *Vassallia* (FMNH P14424). No such depression is described in Wible and Gaudin (2004), but we have subsequently examined specimens of *Euphractus* (UTCM 1486, 1491, 1500) in which a small, circular depression is present in this area. A similar circular depression is also observed in *Proeutatus* (FMNH P13197), whereas *Propalaeohoplophorus* (YPM-PU 15007) appears to have fossa similar in size to that of pampatheres, but much shallower.

The vertical portion of the exoccipital bears a strongly marked, transversely elongated depression immediately dorsal to the occipital condyle (Figure 10). This is the dorsal condyloid fossa of Wible and Gaudin (2004). Dorsal to this depression, the exoccipital is nearly flat. As noted above, the exoccipital forms nearly the entire rim of the foramen magnum, the supraoccipital only contributing a small exposure on the dorsalmost point of the opening. The rim is irregularly shaped due to a small convexity located at roughly the midpoint of its height, the nuchal tubercle. The nuchal tubercle is developed to a similar degree in *Proeutatus* (FMNH P13197) or

Euphractus (Wible and Gaudin 2004), but is less prominent in *Propalaeohoplophorus* (YPM-PU 15007). The latter also has a broader, transversely ovate foramen magnum, in contrast to the taller, more triangular shaped foramen in *Proeutatus* and *H. floridanus*.

The supraoccipital is a broad, hemispherical plate that extends from its ventral contacts with the squamosal, mastoid and exoccipital to its dorsal termination at the nuchal crest, where it is presumably fused to the parietal, as in *Euphractus* (Wible and Gaudin 2004). As in both *Euphractus* (Wible and Gaudin 2004) and *Proeutatus* (Scott 1903-4), the nuchal crest is posteriorly convex laterally and posteriorly concave in the midline. This shape is broadly shared among euphractine and eutatine armadillos, pampatheres, and early glyptodonts, extending all the way back to the oldest known cingulate skull, that of the Eocene taxon *Utaetus* (Barrancan SALMA; Simpson 1948; Gaudin and Croft 2015). In *H. floridanus*, there are prominent, raised tubercles just behind the most posterior point of curvature on the nuchal crest. Low, broadly rounded ridges extend ventromedially from the tubercles toward the foramen magnum. The central region of the supraoccipital between these elevations has a gently concave surface, interrupted in the midline by a very weakly developed external occipital crest (Figure 10). The supraoccipital is very similar in *Vassallia* (FMNH P14424). In *H. septentrionalis* (UF 234224) and *Propalaeohoplophorus* (YPM-PU 15007), the nuchal crest is more rugose, and the external occipital crest is more prominent, the latter also the case in *Euphractus* (Wible and Gaudin 2004). *Proeutatus* lacks the raised tubercles present in the other taxa, it has a large pair of mastoid foramina that perforate the supraoccipital, and it has a characteristic nuchal crest that is very tall to the point of being slightly recurved anteriorly in lateral view (Scott 1903-4; FMHH P13197).

The overall shape of the occiput in *H. floridanus* is rather tall and narrow, almost triangular, with its maximum depth and transverse width (measured at the base of the supraoccipital) nearly equivalent (Tables 1, 2). This is also the case in *H. septentrionalis* (UF 234224), whereas in *Vassallia* (FMNH P14424), *Propalaeohoplophorus* (YPM-PU 15007), *Proeutatus* (FMHH P13197), and *Euphractus* (UTCM 1491), the occiput is lower, broader and more semicircular in shape, with a width/depth ratio ≥ 1.2 .

Mandible



The mandible is preserved in a number of UF *H. floridanus* specimens, including UF 223813, 248500, 275497, 275498, 285000 and 293000. In all but the first two it remains incompletely prepared and attached to the skull, so that the occlusal surfaces of the teeth are not completely visible and the medial mandibular surfaces are also largely obscured. The mandible is prepared free in UF 223813 and 248500, but both are damaged to some extent. The left mandible of UF 224450 has also been prepared free. In this specimen the bone is almost perfectly preserved (Figure 11), although it only retains three of nine lower teeth (the second, sixth and seventh), along with what appears to be a pathological remnant of the fourth. Nevertheless, as the most complete available specimen, it will serve as the primary basis for the description that follows.

The pampathere mandible has been described many times in the literature (e.g., Simpson 1930; Castellanos 1937; James 1957; Edmund 1985; Edmund and Theodor 1997; Vizcaíno et al. 1998; De Iuliis et al. 2000; De Iuliis and Edmund 2002), and, as many of these authors have noted, is broadly similar in its morphology among the various taxa. Since much has already been

written about the comparative morphological differences among pampathere mandibles at the generic level, we will focus our comparisons on the species level variation within *Holmesina*.

The mandible of *H. floridanus* (MML = 182-200 mm; Tables 3, 4) is smaller than that of *H. septentrionalis* [both Simpson (1930) and James (1957) report MML of 240mm] and *H. occidentalis* (MML > 268mm in ROM 4955; Table 3). Proportions are very similar to *H. occidentalis*, with a very similar relative depth of the horizontal ramus (Table 2), whereas the horizontal ramus appears slightly deeper in *H. septentrionalis* (Simpson 1930; James 1957; Edmund 1985). Like *H. occidentalis* (ROM 4955), UF 224450 has two mental foramina that open on the external surface of the horizontal ramus in the symphyseal region (ventral to m3 and m4, respectively). Unlike *H. occidentalis*, both mental foramina are associated with grooves in the surface of the mandible. The more anterior foramen empties into two closely set, parallel, anterodorsally directed grooves, and indeed the foramen itself is partially constricted into an upper and lower opening. The groove emerging from the posterior mental foramen travels posteroventrally. For *H. septentrionalis*, Simpson (1930) illustrates four foramina of varying sizes in the external surface of the mandible anterior to the level of m4, whereas James (1957) describes a single mental foramen beneath m3. It is not clear if all four of Simpson's openings are mental foramina, or if one or more are nutritive foramina that he chose to illustrate.

The anteroventral edge of the symphysis in *H. floridanus* forms roughly a 27° angle with the toothrow (Figure 11C). This appears to be similar to the angle in *H. occidentalis* (ROM 4955), but somewhat more acute than in *H. septentrionalis* [roughly 30° as measured in Simpson (1930, fig. 4) and Edmund (1985, fig. 6)] The posteriormost point of the symphysis extends just below the ventral edge of the horizontal ramus in medial view, as in other *Holmesina*, and the anteriormost point forms a very short triangular extension in front of m1, marked by two small

foramina on its dorsal surface. The length of this short mandibular spout is a little longer than the mesiodistal diameter of the m1 alveolus (spout = 6.3mm, m1 alveolus = 6.0mm), whereas in Edmund's (1985, fig. 6) illustration of *H. septentrionalis* the spout is shorter than m1.

The masseteric fossa of *H. floridanus* (UF 224450) is broad, its anterior terminus marked by a low crest that connects the anteriormost edge of the angular process with the ventralmost edge of the coronoid process (Figure 11A). This crest continues posteriorly across the lateral surface of the coronoid base. This makes the masseteric fossa of *H. floridanus* deeper than that of *Vassallia*, but shallower than that of *H. occidentalis* (Vizcaíno et al. 1998). There are distinct depressions on either side of this upper masseteric crest. The depression above the crest covers most of the lateral surface of the coronoid process, and is bounded anteriorly by the coronoid crest, i.e., the thickened anterolateral margin of the coronoid process. The coronoid crest is continuous dorsally with a distinct crest that crosses the lateral surface of the coronoid process proximal to its tip, which we are designating the lateral coronoid crest. This lateral coronoid crest is found in all euphractine and eutatine armadillos, as well as pampatheres (Gaudin and Wible 2006: char 21[1], an unambiguous synapomorphy of Node A). Because this lateral coronoid depression lies between the coronoid and lateral coronoid crests, which serve as insertion points for the temporalis musculature in *Euphractus* (Smith and Redford 1990; Wible and Gaudin 2004) and presumably in *Holmesina* as well (Vizcaíno et al. 1998), and the upper limit of the masseter, we are labeling this area the "intermuscular fossa." The intermuscular fossa is very similar in size and shape in *H. floridanus* and *H. occidentalis* (ROM 4955), ovate and elongated along an anteroventral to posterodorsal axis. In *H. septentrionalis*, it appears to be narrower anteroposteriorly and more elongated posterodorsally (Cahn 1922; Simpson 1930).

There is also a weak, ovate depression below the upper masseteric crest in UF 224450, its long axis oriented in an anteroventral to posterodorsal direction, bounded posteriorly by the lateral coronoid crest. It is unclear if this area serves as part of the attachment for the masseter, although low ridges crossing its surface suggest that it does, and Smith and Redford (1990) show that the comparable area in *Euphractus* is covered by the masseter muscle.

The coronoid process itself is generally triangular in *H. floridanus*, but varies rather dramatically in its proportions. The ratio of maximum height to basal anteroposterior length ranges from 0.85-1.43, easily encompassing *H. septentrionalis* [as illustrated by James (1957) and Edmund (1985), the ratio is 1.25 or 1.23, respectively] within this range. The process appears to be somewhat more tapered distally in *H. floridanus* than in *H. septentrionalis*. A complete coronoid is not preserved in the specimen of *H. occidentalis* illustrated by Vizcaíno et al. (1998), but the preserved portion is more parallel sided than tapered distally, resembling more closely the condition in *H. septentrionalis*. Although the posterior edge of the coronoid process is slightly inclined posterodorsally in both *H. floridanus* and *H. septentrionalis*, the former taxon possesses an additional small but distinct posterior hook at its distal terminus (Figure 11), a feature lacking in the latter species (James 1957; Edmund 1985). Similar to the lateral coronoid crest described above, the coronoid process of *H. floridanus* carries a thickened anterior edge on its medial face, as well (Figure 11C). This medial crest connects to a second crest near the base of the coronoid. This low crest traces a posteroventrally curved arc, terminating at a point above the space between the last molariform tooth and the mandibular foramen. Anteroposteriorly, the medial surface of the coronoid process is gently concave. The base of the coronoid covers the posterior half of m8 in lateral view, and hides m9 entirely, as in other pampatheres (De Iuliis and Edmund 2002).

When viewed laterally or medially (Figure 11), the condylar process of *H. floridanus* is very short and triangular, closely resembling that of *H. septentrionalis* (Simpson 1930; James 1957; Edmund 1985) and *H. occidentalis* (Vizcaíno et al. 1998). As noted above, there is a single, short condyloid crest on the lateral side of the condylar process. There are two such crests on the medial side. All are short and extend in an anteroventral direction – the lateral crest is straight, whereas the medial crests are curved in an anteriorly concave fashion. Edmund (1985) illustrates three medial condyloid crests in his specimen of *H. septentrionalis*. The condyle itself is ovate, very broad transversely, and narrow anteroposteriorly, its width two to three times its length (Tables 3, 4). Its surface is flat anteroposteriorly, but slightly concave transversely, and inclined posterodorsally in lateral view, as it is in *H. occidentalis* (ROM 4955). At its medial extremity, the condyle of *H. floridanus* hooks sharply anteriorly at nearly a right angle, forming a tall medial wall to an ovate fossa. This fossa extends nearly to the midpoint of the condyle, lying anterior to the articular surface. It likely served as the site of insertion for the lateral pterygoid muscle, since the muscle attaches to this region in the extant *Euphractus* (Wible and Gaudin 2004). The condyle in *H. floridanus* is strongly elevated, located high above the level of the toothrow, like it is in *H. septentrionalis* (Edmund 1985) and *H. occidentalis* (Vizcaíno et al. 1998). Curiously, the condyle of pampatheres is noticeably less elevated than that of *Propalaeohoplophorus*, *Proeutatus*, or *Euphractus* (Table 3).

As in the other *Holmesina*, the angular process of *H. floridanus* extends only a short distance posterior to the base of the condylar process, but forms a very broad, posteroventrally convex curved structure that reaches anteriorly nearly to the midpoint of the last molariform tooth (Figure 11). It extends, at its lowest point, slightly below the ventral edge of the horizontal ramus. The outer surface, part of the very large masseteric fossa, is only slightly convex

anteroposteriorly. Similarly, its inner surface is only slightly concave anteroposteriorly, nearly flat dorsoventrally, but strongly scalloped near its margin by the insertion of the medial pterygoid muscle, which attaches to this same region in *Euphractus* (Wible and Gaudin 2004) and other placental mammals (e.g., *Canis*, Evans and Christiansen 1979; *Homo*, Clemente 1985). Again, this morphology is virtually identical to that of other *Holmesina* (Simpson 1930; Edmund 1985; Vizcaíno et al. 1998). The mandibular foramen lies just above the inner medial pterygoid fossa, just behind and below the level of the third molariform and positioned directly above the most ventral portion of the angular process. In Simpson's (1930) illustration of *H. septentrionalis*, the foramen is located somewhat more anterior and much further ventrally, but this may be due to postmortem damage. In Edmund's (1985) illustration of the same taxon, there appear to be two mandibular foramina, one in a position like that of Simpson's specimen, the other in roughly the same position as in *H. floridanus* (UF 224450).

There is more variation in lower tooth counts than upper tooth counts among crown-group cingulates (Gaudin and Wible 2006) – e.g., *Proeutatus* (Scott 1903-4) and *Euphractus* (Wible and Gaudin 2004) both have 10 lowers, and *Propalaeohoplophorus* has only eight (Scott 1903-4). *Holmesina* has nine, as in other pampatheres (Simpson 1930; Edmund and Theodor 1997; Delulis and Edmund 2002), and this condition is optimized as a synapomorphy of pampatheres plus glyptodonts in Gaudin and Wible's (2006; Node 8) phylogenetic analysis.

Only three teeth are preserved in UF 224450: m2, m6 and m7 (Figure 11). In addition, there appears to be a conical, unerupted m4, but this is likely a pathological condition, as indicated not only by the shape and position of the tooth itself, but by the spongy bone that occupies much of the volume of the alveolus. The shape of the remaining teeth can only be inferred from the outline of their alveoli. There are lower teeth preserved in other FLMNH *H.*

floridanus specimens, though many can only be observed in lateral view because of preservation and degree of preparation. UF 223813 preserves all nine lower molariforms (Table 4), UF 275497 preserves m1, m3-7 and m9, UF 275498 preserves m1-7, and UF 285000 preserves m2, m4-5, and m7-8. The first three lower molariforms in *H. floridanus* are ovate mesiodistally, with their long axis rotated to a slightly mesiolingual to distolabial orientation. The fourth molariform is pathological in UF 224450. The alveolus shape indicates a reniform outline, with a slight labial indentation, but there is no visible external groove on the teeth in the other *H. floridanus* specimens, where the tooth takes on almost a rectangular shape, or perhaps weakly bilobate, in contrast to the reniform m4 (with a lingual groove) of other *Holmesina* (see below). The remaining lower teeth in *H. floridanus* (m5-9) appear to be strongly bilobate in outline. The first and last of these (i.e., m5 and m9) are substantially shorter mesiodistally than the intervening three teeth in between.

The tooth outlines and proportions in *H. septentrionalis* are quite similar (Simpson 1930; Edmund 1985), although both m3 and m4 are clearly reniform (concave lingually) in this species, in clear contrast to *H. floridanus*, and even m2 has a lingual groove as illustrated by Edmund (1985). *Holmesina occidentalis* (Vizcaíno et al. 1998) is even more similar to *H. floridanus*, lacking the reniform anterior teeth of *H. septentrionalis*, although m5 in this taxon is as large as m6-8, contrasting with its reduced length (relative to m6-8) in other *Holmesina*. Simpson (1930) notes that m4 is bilobate in both *Pampatherium* and *Kraglievichia*, and is clearly more elongated mesiodistally than m3, both features contrasting with the condition in *Holmesina*. De Iuliis and Edmund (2002) describe and illustrate an m4 for *Vassallia* that resembles that of *Pampatherium* and *Kraglievichia*, whereas Castellanos (1937, 1946) attributes a *Holmesina*-like morphology to this taxon. De Iuliis and Edmund (2002) suggest the

discrepancy may be due to individual variation, and Edmund and Theodor (1997: p. 230) note that the shape of m4 in *Scirrotherium* varies “from reniform to elongate-elliptical.” In both *Pampatherium* and *Vassallia* (Simpson, 1930; Castellanos 1937, 1946), m5 is reniform rather than bilobate, as it is in *Holmesina*. In *Scirrotherium*, m5 is described as bilobate but illustrated as reniform (Edmund and Theodor 1997: fig.14.2). The long axis of m5-7 in *Vassallia* is obtusely V-shaped with a lingual vertex (FMNH P14424; see illustration in De Iuliis and Edmund, 2002), and is rotated so that the posterior lobe extends further labially than the anterior lobe. Simpson (1930) illustrates a similar if less well developed condition for m6, m7, and m8 in *Kraglievichia*, and m5, m6 and m8 in *Pampatherium*, whereas in *Holmesina* and *Scirrotherium* (Edmund and Theodor 1997), the long axis of the posterior molariforms is essentially straight.

The lower teeth of Santacrucian glyptodonts (*Propalaeohoplophorus* and *Eucinepeltus*; Scott 1903-4) are reminiscent of those in pampatheres in some respects, with the first and second lower molariforms (likely homologous to m2 and m3 of pampatheres) ovate or slightly reniform in outline, and the third (=m4 of pampatheres) clearly reniform, but the remaining lower molariforms show the distinctive trilobate shape characteristic of glyptodonts (Hoffstetter 1958). The lower tooth outlines in *Proeutatus* (FMNH P13197; Scott 1903-4) also display some pampathere-like features. The anterior teeth (m1-3) are ovate, but m4-8 are vaguely heart shaped, with a shallow groove followed by a sharp keel on the lingual surface, with a stronger groove on the labial edge. The long axes of m4-8 are tilted somewhat posterolabially, as described above for *Vassallia*. The m9 in *Proeutatus* is weakly bilobate, like that of pampatheres, but the distal lobe is the broader of the two, whereas the mesial lobe is broader in pampatheres. The tooth outlines in *Euphractus* are like those of most other armadillos, i.e., uniformly circular or ovate in cross section (Wible and Gaudin 2004; Gaudin and Wible 2006).

As was the case with the upper dentition, the preserved teeth in UF 224450 possess a raised central region of osteodentine surrounded by more typical orthodentine (Ferigolo 1985; Kalthoff 2011). In m2, the osteodentine core takes on the shape of a very narrow oval aligned with the long axis of tooth's outline. The osteodentine in m6 and m7 is mostly linear, expanding into a short "Y" at its mesial and distal ends, as was the case with the posterior upper molariforms. The same condition is present in other pampatheres (Simpson 1930; De Iuliis and Edmund 2002; Kalthoff 2011), whereas in glyptodonts the central osteodentine core bears multiple lateral branches (Scott 1903-4; Gillette and Ray 1981; Ferigolo 1985; Kalthoff 2011), and in *Proeutatus* the osteodentine core takes the form of an obliquely oriented oval (Scott 1903-4). *Euphractus* and other cingulates lack this osteodentine core, the central regions of their teeth occupied instead by a variably vascularized "modified orthodentine" (Ferigolo 1985; Gaudin and Wible 2006; Kalthoff 2011).

The occlusal surface of the first three lower molariforms in *H. floridanus* is quite variable. In some instances the teeth are nearly flat, contrasting with the more beveled crowns of the anterior upper molariforms – e.g., in m1 of UF 223813 and 275497 (L only), and m2 and m3 of UF 275498. Other are beveled (some only weakly, e.g., m2 of UF 224450; Figure 11), with a small, mesioventrally sloping anterior facet, usually occupying less than ¼ of the occlusal surface, and the remaining distal facet sloping distoventrally. The other molariforms have single, flat occlusal surfaces, as was the case with the upper posterior teeth. These occlusal surfaces are not horizontal, but inclined distoventrally, giving adjacent tooth crowns a stair-step appearance, as described above for the upper dentition. These occlusal surface patterns are, as far as can be determined, nearly identical in other pampatheres. *Proeutatus* also has beveled wear on the anterior teeth and flat surfaces on the posterior teeth (flat on m8-10 in FMH P13197; see also

allow for the reconstruction of soft tissues, especially the brain and associated cranial nerves and endocranial vasculature, as has recently been done (in part) for the pampathere *Pamphotherium humboldti* (Tambusso and Fariña 2015). Producing and describing detailed CT scans of the skull in *H. floridanus* were deemed beyond the scope of the present study, but are planned for the future. In addition, there is extensive postcranial and carapace material for this species that was not considered in this investigation, but will be the subject of planned future work.

It is particularly fortuitous that this description centers on *H. floridanus*, a taxon represented by such abundant and well preserved material, including at least 10 complete or nearly complete skulls from two sites of similar age in central Florida. As noted by Wible and Gaudin (2004), De Iuliis et al. (2014), and many others, all too often descriptions of fossil species are based on single (or even incomplete) specimens. Whereas this is often due to the limitations of the available material, it makes it difficult to account for intraspecific variation, to distinguish between species level distinctions and sexual dimorphism (e.g., McDonald 2006), or to assess the reliability of systematic characters based on fossil taxa. The present study, like other recent detailed analyses of xenarthran skull morphology (e.g., Wible and Gaudin 2004; Gaudin 2011; McAfee and Naples 2012; DeIuliis et al. 2014; Hautier et al. 2014; Gaudin et al. 2015), has revealed substantial variation in a variety of cranial features in *H. floridanus*. These features include the number, size and /or position of a variety of cranial foramina (anterior palatal foramen, maxillary foramen, minor palatine foramina, foramen for frontal diploc vein, ethmoid foramen, transverse canal foramen, foramina for rami temporalis, suprameatal foramen, hypoglossal foramen); the presence, size and shape of various processes (anteroventral process on premaxilla, lacrimal tubercle, ventral zygomatic process, postorbital process of jugal, orbito-auricularis crest, medial pterygoid process, circular boss on lateral wall of promontorium, medial

shelf of petrosal, coronoid process of mandible) or depressions (digastric fossa, tensor tympani fossa, fossa incudis); and the shape of other cranial (proportions of nasal bone, shape of anterior margin of premaxilla, shape of naso-frontal and jugal/squamosal sutures, shape of external nares and occipital exposure of mastoid) or dental features (e.g., outline of M4 and M5, shape of wear facets on M1).

Whereas the present study reveals a significant amount of intraspecific cranial variability in *H. floridanus*, it has also produced a long list of features that affirm previously hypothesized systematic relationships between this and other purportedly related taxa. Among these are features that are diagnostic of the taxon itself. The only diagnostic feature provided in the original diagnosis of the species by Robertson (1976) was the shape and orientation of the fourth upper molariform, and, as noted above, the shape of this tooth is variable among specimens of *H. floridanus*. Edmund (1987) distinguished this taxon based almost exclusively on size. Hulbert and Morgan (1993) conducted a more extensive analysis, looking at the taxonomic implications of size variation but also a series of qualitative postcranial and dental features for *Holmesina* specimens from Florida only, but they did not list any cranial characteristics that served to distinguish *H. floridanus* from the younger *H. septentrionalis*. The present study recognizes at least 11 distinct, meristic cranial features that may be diagnostic for *H. floridanus* (Table 5), further affirming its status as a distinct pampathere species, currently known only from the late Blancan NALMA of central Florida.

The description has also revealed a large number of characteristics that appear to distinguish the genus *Holmesina* from other pampatheres. As noted in the Introduction section of the present study, *Holmesina* is not recognized as a separate genus by McKenna and Bell (1997), and other authors have suggested the genus may be invalid (James 1957; Robertson

1976). Our description identifies more than a dozen potential diagnostic cranial features (Table 5), strongly affirming the monophyly of this genus, which includes species from both North and South America.

Perhaps the largest suite of features with systematic value are identified as potential synapomorphies of pampatheres as a group (Table 5). The pampatheres have long been recognized as a distinctive group of cingulates, with their flat-topped, bilobate posterior molariforms that are highly dissimilar to the teeth of other cingulates. However, there is less agreement on how this morphological uniqueness should be treated taxonomically, with debate centered on whether pampatheres should be placed in a subfamily Pampatheriinae, a subgroup of the extinct and extant armadillo family Dasypodidae, as was typically the case in traditional classifications (e.g., Hoffstetter 1958; Patterson et al. 1989), or considered a family in their own right, the Pampatheriidae, as they are listed in McKenna and Bell (1997) and in most recent papers (e.g., De Iuliis and Edmund 2002; Tambusso and Fariña 2015; Góis et al. 2015). It should be noted here that if pampatheres are placed in their own family, and if we accept their close relationship to glyptodonts (discussed below), both morphological (Gaudin and Wible 2006; Billet et al. 2011) and molecular phylogenies (Delsuc et al. 2016; Mitchell et al. 2016) would imply that this clade evolved from within armadillos. This in turn would make the family Dasypodidae, a taxon still widely employed in the mammalogical literature (e.g., Wilson and Reeder 2005; Vaughan et al. 2015), a paraphyletic group, necessitating the recognition of multiple armadillo families within “Dasypodidae.” Gibb et al. (2016) propose dividing the Cingulata into two families, Dasypodidae and Chlamyphoridae, the latter including the glyptodonts as a subfamily. It is unclear to us why one of the long-recognized subfamilies of armadillos (and indeed the smallest subfamily in terms of generic level diversity), the

Dasypodinae, is accorded family level status by Gibb et al. (2016), whereas the other three armadillo subfamilies (Euphractinae, Chlamyphorinae and Tolypeutinae) are lumped together, along with the extinct glyptodonts (Glyptodontinae), and presumably their close relatives the pampatheres (now Pampatheriinae), into a single family. It is certainly a minimalist approach to reordering family level diversity among cingulates, but to our mind it fails to adequately reflect the age, morphological disparity, and taxonomic diversity encompassed by this clade, and in particular, the Chlamyphoridae. Moreover, it appears inconsistent with the manner in which taxonomic diversity is distributed in the sister taxon to Cingulata, the Pilosa. It is particularly noteworthy that the Vermilingua, the youngest and least diverse of the three main xenarthran clades (including only four living species; McDonald et al. 2008; Gaudin and Croft 2015), is currently divided into two families. The sloths, which are also a younger radiation than the cingulates (at least as far as they are documented in the fossil record; Gaudin and Croft 2015) are currently arranged in five families (Gaudin 2004). We would therefore advocate recognition of all 4 extant subfamilies of armadillos, as well as the pampatheres and very diverse glyptodonts, respectively, as family level taxa, so that Cingulata would encompass seven families – Dasypodidae (following Gibb et al. 2016), Chlamyphoridae (following Gibb et al. 2016, but restricted to the members of the subfamily Chlamyphorinae, i.e., the living fairy armadillos), Euphractidae (for living euphractines plus their extinct kin), Tolypeutidae, Glyptodontidae, and Pampatheriidae. We suspect this is a better way to arrange cingulate diversity, however we recognize that it does not account for all the taxonomic difficulties posed by the group. For example, it would leave some extinct taxa (e.g., eutatine armadillos, and perhaps some extinct “euphractines” like *Prozaedyus* or *Macro euphractus*; see Gaudin and Wible 2006; Billet et al. 2011) with an unresolved family-level status.

The second largest list of putative synapomorphies recognized in this study support the alliance of pampatheres with the other clade of cingulate herbivores, the much more diverse and specialized glyptodonts (Table 5). An alliance of these two groups of large bodied herbivores was most prominently suggested by Bryan Patterson (Patterson and Pascual 1972; Patterson et al. 1989), and was confirmed by the subsequent cladistic phylogenetic studies of Engelmann (1985), Gaudin and Wible (2006), and Billet et al. (2011). The present study adds to the already extensive list of derived resemblances among these forms (Table 5). The studies by Gaudin and Wible (2006) and Billet et al. (2011) also suggest that the Miocene armadillo *Proeutatus* (Santacrucian SALMA) is the sister taxon to pampatheres plus glyptodonts. This armadillo has been hypothesized to share the herbivorous diet characteristic of pampatheres and glyptodonts (Vizcaíno et al. 2012 and references therein). Table 5 confirms that this relationship is supported by cranial features not directly related to mastication, e.g., features from the ear region.

Lastly, it should be noted that the present study identified a number of cranial features which are shared by some, but not all pampathere genera (e.g., M4 is bilobate in *Pampatherium* and *Kraglievich* but not *Holmesina*; m5 is reniform in *Pampatherium* and *Vassallia* but not *Holmesina*) and some features that appear to be apomorphies of pampatheres other than *Holmesina* (e.g., postorbital process of zygomatic arch on squamosal rather than the jugal, and loss of connection between zygomatic arch and nuchal crest in *Vassallia*). Clearly, and unsurprisingly, cranial data has much to contribute to our understanding of pampathere systematics. To our knowledge, no phylogenetic analysis of pampatheres has yet been performed, but we felt that such an analysis was beyond the scope of the present study, especially given the fact that much of the critical material is available only in South American museums. Nevertheless, such a study is clearly needed in the near future if we are to better

understand the evolution of this distinctive group of large cingulate herbivores, and their place in the history of Cingulata as a whole. Moreover, given their geographic distribution on both sides of the Isthmus of Panama, a better understanding of pampathere internal relationships might also yield insights into their role in the so-called Great American Biotic Interchange (GABI), the extensive exchange of taxa between North and South America that plays such a central role in the evolution of the mammalian fauna of these two continents.

CONCLUSION

The present study represents the first detailed, extensively illustrated, bone-by-bone description of pampathere cranial osteology, including reconstructions of sutural patterns and the position and content of the major cranial foramina. Due to the abundance of fossil material available for this late Pliocene – early Pleistocene species from Florida, we have been able to document extensive interspecific variation in a variety of cranial features. We have also identified a series of new cranial characteristics which appear to be diagnostic for *Holmesina floridanus*. Though the systematics of pampatheres is controversial, our study affirms the monophyly of the genus *Holmesina*, and provides additional characters that support the monophyly of pampatheres as a whole. We advocate the recognition of pampatheres as a distinct family Pampatheriidae within the large clade Cingulata. We also advocate for the recognition of their sister taxon, the glyptodonts, as a family level grouping Glyptodontidae, and for similar family level recognition for the extant cingulate clades historically assigned subfamily status, i.e, the Dasypodidae, Chlamyphoridae, Euphractidae, and Tolypeutidae. Lastly, this analysis highlights the need for further studies of pampatheres in general and *Holmesina floridanus* in particular, including

phylogenetic analyses of pampathere interrelationships, studies of *H. floridanus* postcrania and carapaces, and further studies of *H. floridanus* cranial anatomy using CT-scans.

ACKNOWLEDGMENTS

First and foremost, we thank Richard Hulbert and Jon Bloch of the Florida Museum of Natural History (University of Florida, Gainesville, FL), for all of their help in accessing the wonderful material of *Holmesina floridanus* on which this report is based. For access to other fossil and extant skeletal material used in this study, we thank B. Simpson, J. Flynn and K. Angielczyk of the Field Museum of Natural History (Chicago, IL), J. Wible of the Carnegie Museum of Natural History (Pittsburgh, PA), and W. Joyce and D. Brinkman of the Peabody Museum at Yale University (New Haven, CT). For the exceptional illustrations accompanying this paper, we thank the ever-talented Julia Morgan Scott, and we thank S. Chatzimanolis of the University of Tennessee at Chattanooga for his help in making the stereophotographs in Figure 8. We thank our anonymous reviewers for their insightful reviews of this manuscript.

LITERATURE CITED

- Abba AM, GH Cassini GH, Valverde G, Tilak M-K, Vizcaíno SF, M. Superina M, Delsuc F. 2015. Systematics of hairy armadillos and the taxonomic status of the Andean hairy armadillo (*Chaetophractus nationi*). *Journal of Mammalogy*, 96(4):673–689. DOI:10.1093/jmammal/gyv082
- Aguiar JM, Da Fonseca AB. 2008. Conservation status of the Xenarthra. In: Loughry WJ, Vizcaíno SF, eds. *Biology of the Xenarthra*. Gainesville: University of Florida Press, 215-231.

- 1907 Billet G, Hautier L, de Muizon C, Valentin X. 2011. Oldest cingulate skulls provide congruence
- 1908 between morphological and molecular scenarios of armadillo evolution. *Proceedings of*
- 1909 *the Royal Society of London, B. Biological Sciences*, 278:2791–2797. DOI:
- 1910 10.1098/rspb.2010.2443
- 1911 Bugge J. 1979. Cephalic arterial pattern in New World edentates and Old World pangolins with
- 1912 special reference to their phylogenetic relationships and taxonomy. *Acta Anatomica*,
- 1913 105(1):37–46.
- 1914 Cahn AR. 1922. *Chlamytherium septentrionalis*, a fossil edentate new to the fauna of Texas.
- 1915 *Journal of Mammalogy*, 3:22-24.
- 1916 Cartelle C, Bohórquez GA. 1985. *Pampatherium paulcouthoi*, uma nova espécie de tatu gigante
- 1917 da Bahia, Brasil (Edentata, Dasypodidae). *Revista Brasileira de Zoologia*, 2(4):229-254.
- 1918 Castellanos A. 1937. Anotaciones sobre las líneas filogenéticas de los clamiterios. *Publicaciones*
- 1919 *del Instituto Fisiografía y Geología, Universidad Nacional del Litoral, Rosario*
- 1920 *Argentina. Serie Técnica y Científica*, 8:1 -35.
- 1921 Clemente CD. 1985. *Gray's Anatomy*. Philadelphia: Lea and Febiger.
- 1922 Croft DA. 2016. *Horned Armadillos and Rafting Monkeys. The Fascinating Fossil Mammals of*
- 1923 *South America*. Bloomington: Indiana University Press.
- 1924 De Iuliis G, Edmund AG. 2002. *Vassallia maxima* Castellanos, 1946 (Mammalia: Xenarthra:
- 1925 Pampatheriidae), from Puerta del Corral Quemado (late Miocene to early Pliocene),
- 1926 Catamarca Province, Argentina. Pp. 49-64 in R. J. Emry (ed.), *Cenozoic Mammals of Land*
- 1927 *and Sea: Tributes to the Career of Clayton E. Ray*. Smithsonian Contributions to
- 1928 *Paleobiology* 93, 372 pp.

- 1929 De Iuliis G, Bargo MS, Vizcaíno SF. 2000. Variation in skull morphology and mastication in the
1930 fossil giant armadillos *Pampatherium* spp. and allied genera (Mammalia: Xenarthra:
1931 Pampatheriidae), with comments on their systematics and distribution. *Journal of*
1932 *Vertebrate Paleontology*, 20(4):743-754.
- 1933 De Iuliis G, Gaudin TJ, Vicars MP. 2011. A new genus and species of nothrotheriid sloth
1934 (Xenarthra, Tardigrada, Nothrotheriidae) from the late Miocene (Huayquerian) of Peru.
1935 *Palaeontology*, 54:171–205. DOI: 10.1111/j.1475-4983.2010.01001.x
- 1936 De Iuliis G, Pujos F, Toledo N, Bargo MS, Vizcaíno SF. 2014. *Eucholoeops* Ameghino, 1887
1937 (Xenarthra, Tardigrada, Megalonychidae) from the Santa Cruz Formation, Argentine
1938 Patagonia: implications for the systematics of Santacrucian sloths. *Geodiversitas*, 36:
1939 209–255. DOI: 10.5252/g2014n2a2
- 1940 Delsuc F, Gibb GC, Kuch M, Billet G, Hautier L, Southon J, Rouillard JM, Fernicola JC,
1941 Vizcaíno SF, MacPhee RD, Poinar HN. 2016. The phylogenetic affinities of the extinct
1942 glyptodonts. *Current Biology*, 26(4): R155-R156. DOI: 10.1016/j.cub.2016.01.039
- 1943 Edmund G. 1985. The fossil giant armadillos of North America (Pampatheriinae, Xenarthra _
1944 Edentata). In: Montgomery GG, ed. *The Ecology and Evolution of Armadillos, Sloths,*
1945 *and Vermilinguas*. Washington, DC: Smithsonian Institution Press, 83-93.
- 1946 Edmund AG. 1987. Evolution of the genus *Holmesina* (Pampatheriidae, Mammalia) in Florida,
1947 with remarks on taxonomy and distribution. *Pearce-Sellards Series, Texas Memorial*
1948 *Museum*, 45:1-20.
- 1949 Edmund AG, Theodor JM. 1997. A giant new pampatheriid armadillo. In: Kay RF, Madden RH,
1950 Cifelli RL, Flynn JJ, eds. *Vertebrate Paleontology in the Neotropics: The Miocene Fauna*
1951 *of La Venta, Colombia*. Washington, DC: Smithsonian Institution Press, 227-332.

- 1952 Engelmann G. 1985. The phylogeny of the Xenarthra. In: Montgomery GG, ed. *The Ecology and*
1953 *Evolution of Armadillos, Sloths, and Vermilinguas*. Washington, DC: Smithsonian
1954 Institution Press, 51-63
- 1955 Evans HE, Christiansen GC. 1979. *Miller's Anatomy of the Dog, 2nd edition*. Philadelphia: W.B.
1956 Saunders.
- 1957 Feijó A, Cordeiro-Estrela P. 2016. Taxonomic revision of the *Dasypus kappleri* complex, with
1958 revalidations of *Dasypus pastasae* (Thomas, 1901) and *Dasypus beniensis* Lönnberg,
1959 1942 (Cingulata, Dasypodidae). *Zootaxa*, 4170(2):271-297. DOI:
1960 10.11646/zootaxa.4170.2.3
- 1961 Ferigolo J. 1985. Evolutionary trends of the histological pattern in the teeth of Edentata
1962 (Xenarthra). *Archives of Oral Biology*, 30(1):71–82.
- 1963 Fernicola JC, Toledo N, Bargo MS, Vizcaíno SF. 2012. A neomorphic ossification of the nasal
1964 cartilages and the structure of paranasal sinus system of the glyptodont *Neosclerocalyptus*
1965 Paula Couto 1957 (Mammalia, Xenarthra). *Palaeontologia Electronica*, 15(3):27A, 22p.
1966 palaeo-electronica.org/content/2012-issue-3-articles/305-glyptodont-nasal-anatomy.
- 1967 Fernicola JC, Vizcaíno SF, Fariña RA. 2008. The evolution of armored xenarthrans and a
1968 phylogeny of glyptodonts. In: Loughry WJ, Vizcaíno SF, eds. *Biology of the Xenarthra*.
1969 Gainesville: University of Florida Press, 79-85.
- 1970 Frost DR, Wozencraft WC, Hoffmann RS. 1991. Phylogenetic relationships of hedgehogs and
1971 gymnures (Mammalia: Insectivora: Erinaceidae). *Smithsonian Contributions to Zoology*,
1972 518: 1–69.
- 1973 Gaudin TJ. 1995. The ear region of edentates and the phylogeny of the Tardigrada (Mammalia,
1974 Xenarthra). *Journal of Vertebrate Paleontology*, 15(3): 672-705.

- 1975 Gaudin TJ. 2004. Phylogenetic relationships among sloths (Mammalia, Xenarthra, Tardigrada):
1976 the craniodental evidence. *Zoological Journal of the Linnean Society*, 140(2): 255-305.
- 1977 Gaudin TJ. 2011. On the osteology of the auditory region and orbital wall in the extinct West
1978 Indian sloth genus *Neocnus* (Megalonychidae, Xenarthra, Placentalia). *Annals of the*
1979 *Carnegie Museum of Natural History*, 80(1):5-28.
- 1980 Gaudin TJ, Croft DA. 2015. Paleogene Xenarthra and the evolution of South American
1981 mammals. *Journal of Mammalogy*, special feature, 96(4):622-634.
1982 DOI:10.1093/jmammal/gyv073
- 1983 Gaudin TJ, McDonald HG. 2008. Morphology-based investigations of the phylogenetic
1984 relationships among extant and fossil Xenarthrans. In: Loughry WJ, Vizcaíno SF, eds.
1985 *Biology of the Xenarthra*. Gainesville: University of Florida Press, 24-36.
- 1986 Gaudin TJ, Wible JR. 2006. Chapter 6. The phylogeny of living and extinct armadillos
1987 (Mammalia, Xenarthra, Cingulata): a craniodental analysis. In: Carrano MT, Gaudin TJ,
1988 Blob, RW, Wible, JR, eds. *Amniote Paleobiology: Perspectives on the Evolution of*
1989 *Mammals, Birds, and Reptiles*. Chicago:University of Chicago Press, 153-198.
- 1990 Gaudin TJ, DeIuliis G, Toledo N, Pujos F. 2015. The basicranium and orbital region of the early
1991 Miocene *Eucholoeops ingens* Ameghino, 1887 (Xenarthra, Pilosa, Megalonychidae).
1992 *Ameghiniana*, 52:226-240. DOI: 10.5710/AMGH.04.12.2014.2755
- 1993 Gaudin TJ, Emry RJ, Morris J. 2016. Description of the skeletal anatomy of the North American
1994 pangolin *Patriomanis americana* (Mammalia, Pholidota) from the latest Eocene of
1995 Wyoming (USA). *Smithsonian Contributions to Paleobiology*, 98:1-103.

- 1996 Gaudin TJ, Wible JR, Hopson JA, Turnbull WD. 1996. Reexamination of the morphological
1997 evidence for the Cohort Epitheria (Mammalia, Eutheria). *Journal of Mammalian*
1998 *Evolution*, 3(1): 31-79.
- 1999 Gibb GC, Condamine FL, Kuch M., Enk J, Moraes-Barros N, Superina M, Poinar HN, Delsuc F.
2000 (2016). Shotgun mitogenomics provides a reference phylogenetic framework and
2001 timescale for living xenarthrans. *Molecular Biology & Evolution*, 33(3):621–642.
2002 DOI:10.1093/molbev/msv250.
- 2003 Gillette DD, Ray CE. 1981. Glyptodonts of North America. *Smithsonian Contributions to*
2004 *Paleobiology*, 40:1–255.
- 2005 Góis F, González Ruiz LR, Scillato-Yané GJ, Soibelzon E. 2015. A peculiar new Pampatheriidae
2006 (Mammalia: Xenarthra: Cingulata) from the Pleistocene of Argentina and comments on
2007 Pampatheriidae diversity. *PLoS ONE*, 10(6): e0128296.
2008 DOI:10.1371/journal.pone.0128296
- 2009 Guth C. 1961. La région temporelle des Édentés. D. Phil. Thesis, L'Université de Paris.
- 2010 Hautier L, Billet G, Eastwood B, Lane J. 2014. Patterns of morphological variation of extant
2011 sloth skulls and their implication for future conservation efforts. *The Anatomical Record*,
2012 297:979–1008. DOI: 10.1002/ar.22916
- 2013 Hoffstetter R. 1958. Xenarthra. In: Piveteau P, ed. *Traité de Paléontologie, Vol. 2, no. 6*,
2014 *Mammifères Évolution*. Paris: Masson et Cie, 535– 636.
- 2015 Hulbert RC, Morgan GS. 1993. Quantitative and qualitative evolution in the giant armadillo
2016 *Holmesina* (Edentata: Pampatheriidae) in Florida. In: Martin RA, Barnosky AD, eds.
2017 *Morphological Change in Quaternary Mammals of North America*. New York: Columbia
2018 University Press, 134-177.

- 2019 Hulbert RC, Webb SD. 2001. Chapter 10 – Mammalia 2, Xenarthrans. In: Hulbert RC, ed. *The*
2020 *Fossil Vertebrates of Florida*. Gainesville: University Press of Florida, 175-187.
- 2021 James G. 1957. An edentate from the Pleistocene of Texas. *Journal of Paleontology*, 31(4):796-
2022 808.
- 2023 Kalthoff DC. 2011. Microstructure of dental hard tissues in fossil and recent Xenarthrans
2024 (Mammalia: Folivora and Cingulata). *Journal of Morphology*, 272:641–661. DOI:
2025 10.1002/jmor.10937
- 2026 MacIntyre GT. 1972. The trisulcate petrosal pattern of mammals. *Evolutionary Biology*, 6:275–
2027 303.
- 2028 McAfee RK, Naples VL. 2012. Notice on the occurrence of supernumerary teeth in the two-toed
2029 sloths *Choloepus didactylus* and *C. hoffmanni*. *Mastozoología Neotropical*, 19: 339–344.
- 2030 McDonald HG. 2006. Sexual dimorphism in the skull of Harlan’s ground sloth. *Contributions in*
2031 *Science, Natural History Museum of Los Angeles County*, 510: 1-9.
- 2032 McDonald HG., Vizcaíno SF, Bargo MS. 2008. Skeletal anatomy and the fossil history of the
2033 Vermilingua. In: Loughry WJ, Vizcaíno SF, eds. *Biology of the Xenarthra*. Gainesville:
2034 University of Florida Press, 64-78.
- 2035 McDonough, C. M., and W. J. Loughry. 2008. Behavioral ecology of armadillos. In: Loughry
2036 WJ, Vizcaíno SF, eds. *Biology of the Xenarthra*. Gainesville: University of Florida Press,
2037 281-293.
- 2038 McKenna MC, Bell SK. 1997. *Classification of Mammals Above the Species Level*. New York:
2039 Columbia University Press.
- 2040 Mitchell KJ., Scanferla A, Soibelzon E, Bonini R, Ochoa J, Cooper A. 2016. Ancient DNA from
2041 the extinct South American giant glyptodont *Doedicurus* sp. (Xenarthra: Glyptodontidae)

- 2042 reveals that glyptodonts evolved from Eocene armadillos. *Molecular Ecology*, 25(14):
- 2043 3499-3508. DOI: 10.1111/mec.13695
- 2044 Novacek MJ. 1986. The skull of leptictid insectivorans and the higher-level classification of
- 2045 eutherian mammals. *Bulletin of the American Museum of Natural History*, 183:1–112.
- 2046 Novacek MJ. 1993. Patterns of diversity in the mammalian skull. In: Hanken J, Hall BK, eds.).
- 2047 *The Skull, Volume 2, Patterns of Structural and Systematic Diversity*. Chicago:
- 2048 University of Chicago Press, 438–545.
- 2049 Novacek MJ, Wyss AR. 1986. Higher-level relationships of the recent eutherian orders:
- 2050 morphological evidence. *Cladistics*, 2:257–287.
- 2051 O’Leary MA, Bloch JJ, Flynn JJ, Gaudin TJ, Giallombardo A, Giannini NP, Goldberg SL,
- 2052 Kraatz BP, Luo Z-X, Meng J, Ni X, Novacek MJ, Perini FA, Randall Z, Rougier GW,
- 2053 Sargis EJ, Silcox MT, Simmons NB, Spaulding M, Velazco PM, Weksler M, Wible JR,
- 2054 Cirranello AL. 2013. The placental mammal ancestor and the post-KPg radiation of
- 2055 placentals. *Science*, 339:662–667. DOI: 10.1126/science.1229237
- 2056 Patterson B, Pascual R. 1972. The fossil mammal fauna of South America. In: Keast A, Erk FC,
- 2057 Glass B, eds. *Evolution, Mammals and the Southern Continents*. Albany: State University
- 2058 of New York Press, 247-309.
- 2059 Patterson B, Segall W, Turnbull WD. 1989. The ear region in xenarthrans (= Edentata,
- 2060 Mammalia). Part I. Cingulates. *Fieldiana, Geology, n.s.*, 18:1–46.
- 2061 Patterson B, Segall W, Turnbull WD, Gaudin TJ. 1992. The ear region in xenarthrans (=
- 2062 Edentata, Mammalia). Part II. Pilosa (sloths, anteaters), palaeonodons, and a miscellany.
- 2063 *Fieldiana, Geology, n.s.*, 24:1–79.

- 2064 Robertson JS. 1976. Latest Pliocene mammals from Haile XV A, Alachua County, Florida.
- 2065 *Bulletin of the Florida State Museum, Biological Sciences*, 20(3):111-186.
- 2066 Rose KD, Emry RJ. 1993. Relationships of Xenarthra, Pholidota, and fossil ‘Edentates’: the
- 2067 morphological evidence. In: Szalay FS, Novacek MJ, McKenna MC, eds. *Mammal*
- 2068 *Phylogeny. Volume 2: Placentals*. New York: Springer-Verlag, 81–102.
- 2069 Scott WB. 1903–1904. Mammalia of the Santa Cruz Beds. Part 1: Edentata. *Reports of the*
- 2070 *Princeton Expeditions to Patagonia*, 5:1–364.
- 2071 Simpson GG. 1930. *Holmesina septentrionalis*, extinct giant armadillo of Florida. *American*
- 2072 *Museum Novitates*, 442:1-10.
- 2073 Simpson GG. 1948. The beginning of the age of mammals in South America. Part 1.
- 2074 Introduction. Systematics: Marsupialia, Edentata, Condylarthra, Litopterna, and
- 2075 Notioprogonia. *Bulletin of the American Museum of Natural History*, 91:1–227.
- 2076 Smith KK, Redford KH. 1990. The anatomy and function of the feeding apparatus in two
- 2077 armadillos (Dasypoda): anatomy is not destiny. *Journal of Zoology*, 222:27-47.
- 2078 Stock C. 1925. Cenozoic gravigrade edentates of western North America. *Carnegie Institute of*
- 2079 *Washington Publications*, 331:1–206.
- 2080 Tambusso PS, Fariña RA. 2015. Digital endocranial cast of *Pamphatherium humboldtii*
- 2081 (Xenarthra, Cingulata) from the Late Pleistocene of Uruguay. *Swiss Journal of*
- 2082 *Palaeontology*, 134(1):109-116. DOI: 10.1007/s13358-015-0070-5
- 2083 Vaughan TA, Ryan JM, Czaplewski NJ. 2015. *Mammalogy. 6th ed*. Burlington, MA: Jones and
- 2084 Bartlett Publishers.

- 2085 Vizcaino SF, De Iuliis G, Bargo MS. 1998. Skull shape, masticatory apparatus and diet of
2086 *Vassallia* and *Holmesina* (Mammalia: Xenarthra: Pamphathiidae): when anatomy
2087 constrains destiny. *Journal of Mammalian Evolution*, 5(4):291–322.
- 2088 Vizcaino SF, Fernicola JC, Bargo MS. 2012. Paleobiology of Santacrucian glyptodonts and
2089 armadillos. In: Vizcaino SF, Kay RF, Bargo MS, eds. *Early Miocene Paleobiology in*
2090 *Patagonia*. Cambridge: Cambridge University Press, 194-215.
- 2091 Wible JR. 1990. Petrosals of Late Cretaceous marsupials from North America, and a cladistic
2092 analysis of the petrosal in therian mammals. *Journal of Vertebrate Paleontology*,
2093 10(2):183–205.
- 2094 Wible JR. 2003. On the osteology of the short-tailed opossum *Monodelphis brevicaudata*
2095 (Didelphidae, Marsupialia). *Annals of the Carnegie Museum*, 72:137–202.
- 2096 Wible JR. 2008. On the cranial osteology of the Hispaniolan solenodon, *Solenodon paradoxus*
2097 Brandt, 1833 (Mammalia, Lipotyphla, Solenodontidae). *Annals of the Carnegie Museum*,
2098 70(3):321–402.
- 2099 Wible JR. 2010. Petrosal anatomy of the nine-banded armadillo, *Dasypus novemcinctus*
2100 Linnaeus, 1758 (Placentalia: Xenarthra: Dasypodidae). *Annals of Carnegie Museum*,
2101 79:1–28.
- 2102 Wible JR. 2011. On the treeshrew skull (Mammalia, Placentalia, Scandentia). *Annals of*
2103 *Carnegie Museum*, 79: 149–230.
- 2104 Wible JR, Gaudin TJ. 2004. On the cranial osteology of the yellow armadillo *Euphractus*
2105 *sexcinctus* (Dasypodidae, Xenarthra, Placentalia). *Annals of Carnegie Museum*,
2106 73(3):117–196.

2107 Wible JR, Novacek MJ, Rougier GW. 2004. New data on the skull and dentition in the
 2108 Mongolian Late Cretaceous mammal *Zalambdalestes*. *Bulletin of the American Museum*
 2109 *of Natural History*, 281:1–144.

2110 Wible JR, Rougier GW, Novacek MJ, Asher RJ. 2009. The eutherian mammal *Maelestes*
 2111 *gobiensis* from the Late Cretaceous of Mongolia and the phylogeny of Cretaceous
 2112 Eutheria. *Bulletin of the American Museum of Natural History*, 327:1–123.

2113 Wilson RW, Reeder DM. 2005. *Mammal Species of the World: A Taxonomic and Geographic*
 2114 *Reference*. Baltimore: Johns Hopkins University Press.

2115

2116

FIGURE CAPTIONS

Figure 1. Skull of *Holmesina floridanus* in dorsal view. A, UF 191448; B, UF 248500. Scale bar = 5 cm.

Figure 2. Reconstruction of the skull of *Holmesina floridanus* in dorsal view. Abbreviations: **f**, frontal; **frt**, foramina for rami temporalis; **j**, jugal; **l**, lacrimal; **lf**, lacrimal foramen; **mx**, maxilla; **n**, nasal; **nc**, nuchal crest; **p**, parietal; **pm**, premaxilla; **pop**, paroccipital process of petrosal (= mastoid process of Patterson et al. 1989); **popf**, postorbital process of frontal; **popj**, postorbital process of jugal; **sq**, squamosal; **zp**, zygomatic process of squamosal.

Figure 3. Skull of *Holmesina floridanus* in lateral view. A, UF 191448 in right lateral view; B, UF 248500 in right lateral view; C, UF 248500 in left lateral view. Scale bar = 5 cm.

Figure 4. Reconstruction of the skull of *Holmesina floridanus* in right lateral view. Abbreviations: **as**, alisphenoid; **bo**, basioccipital; **bs**, basisphenoid; **dpj**, descending process of jugal; **f**, frontal; **fdv**, foramen for frontal diploic vein; **fo**, foramen ovale; **frt**, foramina for rami temporalis; **iof**, infraorbital foramen; **j**, jugal; **l**, lacrimal; **lf**, lacrimal foramen; **M1**, first upper molariform tooth; **M9**, ninth upper molariform tooth; **mx**, maxilla; **n**, nasal; **nc**, nuchal crest; **oc**, occipital; **occ**, occipital condyle; **p**, parietal; **pm**, premaxilla; **pop**, paroccipital process of petrosal (= mastoid process of Patterson et al. 1989); **pt**, pterygoid; **sq**, squamosal; **zp**, zygomatic process of squamosal.

2140

2141 Figure 5. Skull of *Holmesina floridanus* in ventral view. A, UF 191448; B, UF 248500. Scale bar
2142 = 5 cm.

2143

2144 Figure 6. Reconstruction of the skull of *Holmesina floridanus* in ventral view. Abbreviations:

2145 **apf**, anterior palatal foramen; **as**, alisphenoid; **bo**, basioccipital; **bs**, basisphenoid; **cf**,
2146 carotid foramen; **dpj**, descending process of jugal; **eo**, exoccipital; **fdv**, foramen for
2147 frontal diploic vein; **fm**, foramen magnum; **fo**, foramen ovale; **gf**, glenoid fossa; **hf**,
2148 hypoglossal foramen; **iof**, infraorbital foramen; **jf**, jugular foramen; **M1**, first upper
2149 molariform tooth; **M9**, ninth upper molariform tooth; **mpf**, minor palatine foramen; **mx**,
2150 maxilla; **n**, nasal; **oc**, occipital; **occ**, occipital condyle; **pal**, palatine; **pcp**, paracondylar
2151 process of exoccipital (=paroccipital process of Patterson et al. 1989); **pgf**, postglenoid
2152 foramen; **pgp**, postglenoid process; **pm**, premaxilla; **pop**, paroccipital process of petrosal
2153 (= mastoid process of Patterson et al. 1989); **popf**, postorbital process of frontal; **popj**,
2154 postorbital process of jugal; **pr**, promontorium of petrosal; **prs**, presphenoid; **pt**,
2155 pterygoid; **zp**, zygomatic process of squamosal; **zpm**, zygomatic process of maxilla.
2156

2157 Figure 7. Reconstruction of right orbital wall of *Holmesina floridanus* in lateral view. Cross-

2158 hatched surfaces indicate where zygomatic arch is “cut.” Abbreviations: **as**, alisphenoid;
2159 **bo**, basioccipital; **bs**, basisphenoid; **cf**, carotid foramen; **cpf**, caudal palatine foramen; **ef**,
2160 ethmoid foramen; **f**, frontal; **fdv**, foramen for frontal diploic vein; **fo**, foramen ovale;
2161 **fr/sof**, fused foramen rotundum and sphenorbital fissure; **ftr**, foramina for rami
2162 temporalis; **fv**, fenestra vestibuli; **iof**, infraorbital foramen; **j**, jugal; **l**, lacrimal; **lf**,

lacrimal foramen; **lfe**, lacrimal fenestra; **lopc**, lateral opening of pterygoid canal; **M9**, ninth upper molariform tooth; **mx**, maxilla; **mx****f**, maxillary foramen; **n**, nasal; **of**, optic foramen; **os**, orbitosphenoid; **p**, parietal; **pgf**, postglenoid foramen; **pgp**, postglenoid process; **pop**, paroccipital process of petrosal (= mastoid process of Patterson et al. 1989); **pr**, promontorium of petrosal; **pt**, pterygoid; **ptp**, post-tympanic process of squamosal; **spf**, sphenopalatine foramen; **sq**, squamosal; **tcf**, transverse canal foramen; **zp**, zygomatic process of squamosal.

Figure 8. Stereophotographs of right auditory region of *Holmesina floridanus* (UF 248500) in ventral view. Abbreviations: **aptt**, anteroventral process of tegmen tympani (= processus crista facialis); **as**, alisphenoid; **bb**, bony bridge between tympanohyal and crista interfenestralis; **bo**, basioccipital; **bs**, basisphenoid; **cf**, carotid foramen; **ci**, crista interfenestralis; **cp**, crista parotica; **ctpp**, caudal tympanic process of petrosal; **eam**, external auditory meatus; **egp**, entoglenoid process; **eo**, exoccipital; **fc**, fenestra cochleae; **fi**, ridge immediately ventral to fossa incudis; **fm**, foramen magnum; **fo**, foramen ovale; **fs**, facial sulcus; **gf**, glenoid fossa; **hf**, hypoglossal foramen; **jf**, jugular foramen; **occ**, occipital condyle; **pcp**, paracondylar process of exoccipital (=paroccipital process of Patterson et al. 1989); **pe**, petrosal; **pgf**, postglenoid foramen; **pgp**, postglenoid process; **pop**, paroccipital process of petrosal (= mastoid process of Patterson et al. 1989); **pr**, promontorium of petrosal; **sq**, squamosal; **stmf**, stylomastoid foramen; **th**, tympanohyal; **tff**, tensor tympani fossa on epitympanic wing of petrosal; **zp**, zygomatic process of squamosal. Scale bar = 1 cm. Photos by S. Chatzimanolis and T. Gaudin.

Figure 9. Isolated left petrosal of *Holmesina floridanus* (UF 248500) in A, B, ventrolateral; C, D, ventral; E, F, lateral; and G, H, medial views. Abbreviations: **aptt**, anteroventral process of tegmen tympani (= processus crista facialis); **av**, aqueductus vestibuli; **bof**, basioccipital facet; **ci**, crista interfenestralis; **coc**, cochlear canaliculus; **cp**, crista parotica; **crp**, crista petrosal; **ctpp**, caudal tympanic process of petrosal; **er**, epitympanic recess; **ew**, epitympanic wing; **fc**, fenestra cochleae; **ff**, facial foramen; **fs**, facial sulcus; **fsi**, foramen singulare; **fv**, fenestra vestibuli; **gps**, sulcus for greater petrosal nerve; **iam**, internal acoustic meatus; **iva**, inferior vestibular area; **pfc**, prefacial commissure; **pop**, paroccipital process of petrosal (= mastoid process of Patterson et al. 1989); **pr**, promontorium of petrosal; **rpp**, rostral process of petrosal; **saf**, subarcuate fossa; **sct**, spiral cribriform tract; **sf**, stapedius fossa; **stmn**, stylomastoid notch; **sva**, superior vestibular area; **tc**, transverse crest; **th**, tympanohyal; **ts**, triangular shelf (=roof of post-promontorial sinus. Scale bar = 1 cm.

Figure 10. Skull of *Holmesina floridanus* in posterior view. A, UF 191448; B, Reconstruction. Abbreviations: **bo**, basioccipital; **dcf**, dorsal condyloid fossa; **dgf**, digastric fossa; **eo**, exoccipital; **eoc**, external occipital crest; **eocc**, exoccipital crest; **fm**, foramen magnum; **nc**, nuchal crest; **oc**, occipital; **occ**, occipital condyle; **og**, groove for occipital artery; **me**, mastoid exposure of petrosal; **pcp**, paracondylar process of exoccipital (=paroccipital process of Patterson et al. 1989); **ptc**, posttemporal canal; **so**, supraoccipital; **sq**, squamosal. Scale bar = 5 cm.

2208 Figure 11. Left mandible of *Holmesina floridanus* (UF 224450) in A, lateral; B, occlusal; and, C,
 2209 medial views. Abbreviations: **ap**, angular process; **cnc**, condyloid crest; **cop**, coronoid
 2210 process; **crc**, coronoid crest; **hr**, horizontal ramus of mandible; **imf**, intermuscular fossa;
 2211 **lcc**, lateral coronoid crest; **m1**, first lower molariform tooth; **m6**, sixth lower molariform
 2212 tooth; **m7**, seventh lower molariform tooth; **maf**, masseteric fossa; **mco**, mandibular
 2213 condyle; **mf**, mental foramen; **maf**, mandibular foramen; **ms**, mandibular symphysis.
 2214 Scale bar = 5 cm.

2215

Table 1 (on next page)

Tables 1. Skull measurements for *Holmesina floridanus* and related taxa.

All measurements reported in millimeters (mm); those reported to the nearest tenth of a millimeter are direct measurements, those rounded to the nearest integer are taken from literature sources or from photographs taken by TJG. Numbers in square brackets are scaled to Greatest Skull Length (GSL)

- 1 Table 1. Skull measurements for *Holmesina floridanus* and related taxa. All measurements reported in millimeters (mm); those
- 2 reported to the nearest tenth of a millimeter are direct measurements, those rounded to the nearest integer are taken from literature
- 3 sources or from photographs taken by TJG. Numbers in square brackets are scaled to Greatest Skull Length (GSL).
- 4

Measurement Description	<i>Holmesina floridanus</i> UF 248500	<i>Holmesina floridanus</i> UF 191448	<i>Holmesina septentrio- nalis</i> UF 234224	<i>Vassalia maxima</i> FMNH P14424	<i>Propalaeo- hoplophorus australis</i> YPMPU 15007	<i>Proeutatus oenophorus</i> FMNH P13197	<i>Euphractus sexcinctus</i> UTCM 1491
Greatest Skull Length (GSL)	227.6*	249.1	293.7	248.0	158.7	117.8*	119.8
Maximum nasal ln	89.9 [0.39]	107.9 [0.43]	134.0 [0.46]	117.0 [0.47]	45 ^c [0.28]	47.9 [0.41]	42.6 [0.36]
Nasal wd at midpoint	35.6	34.9	38	41	23 ^c	10.6	15.4
Ratio nasal width to length	0.40	0.32	0.28	0.35	0.51	0.22	0.36
Rostrum ln (measured from anterior orbital rim)	110.5 [0.49]	124.9 [0.50]	142 [0.48]	117.0 [0.47]	45.2 [0.28]	65* [0.30]	60.1 [0.50]
Premaxilla/nasal suture ln	19.2 [0.08]	21.1 [0.08]	-	-	6.2 ^c [0.04]	13.1 [0.11]	17.6 [0.15]
Mesiodistal ln/ max wd of upper molariforms:	7.0/ 5.5	-	10/ 6	6.8/ 4.5 ^b	n	2.9/ 1.8	4.4/ 2.3
M1							
M2	7.5/ 6.1	-	13/ 9	8.0/ 5.5 ^b	3/ 3.5 ^d	3.4/ 2.1	4.8/ 2.4
M3	9.0/ 6.7	9.9/ 6.4	15/ 8	8.5/ 6.1 ^b	5.5/ 4 ^d	4.4/ 2.7	4.8/ 3.1
M4	10.7/ 7.1	10.3/ 6.8	16/ 8	14.5/ 6.6 ^b	9/ 4 ^d	5.5/ 3.4	5.4/ 3.4
M5	15.9/ 8.3	16.7/ 8.6	18/ 10	18.5/ 8.0 ^b	11/ 4.5 ^d	5.3/ 4.7	5.7/ 3.9
M6	16.8/ 8.7	-	22/ 10	19.0/ 8.6 ^b	12/ 6 ^d	5.2/ 5.0	6.0/ 4.5
M7	15.3/ 8.1	15.0/ 7.8	23/ 11	17.5/ 8.5 ^b	12.5/ 7 ^d	4.9/ 4.6	5.6/ 4.5
M8	13.3/ 7.7	-	21/ 9 ^a	16.7/ 7.5 ^b	12.5/ 7 ^d	4.3/ 4.7	5.3/ 4.0
M9	9.8/ 5.8	-	20/ 8 ^a	13.7/ 7.0 ^b	10.5/ 7 ^d	3.2/ 3.6	4.8/ 2.9
Mean ratio of upper	1.61	-	1.99	1.92	1.75	1.28	1.56

molariform ln/wd							
Palatal ln (in midline)	143.6 [0.63]	163.0 [0.65]	-	146 [0.59]	104 ^d [0.65]	64.0 [0.54]	68.0 [0.57]
Min interpterygoid wd	16.7 [0.07]	17.8 [0.07]	-	12 [0.05]	14 [0.09]	8.1 [0.07]	8.1 [0.07]
Max zygomatic wd	121.1 [0.53]	122.9 [0.49]	-	138 ^b [0.56]	118 [0.74]	70.2 [0.60]	65.6 [0.55]
Min interorbital wd	65.6 [0.29]	76.2 [0.31]	89 [0.30]	79 ^b [0.32]	54 [0.34]	42.5 [0.36]	38.5 [0.32]
Min postorbital wd	38.7 [0.17]	44.3 [0.18]	56 [0.19]	52 ^b [0.21]	28 [0.09]	27.6 [0.23]	27.5 [0.23]
Max wd of glenoid fossa in ventral view (measured along glenoid's long axis)	23.4	23.3	-	32	31 ^e	8.4	9.8
Max anteroposterior ln of glenoid in ventral view	14.9	11.1	17	12	11 ^e	8.0	9.8
Ratio of glenoid wd to ln	1.57	2.10	-	2.7	2.82	1.05	1.00
Postglenoid skull ln	43.5 [0.19]	35.8 [0.14]	47 [0.16]	57 [0.23]	14 [0.09]	17.1 [0.15]	20.5 [0.17]
Max wd of occipital condyles in ventral view (measured along condyle's long axis)	21.7	24	24	25	61	11.4	9.6
Max anteroposterior ln of condyles in ventral view	13.0	14.2	16	15	41	9.5	7.3
Ratio of occipital condyle wd to ln	1.67	1.69	1.5	1.67	1.48	1.2	1.3
Wd of occiput (measured at base of supraoccipital)	73.7	73.5	86	97 ^b	63	52.1	45.6
Max dp of occiput in midline (including ventral edge of foramen magnum)	72.5	70.5	83	67	53	36.2	32.9
Ratio of wd to dp	1.02	1.04	1.04	1.44	1.19	1.44	1.39

6 Abbreviations: “–” = data unavailable; dp = dorsoventral depth; ln = anteroposterior length, Max = maximum; Min = minimum; n =
7 data not applicable; wd = transverse width.
8 *Estimated due to skull breakage; ^a Data from UF 889, multiplied by 0.96 to account for size difference between UF 889 and UF
9 234224; ^b Data from De Iuliis and Edmund (2002); ^c Data from YPMPU 15291; ^d Data from Scott (1903-4), who measured YPMPU
10 15212; ^e Data from FMNH P13205.

Table 2(on next page)

Table 2. Skull measurements for additional specimens of *Holmesina floridanus*.

All measurements reported in millimeters (mm). Numbers in square brackets are scaled to Greatest Skull Length (GSL).

1 Table 2. Skull measurements for additional specimens of *Holmesina floridanus*. All measurements reported in millimeters (mm).

2 Numbers in square brackets are scaled to Greatest Skull Length (GSL).

3

Measurement Description	<i>Holmesina floridanus</i> UF 223813	UF 275496	UF 275497	UF 275498	UF 285000	UF 293000
Greatest Skull Length (GSL)	256*	237.8	-	223*	239.5	-
Maximum nasal ln	81 [0.32]	85.4 [0.36]	69.7	70.0 [0.34]	85.1 [0.36]	88.0
Nasal wd at midpoint	34.4	35.0	33.8	34.2	37.8	35.0
Ratio nasal width to length	0.42	0.41	0.48	0.49	0.44	0.40
Rostrum ln (measured from anterior orbital rim)	122 [0.48]	111 [0.47]	106	103 [0.46]	113 [0.47]	104
Premaxilla/nasal suture ln	-	18.0 [0.08]	19.8	22.3 [0.10]	17.9 [0.07]	17.4
Mesiodistal ln/ max wd of upper molariforms:						
M1	7.1/ 5.4	6.0/ 5.7	-	6.8/ 5.5	5.9/ 5.8	6.9/ 4.3
M2	8.2/ 5.8	-	-	7.9/ 5.6	7.9/ 6.1	8.0/ 4.8
M3	9.5/ 6.1	9.7/ 6.1	-	10.4/ 6.3	9.8/ 6.1	10.2/ 5.4
M4	11.7/ 7.0	11.3/ 7.2	-	11.5/ 7.1	12.3/ 6.7	11.7/ 6.0
M5	16.0/ 9.1	15.6/ 8.7	13*	16.6/ 8.8	15.1/ 8.4	16.6/ 8.0
M6	16.8/ 8.5	16.9/ 8.9	15.7/ 7.6	18.7/ 9.0	17.2/ 8.3	17.9/ 7.9
M7	15.4/ 8.0	15.5/ 8.4	14.9/ 7.0	-	16.6/ 8.2	16.1/ 7.0
M8	13.5/ 7.5	13.7/ 7.9	-	-	14.1/ 8.0	15.7/ 6.6
M9	10.3/ 6.0	8.6/ 6.1	9.3/ 6.0	-	-	10.2/ 5.8
Mean ratio of upper molariform ln/wd	1.68	-	-	-	-	1.99
Palatal ln (in midline)	156* [0.61]	145* [0.61]	-	-	149 [0.62]	155
Min interpterygoid wd	-	-	-	-	-	-

Max zygomatic wd	-	-	-	-	-	-
Min interorbital wd	-	57 [0.24]	-	60 [0.27]	-	55
Min postorbital wd	-	-	-	42 [0.19]	-	-
Max wd of glenoid fossa in ventral view (measured along glenoid's long axis)	-	-	-	-	-	29
Max anteroposterior ln of glenoid in ventral view	12.6 [0.05]	-	13.6	14.5 [0.07]	14.3 [0.06]	12.7
Ratio of glenoid wd to ln	-	-	-	-	-	2.28
Postglenoid skull ln	46* [0.18]	44 [0.19]	-	42 [0.19]	40 [0.17]	-
Max wd of occipital condyles in ventral view (measured along condyle's long axis)	22.2	22.7	20.8	21.3	-	24.2
Max anteroposterior ln of condyles in ventral view	13.5	13.3	12.7	14.0	-	14.0
Ratio of occipital condyle wd to ln	1.64	1.71	1.64	1.52	-	1.73
Wd of occiput (measured at base of supraoccipital)	69.8	73.7	-	66.7	70.6	68
Max dp of occiput in midline (including ventral edge of foramen magnum)	-	77*	-	64.0	-	64.7
Ratio of wd to dp	-	0.96	-	1.04	-	1.05

4

5 Abbreviations: “-” = data unavailable; dp = dorsoventral depth; ln = anteroposterior length, Max = maximum; Min = minimum; wd
6 = transverse width.

7 *Estimated due to skull breakage.

Table 3 (on next page)

Table 3. Mandibular measurements for *Holmesina floridanus* and related taxa.

All measurements reported in millimeters (mm); those reported to the nearest tenth of a millimeter are direct measurements, those rounded to the nearest millimeter are taken from literature sources or from photographs taken by TJG. Numbers in square brackets are scaled to Maximum Mandibular Length (MML).

- 1 Table 3. Mandibular measurements for *Holmesina floridanus* and related taxa. All measurements reported in millimeters (mm); those
- 2 reported to the nearest tenth of a millimeter are direct measurements, those rounded to the nearest millimeter are taken from literature
- 3 sources or from photographs taken by TJG. Numbers in square brackets are scaled to Maximum Mandibular Length (MML).
- 4

Measurement Description	<i>Holmesina floridanus</i> UF 224450	<i>Holmesina occidentalis</i> ROM 4955	<i>Vassalia maxima</i> FMNH P14424 ^a	<i>Propalaeo- hoplophorus australis</i> MLP 16-15 ^b	<i>Proeutatus oenophorus</i> FMNH P13197	<i>Euphractus sexcinctus</i> UTCM 1491
Maximum Mandibular Length (MML)	200.5	268*	180*	139	98.3	93.0
Max dp of horizontal ramus	40.0 [0.20]	52 [0.19]	47.5 ^a [0.26]	37 [0.27]	16.1 [0.16]	13.5 [0.15]
Max dp of ascending ramus	120.5 [0.60]	155 [0.58]	132.0 ^a [0.73]	98 [0.71]	53.8 [0.55]	49.5 [0.53]
Condyle, max wd	23.4	-	31.2 ^a	-	9.0	9.9
Condyle, max ln	7.0	-	11.0 ^a	-	4.7	5.9
Ratio of condyle wd to ln	3.34	-	2.84	-	1.91	1.68
Height of condyle above toothrow	39.3 [0.20]	84 [0.31]	60 [0.33]	59 [0.42]	37.3 [0.38]	41.7 [0.45]
Symphysis ln	59.0 [0.29]	79* [0.29]	54.0 ^a [0.30]	41 [0.29]	23.5 [0.24]	25.7 [0.28]
Coronoid process, anteroposterior ln at base	31.0	40	33	31	12.4	9.8
Coronoid process, maximum dp	42.0	-	50	31	16.2	15.5
Ratio of coronoid process dp to ln	1.35	-	1.52	1.0	1.31	1.58
Mesiodistal ln/ max wd of lower molariforms in <i>Holmesina floridanus</i>	m1: 5.8/ 5.1** m2: 7.5/ 5.6 m3: 11.7/ 7.1** m4: 14.9/ 7.7** m5: 17.3/ 9.3** m6: 16.9/ 8.6 m7: 16.2/ 8.0 m8: 16.7/ 8.5** m9: 12.3/ 7.6** [Mean ratio of lower molariform ln/wd: 1.72]					

UF 224450

5
6
7
8
9
10

Abbreviations: “–” = data unavailable; dp = dorsoventral depth; ln = anteroposterior length, Max = maximum; Min = minimum; n = data not applicable; wd = transverse width.
*Estimated due to breakage; **Estimated from alveolus diameter.
^a Data from De Iuliis and Edmund (2002); ^b Estimated from photograph, Vizcaíno et al. 1998, Fig. 2.

Table 4(on next page)

Table 4. Mandibular measurements for additional specimens of *Holmesina floridanus*.

All measurements reported in millimeters (mm). Numbers in square brackets are scaled to Maximum Mandibular Length (MML).

1 Table 4. Mandibular measurements for additional specimens of *Holmesina floridanus*. All measurements reported in millimeters
 2 (mm). Numbers in square brackets are scaled to Maximum Mandibular Length (MML).

3

Measurement Description	<i>Holmesina floridanus</i> UF 223813	UF 275497	UF 275498	UF 285000	UF 293000
Maximum Mandibular Length (MML)	182.2	187*	191*	-	185*
Max dp of horizontal ramus	38* [0.21]	41.0 [0.22]	40.4 [0.21]	44	39.3 [0.21]
Max dp of ascending ramus	106.5 [0.58]	120.3 [0.64]	-	-	113* [0.61]
Condyle, max wd	24.0	21.4	18.3	23.0	23.8
Condyle, max ln	7.4	9.5	7.5	10.0	9.1
Ratio of condyle wd to ln	3.24	2.25	2.44	2.30	2.62
Height of condyle above toothrow	45.6 [0.25]	43.0 [0.23]	-	30.0	37.0 [0.20]
Symphysis ln	54.3 [0.30]	-	50.3 [0.26]	-	58.4 [0.32]
Coronoid process, anteroposterior ln at base	31.2	33.3	-	-	31.7
Coronoid process, maximum dp	26.6	47.7	-	-	36.0
Ratio of coronoid process dp to ln	0.85	1.43	-	-	1.14
Mesiodistal ln/ max wd of lower molariforms in <i>Holmesina floridanus</i> UF 223813	m1: 5.0/ 4.8 m2: 7.2/ 5.7 m3: 8.2/ 6.0 m4: 11.5/ 6.8 m5: 16.0/ 8.6 m6: 17.0/ 8.4 m7: 15.2/ 8.0 m8: 13.6/ 7.0 m9: 10.7/ 5.9 [Mean ratio of lower molariform ln/wd: 1.65]				

4

5 Abbreviations: “–” = data unavailable; dp = dorsoventral depth; ln = anteroposterior length, Max = maximum; Min = minimum; wd
6 = transverse width.

7 *Estimated due to breakage.

8

Table 5(on next page)

Table 5. Listing of cranial features with potential systematic value (i.e., diagnostic features or putative synapomorphies) identified in the description from the present study.

1 Table 5. Listing of cranial features with potential systematic value (i.e., diagnostic features or putative synapomorphies) identified in
2 the description from the present study.

3

4 *Holmesina floridanus*: 1) ovate shape of M3; 2) absence of vomer/premaxilla contact within nasal cavity; 3) lacrimal foramen situated
5 on the antorbital ridge; 4) medial pterygoid exposure that fails to reach nasopharyngeal roof; 5) inflated pterygoid; 6) presence
6 of a bony bridge connecting the tympanohyal and crista interfenestralis; 7) presence of a raised circular boss on the lateral
7 surface of the promontorium; 8) elongate, narrow basioccipital; presence of well-developed rectus capitis fossae and
8 pharyngeal tubercle on basioccipital; 9) distinct grooves emerging anteriorly from mental foramina; and 10) mandibular spout
9 with anteroposterior $ln > m1$; 11) rectangular shape of m4.

10

11 Genus *Holmesina*: 1) nasals become narrower posteriorly; 2) maxillary/premaxillary suture M-shaped in ventral view; 3)
12 maxillary/palatine suture U-shaped in ventral view; 4) presence of prominent lateral maxillary ridge and deep antorbital fossa;
13 5) reniform M4 and bilobate m5; 6) lack of orbital exposure of palatine; 7) ethmoid foramen entirely within frontal, lacking
14 orbitosphenoid participation in rim; 8) no orbitosphenoid participation in rim of sphenopalatine foramen; 9) fenestra cochleae
15 very low and wide, ratio of $wd/dp > 3$; 10) triangular stylohyal fossa with distally expanded tympanohyal; 11) strong medial
16 flange of petrosal marked by pits and ridges; 12) low stapedial ratio (<1.4); and 13) ventrally displaced internal acoustic
17 meatus.

18

19 Pamphathes: 1) nasal $ln > 45\%$ of GSL; 2) presence of median anteroventral processes on premaxilla; 3) incisive foramina open
20 ventrally into single, deeply recessed, midline fossa; 4) infraorbital canal elongate, extending from level of M6-M8; 5)
21 reniform anterior molariforms and bilobate posterior molariforms; 6) posterior molariforms with linear, unbranched core of

osteodentine; 7) partially closed (anteriorly) upper toothrows; 8) teeth wear in stairstep fashion in lateral view; 9) triangular facial process of lacrimal; 10) triangular glenoid fossa (apex lateral); 11) no horizontal portion of jugal/squamosal suture; 12) ridged, anteroposteriorly expanded ventral zygomatic process formed by maxilla and anterior jugal [mostly the latter]; 13) zygomatic process of squamosal increases in dp anteriorly; 14) reduced midline crest on endocranial exposure of orbitosphenoid; 15) ventral flange of basisphenoid forms portion of the lateral wall of the nasopharynx; 16) Elongate groove on petrosal for greater petrosal nerve; 17) broad crista interfenestralis of petrosal; 18) enormously enlarged paroccipital process of petrosal; 19) caudal tympanic process of petrosal forms posterior wall to stapedial fossa; 20) large epitympanic wing of petrosal (as in *Euphractus*), forms shelf above rostral process of promontorium; 21) Groove for auricular branch of vagus nerve between caudal tympanic process and triangular shelf [= roof of postpromontorial sinus]; 22) Sharp, narrow transverse crest within internal acoustic meatus; 23) low rounded ridges subdivide subarcuate fossa; 24) prefacial commissure enlarged, bulbous; 25) crista petrosa rounded, divided by groove into medial and lateral parts; 26) paracondylar process of exoccipital hooked medially; 27) ventral surface of exoccipital convex transversely; 28) mandibular condyle less elevated above toothrow than glyptodonts, *Proeutatus*, *Euphractus*; and 29) coronoid process covers m9 and part of m8 in lateral view.

Pamphateres plus glyptodonts: 1) presence of semicircular notch in anterolateral edge of premaxilla; 2) dp of external nares \geq wd; 3) teeth with essentially linear core of osteodentine; 4) anterior molariforms slanted lingually in posterior view, posterior molariforms slanted labially; 5) narrow, U-shaped postpalatal margin (also in Gaudin and Wible 2006); 6) pterygoid processes form thickened, rugose bosses (also in Gaudin and Wible 2006); 7) pterygoid participation in hard palate; 8) lacrimal foramen positioned on facial process of lacrimal; 9) lacrimal foramen situated within distinct fossa; 10) presence of an enlarged ventral zygomatic process near anterior terminus of zygomatic arch; 11) sphenopalatine foramen in common fossa with sphenorbital fissure (also in Gaudin and Wible 2006); 12) raised ridge along squamosal/parietal suture; 13) posterior zygomatic root directed laterally (also in Gaudin and Wible 2006); 14) postglenoid foramen visible in ventral view (also in Gaudin and Wible

2006); 15) broad triangular shelf [= roof of postpromontorial sinus]; 16 & 17) enlarged paroccipital process of petrosal and paracondylar process of exoccipital; 18) well-developed external occipital crest; 19) anterior portion of occipital condyle extends lateral to dorsal portion in ventral view; 20) nine lower molariforms present; 21) ratio between maximum depth of mandibular horizontal ramus vs. MML > 0.2 (also in Gaudin and Wible 2006); and 22) maximum wd of mandibular condyle $\geq 3 \times$ its ln (also in Gaudin and Wible 2006).

Pamphathères plus glyptodonts plus *Proeutatus*: 1) nasal ln $> 35\%$ of GSL (also in Gaudin and Wible 2006); 2) presence of osteodentine core in molariforms (also in Gaudin and Wible 2006); 3) beveled wear on anterior molariforms, posterior molariforms worn flat (also in Gaudin and Wible 2006); 4) lateral portion of frontal/parietal suture even with anterior edge of the glenoid; 5) optic foramen hidden in lateral view (also in Gaudin and Wible 2006); 6) dorsal edge of zygomatic process of squamosal connected to nuchal crest posteriorly; 7) middle of infratemporal crest marked by large boss, the ossified ala hypochiasmata; 8) open groove for vidian nerve in roof of nasopharynx; 9) large entoglenoid process of squamosal; 10) groove for greater petrosal nerve uncovered by anteroventral process of tegmen tympani [=processus crista facialis]; 11) anteroventral process of tegmen tympani reduced in size, only contacts squamosal; 12) tensor tympanic muscle originates on anteroventral promontorium; 13) caudal tympanic process of petrosal lacks contact for ectotympanic; 13) Rostral process of petrosal enlarged, promontorium elongated anteromedially; 14) presence of epitympanic recess [as opposed to a sinus]; and 15) triangular shelf of petrosal with raised posterolateral corner

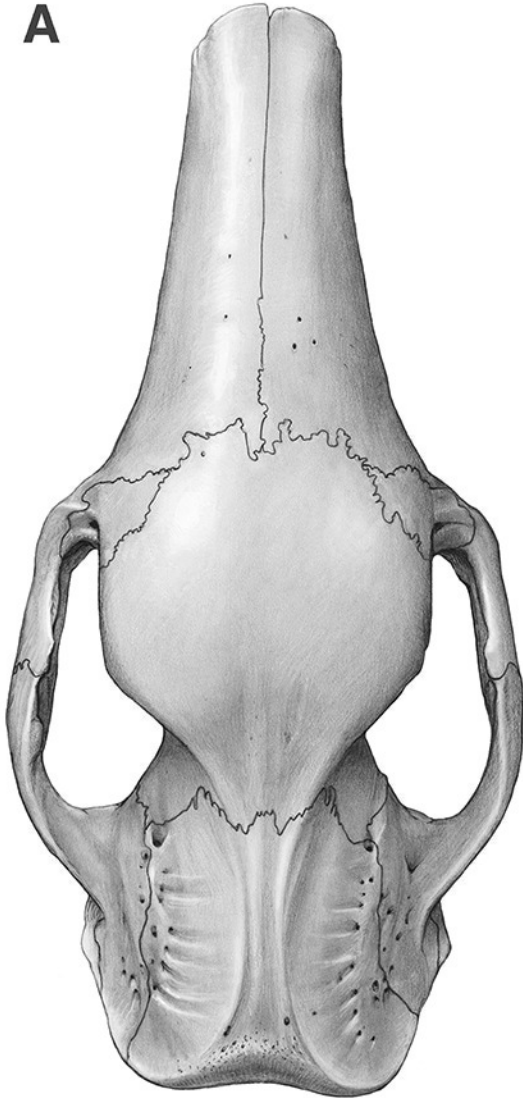
Abbreviations: GSL = greatest skull length; dp = dorsoventral depth; ln = anteroposterior length; M1...9 = upper molariform teeth; MML = maximum mandibular length; wd = transverse width.

Figure 1(on next page)

Skull of *Holmesina floridanus* in dorsal view

A, UF 191448; B, UF 248500. Scale bar = 5 cm.

A



B

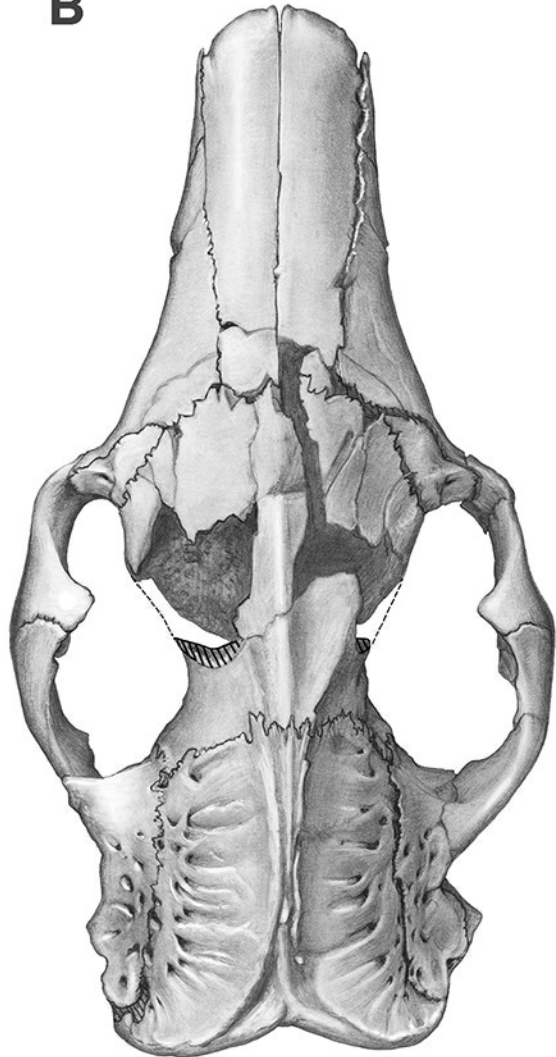


Figure 2 (on next page)

Reconstruction of the skull of *Holmesina floridanus* in dorsal view

Abbreviations: **f**, frontal; **ftr**, foramina for rami temporalis; **j**, jugal; **l**, lacrimal; **lf**, lacrimal foramen; **mx**, maxilla; **n**, nasal; **nc**, nuchal crest; **p**, parietal; **pm**, premaxilla; **pop**, paroccipital process of petrosal (= mastoid process of Patterson et al. 1989); **popf**, postorbital process of frontal; **popj**, postorbital process of jugal; **sq**, squamosal; **zp**, zygomatic process of squamosal.

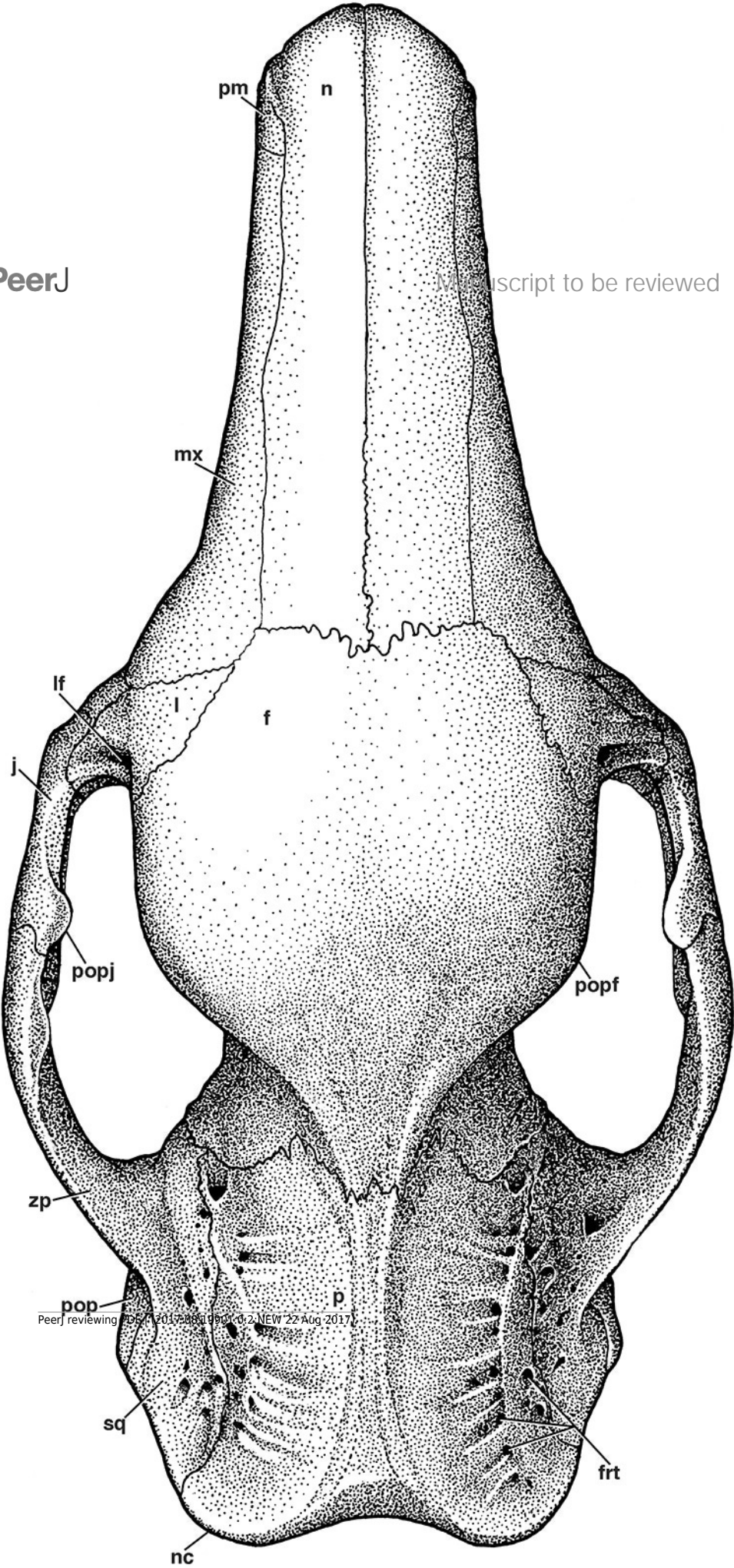
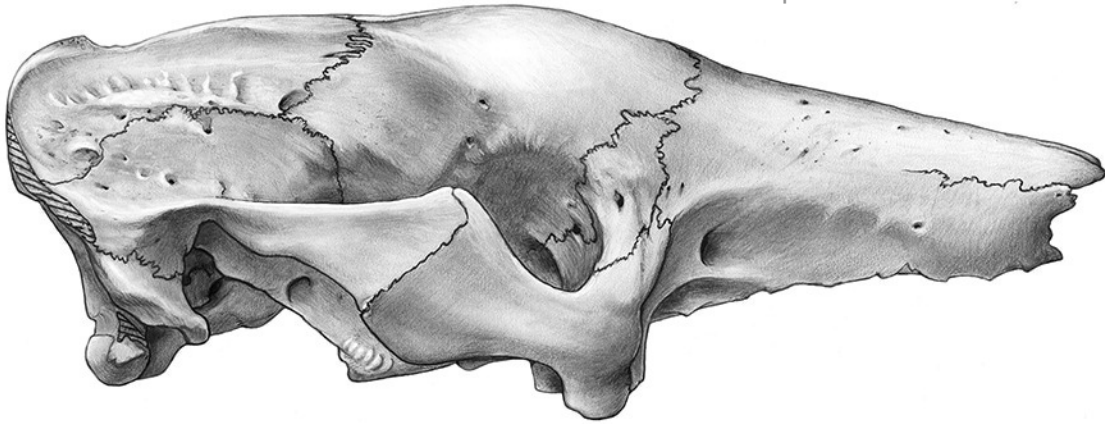


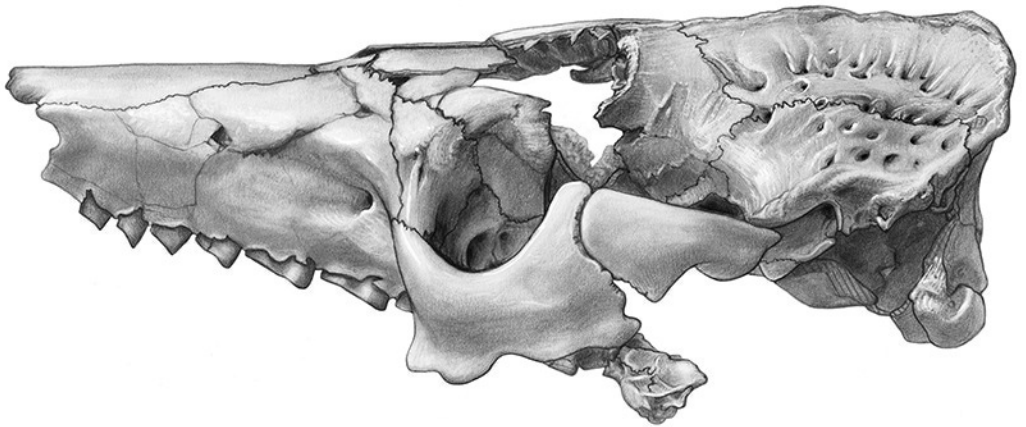
Figure 3(on next page)

Skull of *Holmesina floridanus* in lateral view

A, UF 191448 in right lateral view; B, UF 248500 in right lateral view; C, UF 248500 in left lateral view. Scale bar = 5 cm.



B



C

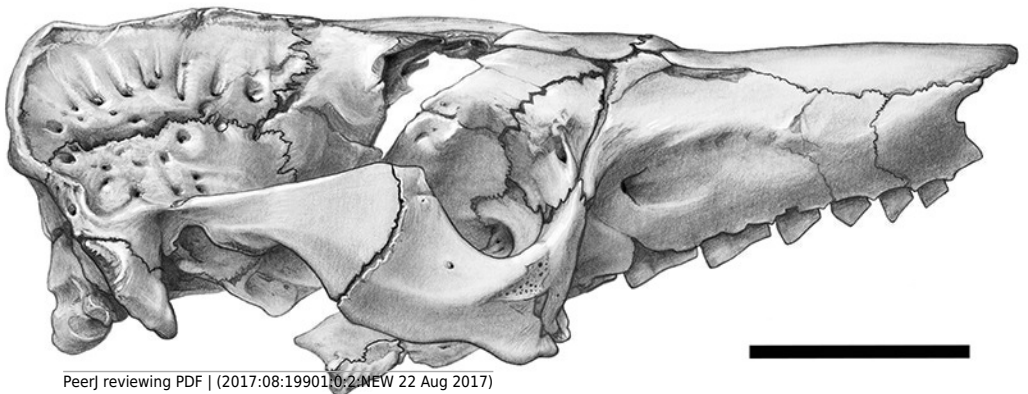


Figure 4(on next page)

Reconstruction of the skull of *Holmesina floridanus* in right lateral view

Abbreviations: **as**, alisphenoid; **bo**, basioccipital; **bs**, basisphenoid; **dpj**, descending process of jugal; **f**, frontal; **fdv**, foramen for frontal diploic vein; **fo**, foramen ovale; **ftr**, foramina for rami temporales; **iof**, infraorbital foramen; **j**, jugal; **l**, lacrimal; **lf**, lacrimal foramen; **M1**, first upper molariform tooth; **M9**, ninth upper molariform tooth; **mx**, maxilla; **n**, nasal; **nc**, nuchal crest; **oc**, occipital; **occ**, occipital condyle; **p**, parietal; **pm**, premaxilla; **pop**, paroccipital process of petrosal (= mastoid process of Patterson et al. 1989); **pt**, pterygoid; **sq**, squamosal; **zp**, zygomatic process of squamosal.

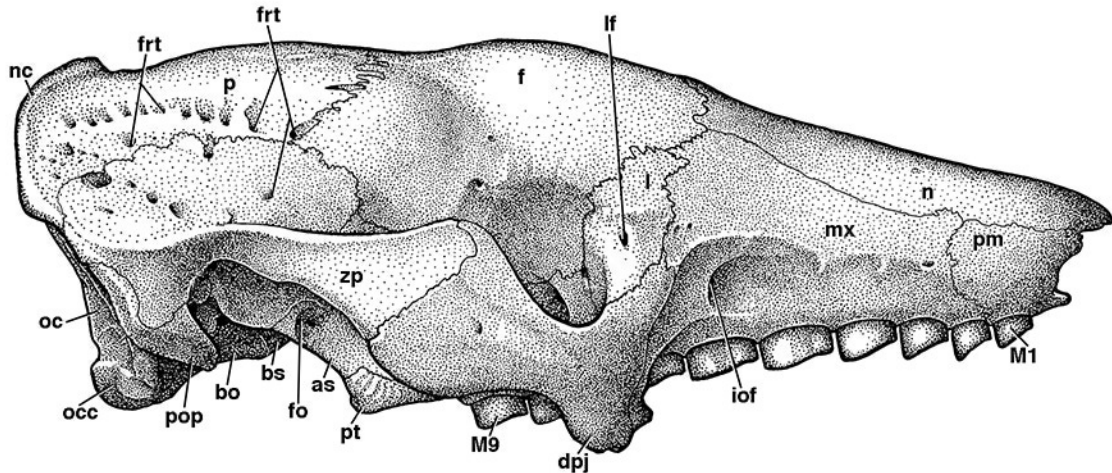


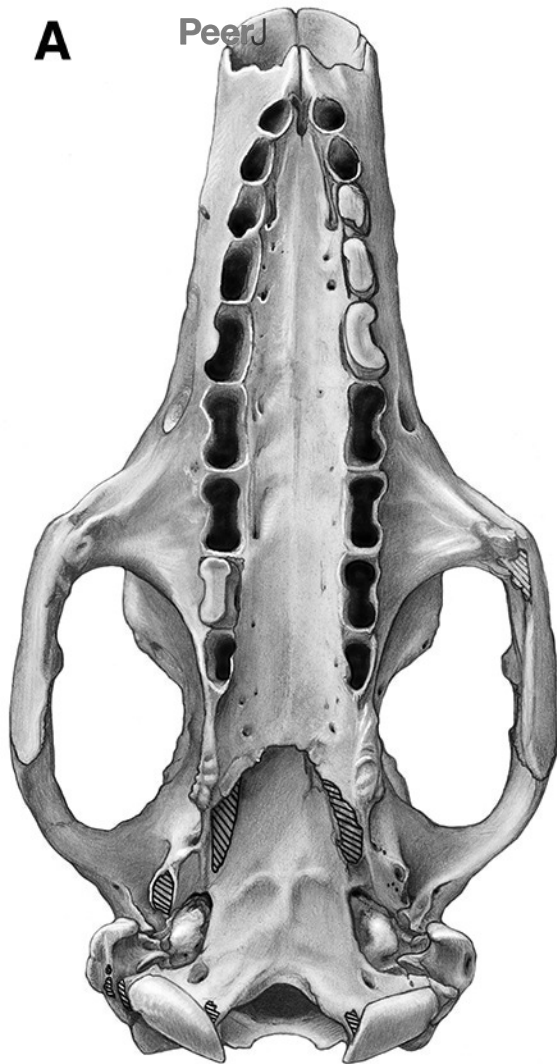
Figure 5(on next page)

Skull of *Holmesina floridanus* in ventral view

A, UF 191448; B, UF 248500. Scale bar = 5 cm.

A

PeerJ

**B**

Manuscript to be reviewed

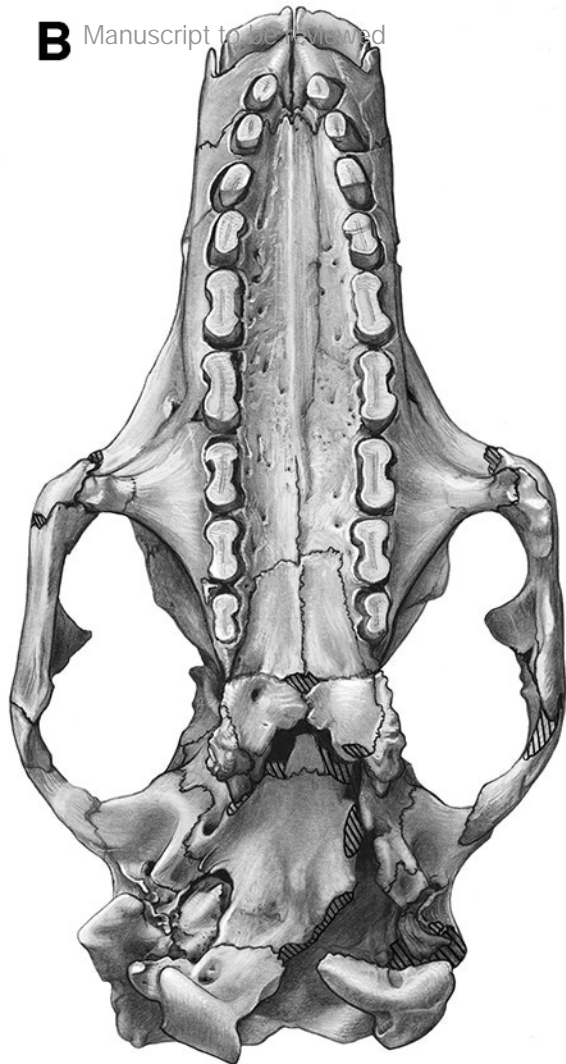


Figure 6(on next page)

Reconstruction of the skull of *Holmesina floridanus* in ventral view

Abbreviations: **apf**, anterior palatal foramen; **as**, alisphenoid; **bo**, basioccipital; **bs**, basisphenoid; **cf**, carotid foramen; **dpj**, descending process of jugal; **eo**, exoccipital; **fdv**, foramen for frontal diploic vein; **fm**, foramen magnum; **fo**, foramen ovale; **gf**, glenoid fossa; **hf**, hypoglossal foramen; **iof**, infraorbital foramen; **jf**, jugular foramen; **M1**, first upper molariform tooth; **M9**, ninth upper molariform tooth; **mpf**, minor palatine foramen; **mx**, maxilla; **n**, nasal; **oc**, occipital; **occ**, occipital condyle; **pal**, palatine; **pcp**, paracondylar process of exoccipital (=paroccipital process of Patterson et al. 1989); **pgf**, postglenoid foramen; **pgp**, postglenoid process; **pm**, premaxilla; **pop**, paroccipital process of petrosal (= mastoid process of Patterson et al. 1989); **popf**, postorbital process of frontal; **popj**, postorbital process of jugal; **pr**, promontorium of petrosal; **prs**, presphenoid; **pt**, pterygoid; **zp**, zygomatic process of squamosal; **zpm**, zygomatic process of maxilla.

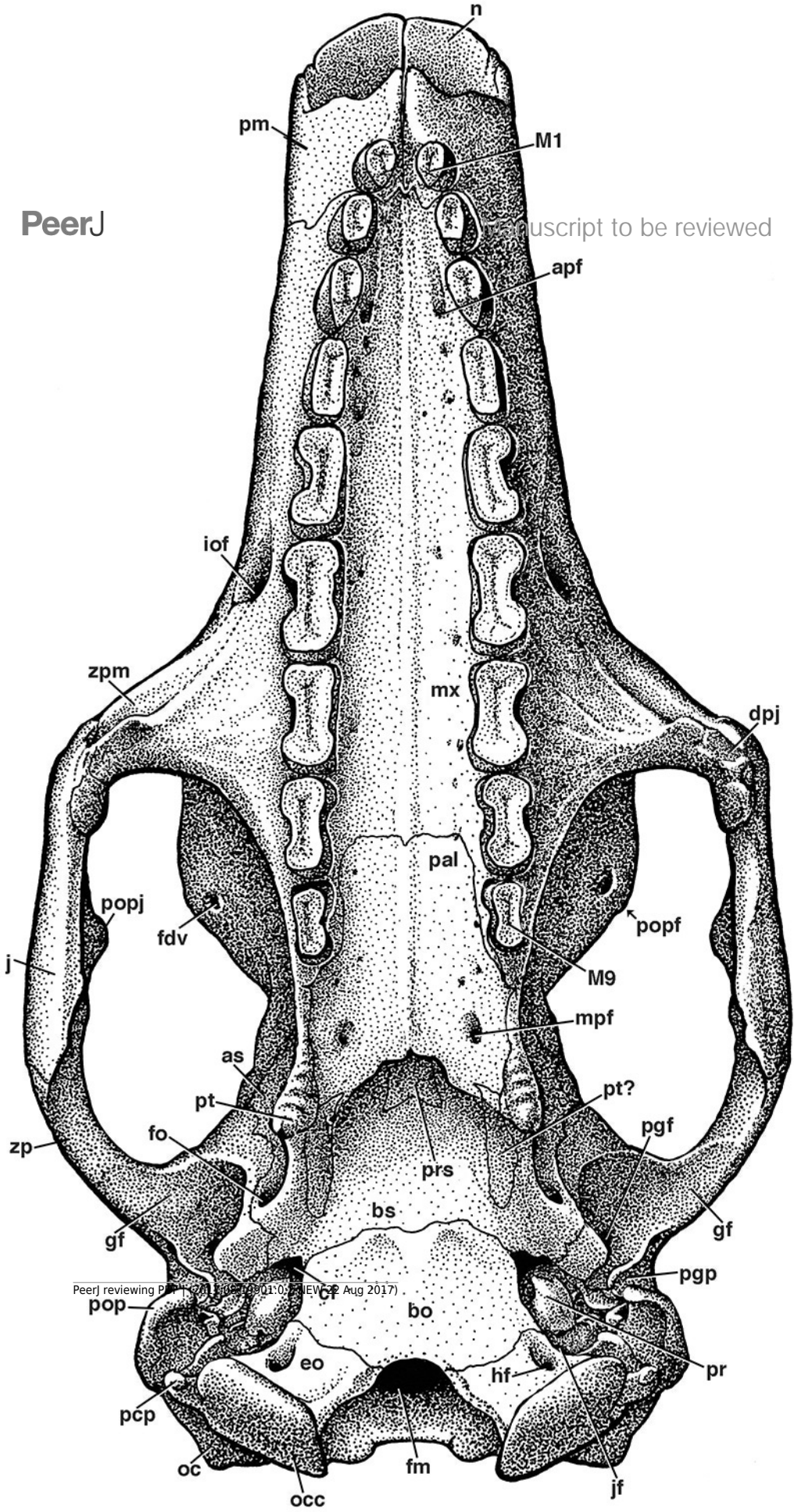


Figure 7 (on next page)

Reconstruction of right orbital wall of *Holmesina floridanus* in lateral view

Cross-hatched surfaces indicate where zygomatic arch is “cut.” Abbreviations: **as**, alisphenoid; **bo**, basioccipital; **bs**, basisphenoid; **cf**, carotid foramen; **cpf**, caudal palatine foramen; **ef**, ethmoid foramen; **f**, frontal; **fdv**, foramen for frontal diploic vein; **fo**, foramen ovale; **fr/sof**, fused foramen rotundum and sphenorbital fissure; **ftr**, foramina for rami temporalis; **fv**, fenestra vestibuli; **iof**, infraorbital foramen; **j**, jugal; **l**, lacrimal; **lf**, lacrimal foramen; **lfe**, lacrimal fenestra; **lopc**, lateral opening of pterygoid canal; **M9**, ninth upper molariform tooth; **mx**, maxilla; **mx****f**, maxillary foramen; **n**, nasal; **of**, optic foramen; **os**, orbitosphenoid; **p**, parietal; **pgf**, postglenoid foramen; **pgp**, postglenoid process; **pop**, paroccipital process of petrosal (= mastoid process of Patterson et al. 1989); **pr**, promontorium of petrosal; **pt**, pterygoid; **ptp**, post-tympanic process of squamosal; **spf**, sphenopalatine foramen; **sq**, squamosal; **tcf**, transverse canal foramen; **zp**, zygomatic process of squamosal.

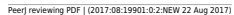


Figure 8(on next page)

Stereophotographs of right auditory region of *Holmesina floridanus* (UF 248500) in ventral view

Abbreviations: **aptt**, anteroventral process of tegmen tympani (= processus crista facialis); **as**, alisphenoid; **bb**, bony bridge between tympanohyal and crista interfenestralis; **bo**, basioccipital; **bs**, basisphenoid; **cf**, carotid foramen; **ci**, crista interfenestralis; **cp**, crista parotica; **ctpp**, caudal tympanic process of petrosal; **eam**, external auditory meatus; **egp**, entoglenoid process; **eo**, exoccipital; **fc**, fenestra cochleae; **fi**, ridge immediately ventral to fossa incudis; **fm**, foramen magnum; **fo**, foramen ovale; **fs**, facial sulcus; **gf**, glenoid fossa; **hf**, hypoglossal foramen; **jf**, jugular foramen; **occ**, occipital condyle; **pcp**, paracondylar process of exoccipital (=paroccipital process of Patterson et al. 1989); **pe**, petrosal; **pgf**, postglenoid foramen; **pgp**, postglenoid process; **pop**, paroccipital process of petrosal (= mastoid process of Patterson et al. 1989); **pr**, promontorium of petrosal; **sq**, squamosal; **stmf**, stylomastoid foramen; **th**, tympanohyal; **ttf**, tensor tympani fossa on epitympanic wing of petrosal; **zp**, zygomatic process of squamosal. Scale bar = 1 cm.

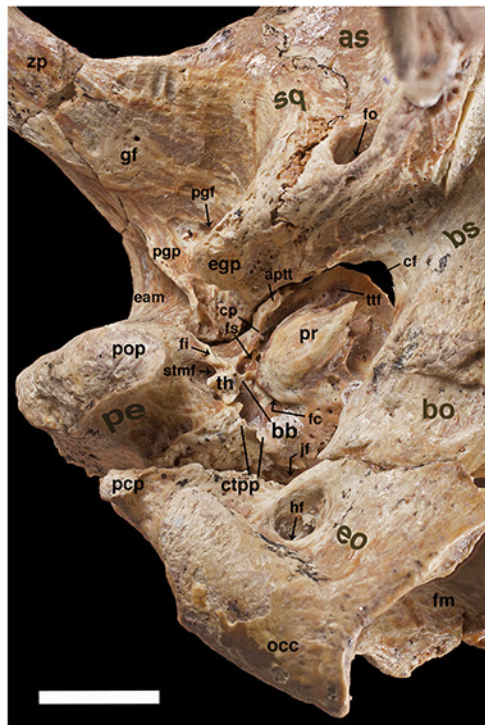
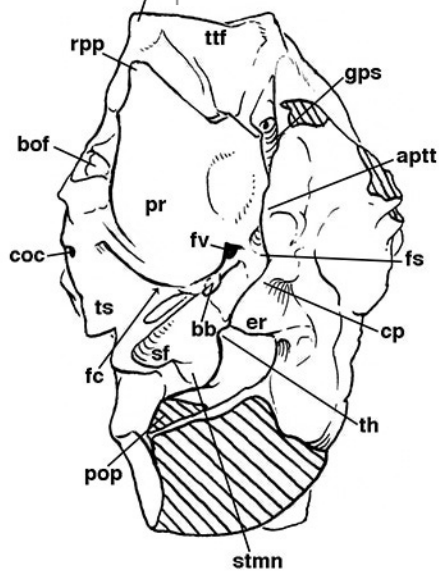
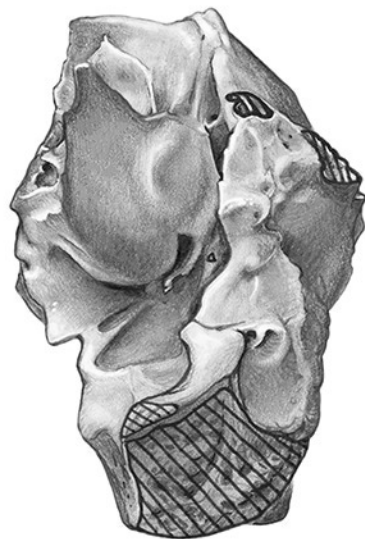


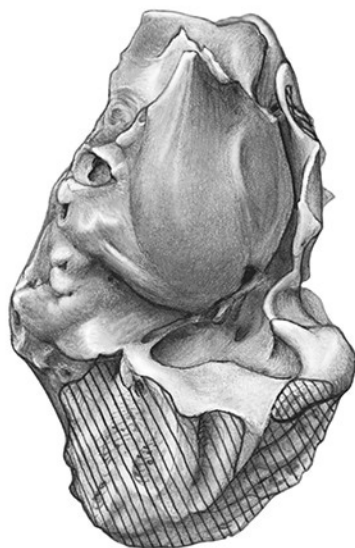
Figure 9(on next page)

Isolated left petrosal of *Holmesina floridanus* (UF 248500)

A, B, ventrolateral; C, D, ventral; E, F, lateral; and G, H, medial views. Abbreviations: **aptt**, anteroventral process of tegmen tympani (= processus crista facialis); **av**, aqueductus vestibuli; **bof**, basioccipital facet; **ci**, crista interfenestralis; **coc**, cochlear canaliculus; **cp**, crista parotica; **crp**, crista petrosal; **ctpp**, caudal tympanic process of petrosal; **er**, epitympanic recess; **ew**, epitympanic wing; **fc**, fenestra cochleae; **ff**, facial foramen; **fs**, facial sulcus; **fsi**, foramen singulare; **fv**, fenestra vestibuli; **gps**, sulcus for greater petrosal nerve; **iam**, internal acoustic meatus; **iva**, inferior vestibular area; **pfc**, prefacial commissure; **pop**, paroccipital process of petrosal (= mastoid process of Patterson et al. 1989); **pr**, promontorium of petrosal; **rpp**, rostral process of petrosal; **saf**, subarcuate fossa; **sct**, spiral cribriform tract; **sf**, stapedius fossa; **stmn**, stylomastoid notch; **sva**, superior vestibular area; **tc**, transverse crest; **th**, tympanohyal; **ts**, triangular shelf (=roof of post-promontorial sinus. Scale bar = 1 cm.



C



D

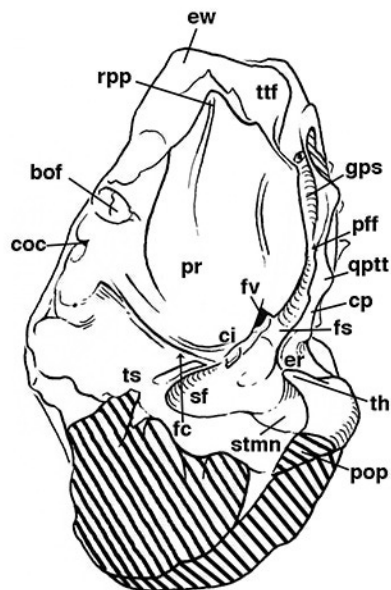


Figure 10(on next page)

Isolated left petrosal of *Holmesina floridanus* (UF 248500)

Isolated left petrosal of *Holmesina floridanus* (UF 248500) in A, B, ventrolateral; C, D, ventral; E, F, lateral; and G, H, medial views. Abbreviations: **aptt**, anteroventral process of tegmen tympani (= processus crista facialis); **av**, aqueductus vestibuli; **bof**, basioccipital facet; **ci**, crista interfenestralis; **coc**, cochlear canaliculus; **cp**, crista parotica; **crp**, crista petrosal; **ctpp**, caudal tympanic process of petrosal; **er**, epitympanic recess; **ew**, epitympanic wing; **fc**, fenestra cochleae; **ff**, facial foramen; **fs**, facial sulcus; **fsi**, foramen singulare; **fv**, fenestra vestibuli; **gps**, sulcus for greater petrosal nerve; **iam**, internal acoustic meatus; **iva**, inferior vestibular area; **pfc**, prefacial commissure; **pop**, paroccipital process of petrosal (= mastoid process of Patterson et al. 1989); **pr**, promontorium of petrosal; **rpp**, rostral process of petrosal; **saf**, subarcuate fossa; **sct**, spiral cribriform tract; **sf**, stapedius fossa; **stmn**, stylomastoid notch; **sva**, superior vestibular area; **tc**, transverse crest; **th**, tympanohyal; **ts**, triangular shelf (=roof of post-promontorial sinus. Scale bar = 1 cm.

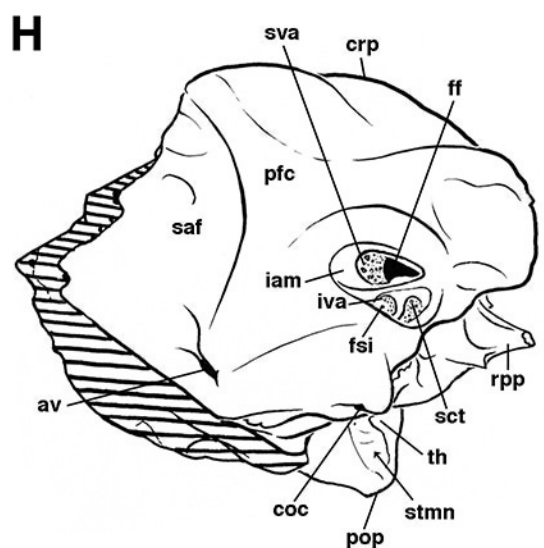
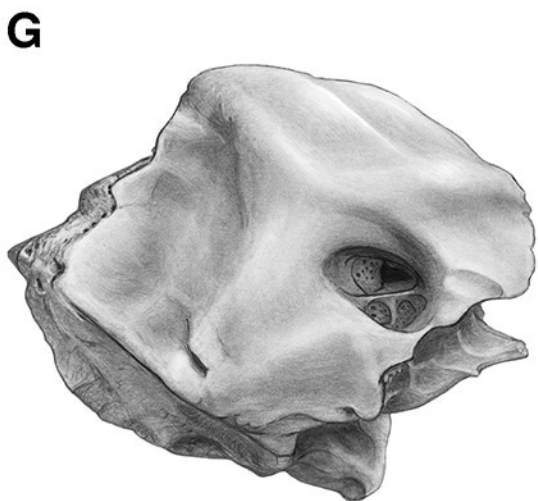
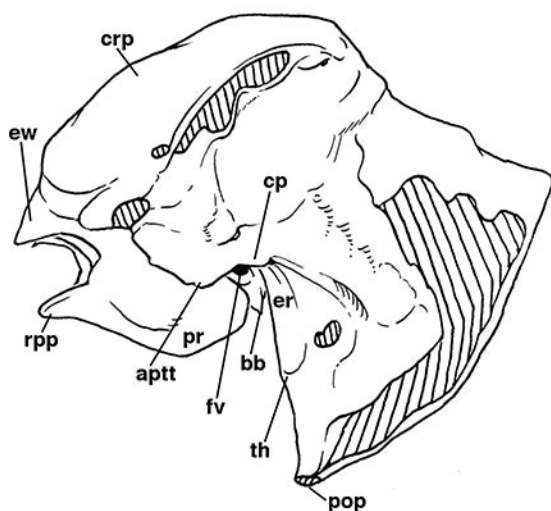
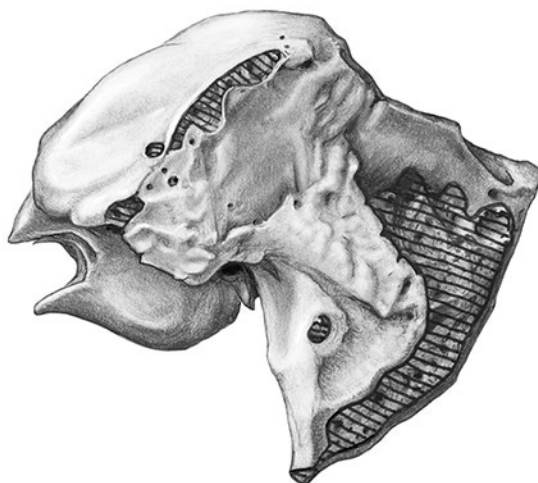
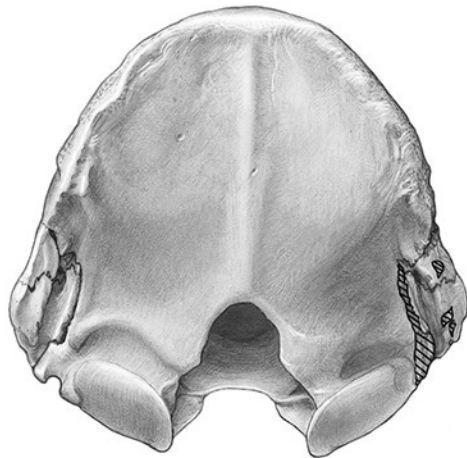


Figure 11(on next page)

Skull of *Holmesina floridanus* in posterior view

A, UF 191448; B, Reconstruction. Abbreviations: **bo**, basioccipital; **dcf**, dorsal condyloid fossa; **dgf**, digastric fossa; **eo**, exoccipital; **eo**, external occipital crest; **eo**, exoccipital crest; **fm**, foramen magnum; **nc**, nuchal crest; **oc**, occipital; **oc**, occipital condyle; **og**, groove for occipital artery; **me**, mastoid exposure of petrosal; **pcp**, paracondylar process of exoccipital (=paroccipital process of Patterson et al. 1989); **ptc**, posttemporal canal; **so**, supraoccipital; **sq**, squamosal. Scale bar = 5 cm.

A



B

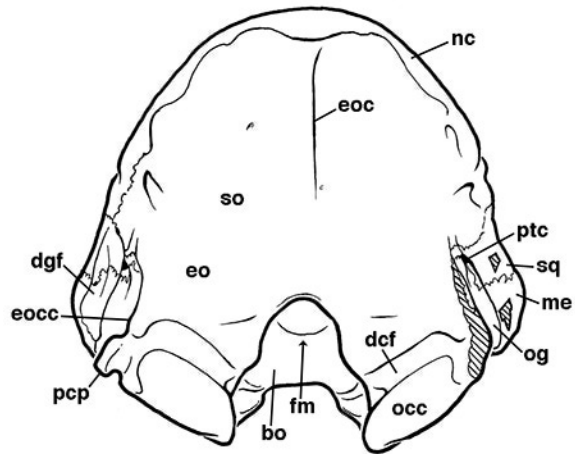


Figure 12(on next page)

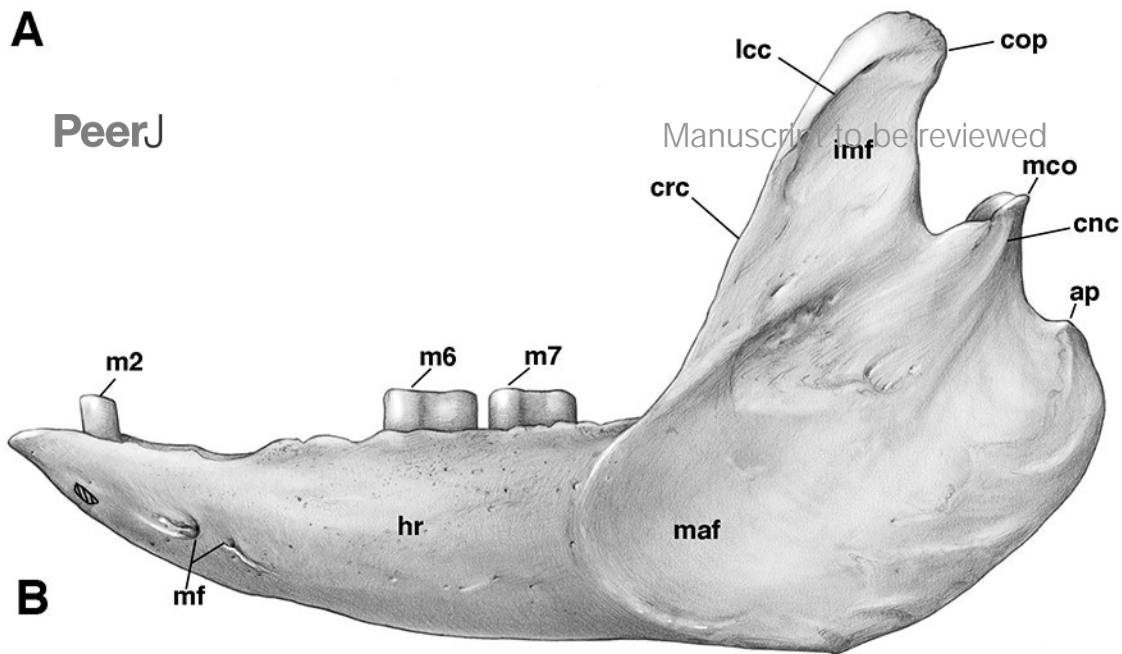
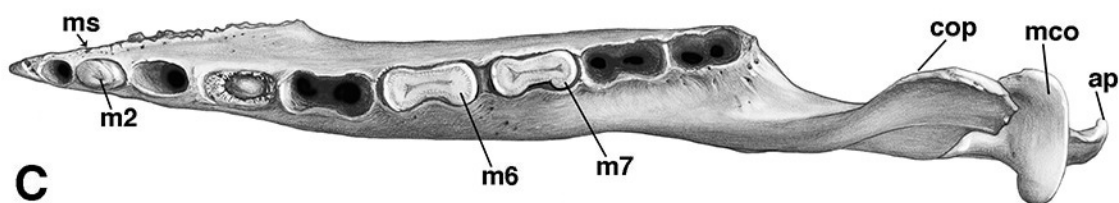
Left mandible of *Holmesina floridanus* (UF 224450)

A, lateral; B, occlusal; and, C, medial views. Abbreviations: **ap**, angular process; **cnc**, condyloid crest; **cop**, coronoid process; **crc**, coronoid crest; **hr**, horizontal ramus of mandible; **imf**, intermuscular fossa; **lcc**, lateral coronoid crest; **m1**, first lower molariform tooth; **m6**, sixth lower molariform tooth; **m7**, seventh lower molariform tooth; **maf**, masseteric fossa; **mco**, mandibular condyle; **mf**, mental foramen; **maf**, mandibular foramen; **ms**, mandibular symphysis. Scale bar = 5 cm.

A

PeerJ

Manuscript to be reviewed

**B****C**